Studies on dose delivery errors and quality assurance methods using Volumetric Modulated high energy X-rays from Linear Accelerator.

Thesis submitted to the University of Calicut

in partial fulfillment of the requirements

for the degree of

Doctor of Philosophy

in

Physics

Noufal M P

Department of Physics

Farook College

P.O. Farook College, PIN-673632

Kozhikode Dt., Kerala.

May 2018

CERTIFICATE

Certified that the work presented in this thesis entitled 'Studies on dose delivery errors and quality assurance methods using Volumetric Modulated high energy X-rays from Linear Accelerator' is a bonafide work done by Mr. Noufal. M.P., under my guidance in the Department of Physics, Farook College and that this work has not been included in any other thesis submitted previously for the award of any degree.

Farook College
May 2018

Dr. K. K. Abdullah
(Supervising Guide)

DECLARATION

I hereby declare that the work presented in this thesis entitled 'Studies on dose delivery errors and quality assurance methods using Volumetric Modulated high energy X-rays from Linear Accelerator' is based on the original work done by me under the guidance of Dr. K. K. Abdullah, Department of Physics, Farook College and has not been included in any other thesis submitted previously for the award of any degree.

Farook College

May 2018 Noufal M.P.

Acknowledgements

I would like to express my sincere gratitude to Dr K.K.Abdullah, my research guide, for his continuous support throughout my Ph.D program and related research. His guidance, motivation and vast knowledge has helped me immensely during the research and thereafter. I could not have imagined having a better advisor and mentor for my study.

I would also like to express my sincere thanks to Dr P.A.Subha, Head of the Department of Physics, Farook College, for providing her valuable suggestions during various stages of the work. I am indebted to her for taking her valuable time to provide me with continuous encouragement and informative discussions and for the constant support she provided to overcome the many difficulties during the time of research.

I express my special thanks to Prof.E.P.Imbichikoya, and Dr.K.M.Naseer, the former and present principals of Farook College, for their support and encouragement. I would also like to thank my colleagues in the Department of Physics, Farook College, for their keen interest and encouragement in my research work.

I am really grateful to Prof Sankaran Nair, Chief Medical Physicist, Baby Memorial Hospital and Dr Sasindran, Head of the Department of Radiation Oncology, Baby Memorial Hospital, Calicut for providing me the academic support and necessary facilities to accomplish this research. I would like to thank my co-researchers and colleagues in the the department of Medical physics at Baby Memorial Hospital, P Niyas and Dr Sanudev for their active involvement in in-

formative discussions.

Above all, I am thankful to Almighty for granting me the wisdom, health and strength to undertake this research task and complete it. Finally, I would like to dedicate this thesis work to my wife and to my parents who inspired me to take up this task and encouraged me throughout my research. I thank them for their patience and great support.

Noufal.M.P

List of Figures

List of Tables

Contents

List of papers published

1. Analysis of Influence of Errors in Angular Settings of Couch and Collimator on the Dosimetric and Radiobiological Parameters in VMAT Plans. **M.P.Noufal***, K.K.Abdullah P. Niyas, and R. Vishnu. Journal of Medical Imaging and Radiation Sciences, 48 (2017), 166-177.

2. Effect of translational couch shifts in volumetric modulated arc therapy (VMAT) plans and predicting its impact on daily dose delivery. **M.P.Noufal***, K.K. Abdullah , P. A. R. Subha and Sanudev Sadanadan. Journal of Radiotherapy in Practice, 1-14.

3. Analysis of Dosimetric Impacts of Cone Beam Computed Tomography-Based Volumetric Modulated Arc Therapy Planning. **M.P.Noufal***, K. K. Abdullah, P. Niyas. Journal of Medical Imaging and Radiation Sciences, 47, Issue 2, June 2016, Pages 160-170, (2016).

4. A Study of impacts of different evaluation criteria on gamma pass rates in VMAT QA using MatriXX and EPID. **M.P.Noufal***, K. K. Abdullah, P. Niyas, R. Subha. Polish Journal of Medical Physics and Engineering 2017;23(4):99-107.

List of Conference presentations

1. Dosimetry Validation of Volumetric Modulated Arc Therapy by four independent Quality Assurance Methods. 33^{rd} National conference of association of Medical Physicist of India, Department of Radiotherapy and Oncology, Kasturba Medical College, Manglore, 2012.

2. Analysis of RapidArc (VMAT) Optimization and Planning Strategies in Head Neck Tumour. 33^{rd} National conference of association of Medical Physicist of India, Department of Radiotherapy & Oncology,Kasturba Medical College, Manglore, 2012.

3. Study of Performance of Electron Montecarlo Algorithm in High Energy electron beams from a Linear Aceelarator. 19^{th} National Symposium on Radiation Physics(NSRP), 2012, Chennai.

4. A study on Adaptive Volumetric Modulated Arc treatment planning using kV cone-beam CT. 34^{th} National conference of association of Medical Physicist of India, Saha Instutute of Nuclear Physics, Kolkata, 2013

5. Predicting the outcome of radiotherapy treatment in cancer patients using polynomial curve fitting method. International Conference on Nonlinear Physics, Department of Physics & Research centre, Farook College, Calicut, 2016.

6. Predicting the impacts of daily translational couch shifts on DVH and radio biological parameters of VMAT plans using curve fitting method. 38^{th} National conference of association of Medical Physicist of India, Jaipur, 2017.

Preface

Radiation is the emission or transmission of energy in the form of waves or particles through space or through a material medium. It includes electromagnetic radiation such as radio waves, microwaves, visible light, x-rays, and gamma radiation (γ) and particle radiation, such as alpha radiation (α), beta radiation (β), and neutron radiation as well. Radiation therapy involves delivering powerful doses of electromagnetic waves of energy such as x-rays to disrupt the ability of cancer cells to grow and divide, killing cancer cells, slowing their growth, and shrinking tumours.

In the present work, we have studied the impact of dose delivery errors in Volumetric Modulated Arc Therapy (VMAT) treatment plans and its method of quality assurance test to ensure the correct dose delivery during radiotherapy patient treatment. We have concentrated on the effects on VMAT plans due to couch, collimator angular settings variation, systematic and random couch translation errors which lead us to suggest a new method to predict their impacts before dose delivery. We have also studied the feasibility of direct dose calculation on Cone Beam Computed Tomography (CBCT) to predict the dose delivery errors due to anatomical changes in the patients due to weight loss, tumour shrinkage and soft tissue changes during VMAT treatment. The quality of overall treatment of VMAT was assessed by array of ionisation chambers and amorphous-silicon photodiodes.

The thesis is divided into five chapter. **Chapter 1** briefly describes the prduction of high energy x-rays and their uses in medicine. An overview of the thesis highlighting the need for carrying out this work is also included in this

chapter. A brief review of literature related to work is referred in every chapter. The variations in the Dose Volume Histogram (DVH) and radio biological parameters due to deviations in the collimator and couch angular settings have been investigated in different types of VMAT planning situations. In **chapter-3**, we have extensively studied the effect of systematic couch translational errors in Right Left, Superior Inferior and Anterior Posterior directions of the couch shifts in VMAT plans. We have also developed a simple method to predict these effects on a daily basis using curve fitting method which is explained in **chapter-3**.

In **chapter 4**, we have studied the feasibility of using the CBCT for VMAT planning and finding daily dose variation. The Hounsfield Unit (HU) values for the CT and CBCT images for the comparison between CT and CBCT images using a Catphan 504 phantom is also calculated and evaluated. In **chapter 5**, the study of impacts of different evaluation criteria on gamma pass rates in VMAT QA using Matrixx and EPID is described and evaluated. Our investigation of differently shaped hypothetical PTVs and different clinical situations has provided us with an improved perspective of the plan verification process in different complex situations. Results obtained and future prospectives of the work are included at the end of each chapter.

Chapter 1

Introduction and Thesis Outline

1.1 Production of High energetic X-rays

High energetic X-rays are produced using two methods; the bremsstrahlung process and the characteristic X-rays production method. In the bremsstrahlung process, X-rays are produced as a result of the interaction between a high-speed electron and a nucleus as phenomenon predicted by Maxwell's general theory of electromagnetic radiation. According to this theory, when an electron, with its associated electromagnetic field, passes in the vicinity of a nucleus, it suffers a sudden deflection and acceleration. As a result, a part or all of its energy is dissociated from it and propagates in space as electromagnetic radiation. The mechanism of bremsstrahlung production is illustrated in Figure 1.1.

In the second method, when an electron with kinetic energy may interact with the atoms of the target by ejecting an orbital electron, such as a K, L, or M electron, it leaves the atom ionized. The original electron will recede from the collision with energy Eo - ΔE, where ΔE is the energy given to the orbital electrons (Figure 1.2). A part of ΔE is spent in overcoming the binding energy of the electron and the rest is carried by the ejected electron. When a vacancy is created in an orbit, an outer orbital electron will fall down to fill that vacancy. In doing so, the energy is radiated in the form of electromagnetic radiation. This

is called characteristic radiation.

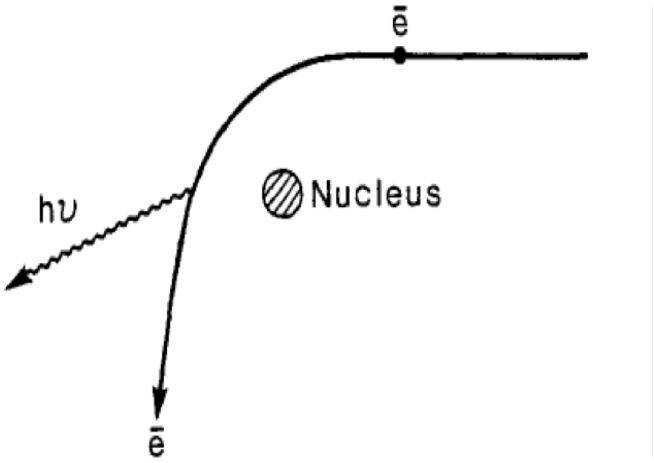

Figure 1.1: Illustration of bremsstrahlung X-ray production

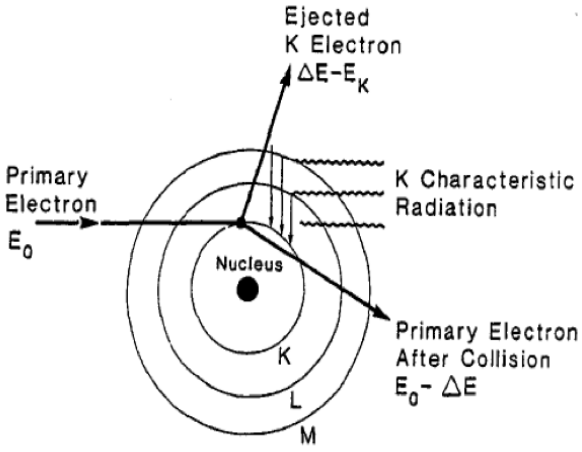

Figure 1.2: Illustration of characteristic X-ray production

1.2 Use of High energy X-rays in Medicine

High energy X-rays, using their ionization capacities are used to either kill or inhibit the growth of cancer cells by damaging its DNA. Linear Accelerator (LINAC) is usually used to emit high energetic X-rays in the external beam radiation therapy [1]. LINAC uses high frequency electromagnetic waves to accelerate electrons to high energies and when these electrons collide with a target, Mega Voltage (MV) X-rays are produced. The X-rays are then modulated in

such a way as to conform to the shape of the tumor before delivering to the tumor site. LINAC delivers maximum radiation exposure to the tumor while ensuring minimum radiation on the surrounding normal tissues. This is achieved by dynamically modulating the intensity of each x-ray beam's radiation dose using Multi-Leaf Collimator (MLC), and this type of treatment delivery is called Intensity Modulated Radiation Therapy (IMRT) [2]. IMRT conforms the radiation dose more precisely to the three-dimensional shape of the tumor by varying the intensity of the radiation beam in many small volumes. Volumetric Modulated Arc Therapy (VMAT) is a new, highly advanced rotational type of IMRT technique based on the concept of Otto [3]. In VMAT, the treatment plans are produced by the modulation of gantry speed, dose rate and the position of the MLC. It has the ability to produce complex dose distribution in a single rotation of gantry and produces highly conformal dose distribution in a shorter time than that of the IMRT. We have used the LINAC made by Varian Medical Systems, Palo Alto, named Clinac-iX which was installed and commissioned at Baby Memorial Hospital, Calicut in 2011 for the study (Figure 1.3). This LINAC is capable of providing multiple electron energies of 4, 6, 9, 12, and 15 MeV and X-ray photon beam energies of 6 MV and 15 MV.

1.3 Components of Clinac-iX

1.3.1 Modulator cabinet, console control and gantry stand

The modulator converts the incoming alternating current into pulses of direct current and these high-voltage pulses are fed to the electron gun and to the microwave power source (klystron). Console control is used to give commands to the LINAC. The console control is located outside the shielded treatment room and all the operations of the LINAC are initiated, monitored and controlled from there. Driver stand or gantry stand is a stand to contain the apparatus that drives

Figure 1.3: Diagram of a Varian Clinac iX

the linear accelerator. It provides the support to the gantry that rotates around the patient and to which the LINAC is mounted. When the beam is initiated, the high voltage pulses from the modulator are sent to a microwave-producing tube called a klystron and also to the electron gun which is positioned at the starting of the accelerating structure in the gantry.

1.3.2 Klystron

The klystron amplifies the signal from the modulator. It is driven by a low-power microwave oscillator. The electrons produced by the cathode are accelerated by a negative pulse of voltage into the first cavity, called the buncher cavity. The microwaves set up an alternating electric field across the cavity due to which the velocity modulation of the electrons takes place. Some electrons are speeded

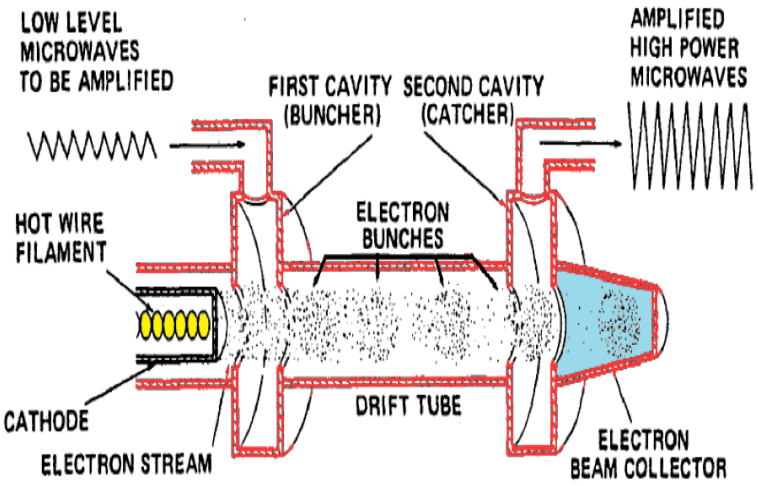

Figure 1.4: Schematic diagram of a klystron amplifier

up while others are slowed down and some remain unaffected. This results in bunching of electrons as the velocity modulated beam passes through a field-free space in the drift tube. When electron bunches reach the catcher cavity (Figure 1.4), they induce charges on the ends of the cavity and thereby generating a retarding electric field. Due to this, the electrons suffer deceleration, and its kinetic energy gets converted into high power micro waves. The amplified microwave signal from the klystron travels to the circulator first and then to the accelerating system via a waveguide. The circulator acts as a one-way gate so that the microwave power may go towards the accelerator but not be reflected back towards the klystron. A cooling water system incorporated in the gantry cools the entire system.

1.3.3 Electron gun and accelerator structure

The electron gun produces electrons by heating the tungsten filament inside the cathode. The number of electrons ejected is controlled by adjusting the temperature of the filament. The electrons ejected from the gun are coupled with the microwave pulses arriving from the waveguide and travel down the accelerator tube by interacting with the electromagnetic field of the microwaves. Intense electric fields are created inside the tube by resonant cavities positioned

at each side of the wave guide which accelerates the electrons and also helps to focus the beam. The vacuum inside the tube ensure that the electron beam is not obstructed by other particles. There are two quadra pole magnets to control the path of the negatively charged electron beam called steering coils. An additional coil called the focusing coil helps to redefine the electron beam so that its diameter becomes same as that of the pin head when it hits the target. At the distal end of the waveguide, the electrons then pass through a bending magnet assembly where they are directed towards the treatment head.

1.3.4 Treatment Head and beam collimation

The treatment head provides the necessary shielding against radiation leakage in accordance with radiation protection guidelines. The high energy electrons emerging from the exit window of the accelerator structure, in the form of a pencil beam of about 3 mm in diameter, falls on the Tungsten target placed in the path of the beam produces bremsstrahlung X-rays.

The treatment X-ray is first collimated by a fixed primary collimator located immediately after the X-ray target. The primary collimator minimizes leakage and absorbs scattered X-rays in the lateral direction. It defines the maximum size of the resulting radiation beam. The electrons hitting the target are in the MeV range and as a result the X-rays produced from the target are forward peaked. To obtain a more uniform intensity, a flattening filter is inserted after the primary collimator as shown in Figure 1.5. In the electron, mode the filter is moved out of the way and instead of striking the target, it is made to strike an electron scattering foil to spread the beam as well as to get uniform electron fluence across the treatment field as shown in Figure 1.5B. The scattering foil consists of a thin metallic foil, usually of lead. The thickness of the foil is such that most of the electrons are scattered instead of suffering bremsstrahlung.

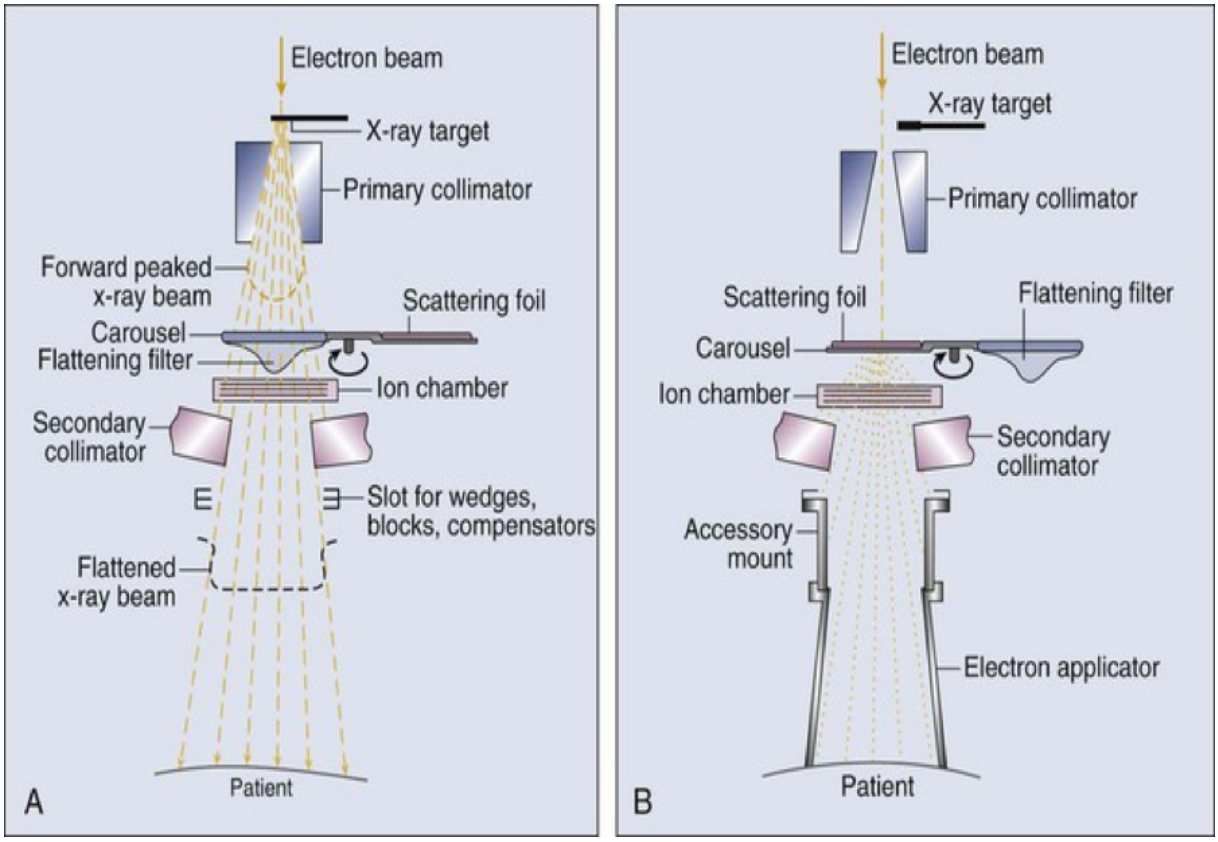

Figure 1.5: Components of treatment head A: X-ray therapy mode. B: Electron therapy mode.

1.3.5 Beam Monitoring and Multileaf collimators

The flattened X-ray beams or the electron beams is then made to fall on the dose monitoring chambers which monitors the dose rate, integrated dose, and field symmetry. The dose delivered to the patient is measured and controlled simultaneously in two independent ionization chambers. After passing through the ion chambers, the beam is further collimated by a continuously movable x-ray collimator, called jaws. This secondary collimator consists of two pairs of lead or tungsten blocks (jaws) which provide a rectangular opening from 0×0 to the maximum field size (40×40 cm) projected at a standard distance such as 100 cm from the X-ray source (focal spot on the target). The collimator blocks are constrained to move so that the block edge is always along a radial line passing through the target.

The IMRT/VMAT treatment and other conformal radiation therapy tech-

niques, a collimator system is employed, is called the multileaf collimators (MLC) (Figure 1.6). A multi-leaf collimator consist of a large number of leaves that can be driven automatically, independent of each other, to generate a field of any shape. The MLC system in linac contains 120 leaves (60 opposing pairs), where the bottom and top 10 pairs are 1cm wide and the middle 40 pairs are 0.5 cm wide projected at the isocenter. The leaves are made of Tungsten alloy, are 6 cm thick (in the vertical direction), and have rounded leaf ends.

Figure 1.6: Diagram of a Multileaf collimators attached to Clinac iX

1.3.6 Treatment couch/Patient support assembly

Patient support assembly is mainly the couch on which the patient to be irradiated lies down (Figure 1.7). It has the control panel with which gantry rotation and couch movement are done. The treatment couch has four degrees of freedom, including the three translational motions in the x, y, and z directions and

rotation about the vertical axis which passes through the point of intersection of the collimator axis and the axis of rotation of the gantry, known as the isocenter.

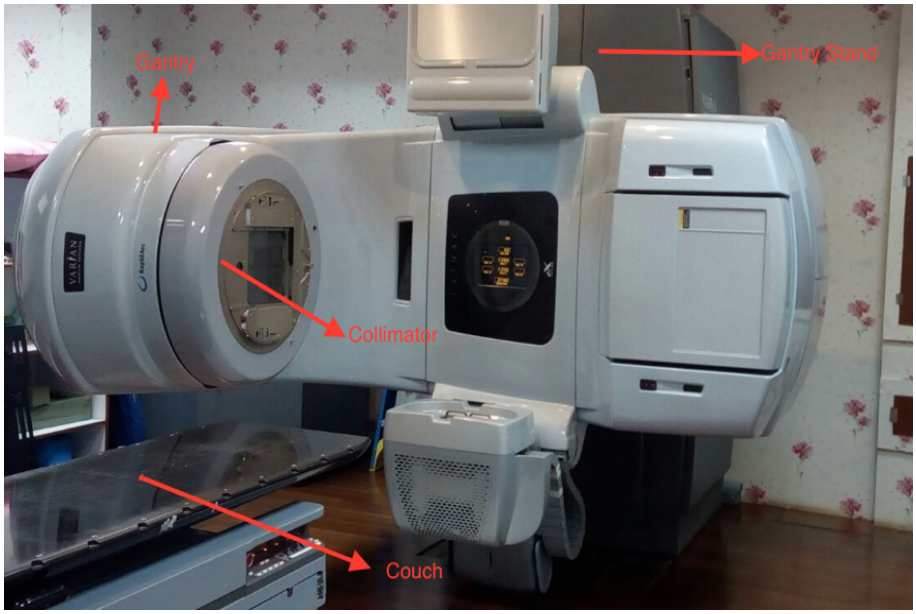

Figure 1.7: Clinac-iX with Gantry, Gantry stand, couch and collimator

1.4 Thesis outline

The treatment planning is done based on the assumption that patient anatomy is static over the course of treatment. But during treatment delivery, patient repositioning and motion of internal organs give rise to uncertainties. In addition, MLC positional errors or small calibration errors in the angular settings of the collimator, couch or gantry may create difference in dose. In combination, the patient set up variations and the machine delivery errors produce a delivered dose different from that of the planned dose. These effects are especially significant in VMAT techniques, where there is a steep dose gradient between the tumor and the Organ At Risk (OAR).

In the present work, we have studied the impact of dose delivery errors in VMAT treatment plans and its methods of quality assurance tests to ensure the correct dose delivery during radiotherapy patient treatment. We have concentrated on the effects on VMAT plans due to couch, collimator angular settings

variation, systematic and random couch translation errors which lead us to suggest a new method to predict their impacts before dose delivery. We have also studied the feasibility of direct dose calculation on Cone Beam Computed Tomography (CBCT) to predict the dose delivery errors due to anatomical changes in the patients due to weight loss, tumour shrinkage and soft tissue changes during VMAT treatment. The quality of overall treatment of VMAT was assessed by array of ionisation chambers and amorphous-silicon photodiodes.

The thesis is divided into five chapter. Chapter-1 briefly describes the production of high energy x-rays and their uses in medicine. An overview of the thesis highlighting the need for carrying out this work is also included in this chapter. A brief review of literature related to work is referred in every chapter. In chapter-2, the variations in the Dose Volume Histogram (DVH) and radio biological parameters due to deviations in the collimator and couch angular settings have been investigated in different types of VMAT planning situations. The variation on radiobiological parameters such as Tumour Control Probability (TCP) and Equivalent Uniform Dose (EUD) for the Planning Target Volumes (PTVs) and Normal Tissue Complications (NTCP) values for the OARs are evaluated. EUD was calculated using the Niemierko phenomenological model [4] according to which, if the biologically equivalent dose is given uniformly, it will lead to the same biological effect as the actual non uniform dose distribution. The NTCP values were calculated using the Lyman-Kutcher-Burman (LKB) model [5].

To study the dose delivery errors due to deviations in the collimator and couch angular settings in DVH and radio biological parameters of VMAT technology based stereotactic radio surgery (SRS)/ stereotactic body radiation therapy (SBRT) treatment, we have created three hypothetical PTV based planning situations and also used 30 clinical plans, which included prostate, head and neck (HN) and brain cases. Couch and collimator angular errors of 1^0, 2^0 and 3^0 were introduced in these plans and the variations were studied and explained in chapter-2.

In chapter-3, we have extensively studied the effect of systematic couch trans-

lational errors in Right Left (R-L), Superior Inferior (S-I) and Anterior Posterior (A-P) directions in VMAT plans. We have also developed a simple method to predict these effects on a daily basis using curve fitting method, which can be described as follows: Let $D_j(x_0, y_0, z_0)$ be the dose received by V_j^{th} volume of a structure in the DVH of the base plan, planned with an isocenter (IC) co-ordinate (x_0, y_0, z_0). When there is a translational couch shift of 'i' on either side of the IC position (x_{0+i} in the right or positive x direction and x_{0-i}in the left or negative x direction), the dose received by V_j^{th} volume due to translational couch shift now becomes $D_j(x_{0+i}, y_0, z_0)$ and $D_j(x_{0-i}, y_0, z_0)$, provided there are no shifts in the y and z axis. Thus, the variations in $D_j(x_0, y_0, z_0)$ along the x direction can be represented by the fitted function f(x, v_j). Similarly variations along the y and z axis can be represented by functions f(y, v_j) and f(z, v_j) respectively. For each point on V_j, corresponding functions can be calculated and can be used to predict the effect of daily random couch shifts on DVH by the mathematical modeling of the base plan DVH without using any further dose computation on Computed Tomography (CT). To demonstrate this, we have selected 10 prostate patients treated with VMAT technology. Systematic couch shifts were introduced in the clinically accepted base plans with an increment of 1 mm and up to 5 mm from the IC in both directions on each of the three axis, x (R-L), y (S-I) and z (A-P). The DVHs of the base plan and the error plans were imported into MATLAB software (R2013a, The MathWorks, Natick, MA) and in-house MATLAB code was generated to find the best curve fitted functions f(x, v_j), f(y, v_j) and f(z, v_j) for each points on the DVH and thereby generating the predicted DVH for PTV and OARs. It is then used to find the daily radio biological parameters, EUD, TCP and NTCP. EUD and NTCP were calculated using the Niemierko model [4] and LKB model [5] respectively. Finally, the MATLAB predicted and the treatment planning system (TPS) calculated DVHs were compared to validate our method and percentage variation between the two also was evaluated. All this methods and results are explained in chapter-3.

In the new era of radiotherapy, the kilo voltage CBCT has become a potential

tool for evaluating the deviations in the positioning set up and the changes in the organ dimensions of the patient during the course of treatment. It helps to assess the anatomical changes in the patients due to weight loss, tumour shrinkage and soft tissue changes. The changes in anatomy and organ motion can lead to variations in the dose distributions calculated based on planning the CT. These changes may end up with a daily dose which does not match with the prescribed dose. Therefore, we have also studied the feasibility of direct dose computation on CBCT and predict the dose variation due to the anatomical changes on daily basis.

In chapter 4, we have studied the feasibility of using the CBCT for VMAT planning and finding daily dose variation. The Hounsfield Unit (HU) values for the CT and CBCT images for the comparison between CT and CBCT images using a Catphan 504 phantom (The Phantom Laboratory, Salem, NY) is also calculated. The HU values in this case is defined by

$$HU = (\frac{\mu_{materail} - \mu_{water}}{\mu_{water}}) \times 1000$$

where $\mu_{material}$ and μ_{water} are the attenuation coefficients of the material and water respectively. The Catphan contains seven different materials which are: air (0 gm/cm^3), polymethylpentene (PMP) (0.83 gm/cm^3), low density polyethylene (LDPE) (0.92 gm/cm^3), Polystyrene (1.05 gm/cm^3), Acrylic (1.18 gm/cm^3), Delrin (1.41 gm/cm^3) and Teflon (2.16 gm/cm^3). The HU values for the CT and CBCT images of the Catphan were analysed at different areas of interest defined on the seven materials. Besides that, we have compared the dose calculation accuracy of the CBCT images of different treatment sites based on the analysis and also proposed a method for CBCT dose calculation in VMAT plans which can predict the daily dose variation due to anatomical changes such as weight loss, tumour shrinkage and soft tissue changes in patients.

In IMRT, MLC is the only varying parameter. However the level of complexity in VMAT is increased owing to the gantry speed and the dose rate change

during treatment delivery. The real-time correlation between these parameters is inevitable during VMAT delivery because any such variations generates a potential error [6]. Considerable differences also exist between the optimization processes of VMAT and IMRT, which complicates VMAT plans. These factors necessitate stringent quality assurance (QA) to be performed before treatment delivery. Therefore, we have finally analysed the methods of QA tests in VMAT with different systems. For the pupose, an ionization chamber based array called MatriXX, which is an array consisting of 1020 single air-vented plane-parallel cylindric ionization chambers (0.55 cm height, 0.4 cm diameter, centre-to-centre distance 0.76 cm) arranged in a 32 $\times$ 32 matrix. The QA test analysis is also done using amorphous-silicon (aSi 1000) photodiodes called EPID, which are arranged in a 40 $\times$ 30 cm active detector area (1024 $\times$ 768 pixels, 0.039 $\times$ 0.034 cm pixel pitch). We have analysed the dose distribution by a method called gamma index (γ), which is the most widely accepted method for the evaluation of 2D dose distributions. The measured and calculated 2D dose distributions in both systems were compared using this method, as recommended by Low et al [7].

In chapter 5, the study of impacts of different evaluation criteria on gamma pass rates in VMAT using Matrixx and EPID is discribed. The results obtained for the two systems are comparable in terms of the measured and calculated doses, which confirmed the suitability of the equipments used and the validity of the plans. Our investigation of differently shaped hypothetical PTVs and different clinical situations has provided us with an improved perspective of the plan verification process in different complex situations. The study results emphasize that the threshold settings significantly affect the gamma pass rates, especially in the lower gamma criteria. All the results obtained and methods adopted about this evolution is described in chapter-5.

References

[1] David I, Thwaites et al. (2006). Back to the future: the history and development of the clinical linear accelerator Phys. Med. Biol. 51 343-362.

[2] Fogliata A, Clivio A, Nicolini G, Vanetti E & Cozzi L. (2008). Intensity modulation with photons for benign intracranial tumours: a planning comparison of volumetric single arc, helical arc and fixed gantry techniques. Radiother Oncol 89, 254-62.

[3] Otto K. (2008). Volumetric modulated arc therapy: IMRT in a single gantry arc. Med Phys 35, 310-7.

[4] Gay HA & Niemierko A. (2007). A free program for calculating EUD-based NTCP and TCP in external beam radiotherapy. Phys Med. 23,115-25.

[5] Semenenko VA & Li XA. (2008). Lyman-Kutcher-Burman NTCP model parameters for radiation pneumonitis and xerostomia based on combined analysis of published clinical data. Phys Med Biol. 53,737-55.

[6] Bedford J L & Warrington A P. (2009). Commissioning of volumetric modulated arc therapy (VMAT) Int. J. Radiat. Oncol. Biol. Phys; 73:537-45.

[7] Low DA, Harms WB & Mutic S, Purdy JA. (1998). A technique for the quantitative evaluation of dose distributions. Med Phys.; 25(5):656-61.

Chapter 2

Analysis of influence of errors in angular settings of couch and collimator

2.1 Introduction

The field of radiation delivery has undergone many innovative developments over the past few years. The volumetric modulated arc therapy (VMAT) is one of the modern techniques which have become an indispensable part of the radiotherapy department. The VMAT is a highly advanced rotational intensity modulated radiation therapy (IMRT) technique based on the concept of Otto [1]. It has the ability to produce complex dose distribution in a single rotation of gantry. It has become quite popular because of its ability to produce highly conformal dose distribution in a shorter time than that of the IMRT. VMAT plans are now being used for almost all tumor sites [2-5]. In VMAT, the plans are produced by the modulation of gantry speed, dose rate and the position of the multileaf collimator (MLC). A real time correlation between these parameters plays a key role in the dose delivery. Any error in these parameters raises potential changes in the delivered dose from that of the planned one. RapidArc is the commercial

implementation of VMAT on the Varian linear accelerator (LINAC). RapidArc uses progressive resolution optimizer (PRO) algorithm where the optimisation starts with a few number of control points and as the process progress, number of the points get increased. The final single arc plan, with gantry control points, is sampled approximately every 2^0. A continuous and real time interpolation between the control points, used by the treatment planning system (TPS) for the optimization process, is also required during the delivery [6].

In both VMAT and IMRT, there always exist a sharp dose gradient between the planning target volume (PTV) and the organ at risk (OAR) than that found in conventional three dimension conformal radiotherapy techniques. Any positional error in the MLC or small calibration errors in the angular settings of the collimator, couch or gantry can create an under dose on the tumor or an over dose on the critical structure [7-13]. This is especially important when the complex nature of the VMAT is considered. More investigation is needed to be done in these areas to study how the delivery errors affect the dose volume histogram (DVH) parameters and how these errors significantly change the tumor control probability (TCP) and the normal tissue complication probability (NTCP).

The MLC plays a vital role in the treatment delivery in dynamic treatment techniques like VMAT and IMRT. Several investigations had been done to study the effects of systematic and random positional errors of the MLC on VMAT and IMRT plans. IMRT is more prone to the delivery errors than the VMAT plans [14]. Systematic errors in the MLC leaf bank position produce a 2% to 4% higher dose difference in sliding window (SW) IMRT than in VMAT plans [14]. The gantry error also has a greater effect on the SW-IMRT compared to the latter [14]. G. Mu et al [7] reported that random MLC positional error up to 2 mm have only a negligible effect on the dosimetric parameters in the head and neck (HN) IMRT plans, while systematic MLC error of 1mm produces a significant impact. It created a 4% and an 8% variation in the dose received by 95% of PTV volume in simple and complex IMRT plans respectively [7]. Another study reported that a 1.5 mm random error in MLC or back up jaws in IMRT plan delivery can

produce a 5% dose difference in the plan, while a systematic error of ±0.5 mm is enough to produce a significant dose variation [8]. Rangel and Dunscombe [9] also reported that a 2 mm random error in dynamic MLC for prostate and HN IMRT plans led to negligible dose difference; but in order to limit the target dose change within 2%, the systematic error needed to be less than 0.3 mm. Similar studies have been done for VMAT plans also. M. Oliver et al [11] have investigated the effect of MLC position errors on the VMAT plans in HN cases. They studied the systematic and random errors in the MLC and their impact on the equivalent uniform dose (EUD) and reported that the correlation between all MLC error types and the EUD was linear. The EUD dose sensitivities with random, systematic shift, systematic close and systematic open MLC errors for the PTV were -0.2, -0.9, -2.8 and 1.9 Gy/mm respectively [11].

Several collimator and couch angular settings are used in both IMRT and VMAT plans, depending upon the complexity of the plan. The VMAT planning technique is now being used for the Stereotactic radiosurgery (SRS) and Stereotactic body radiation therapy (SBRT), treatments [15-17]. Here, the non coplanar beam arrangement is achieved by varying the couch angles for producing a highly conformal dose distribution and for better organ sparing. Moreover, to reduce the impact of tongue and groove effect during the arc rotation in VMAT plans, the collimator rotation need to be set at values different from zero. Several investigations have been done on the effect of MLC, gantry and MU errors on the VMAT plans [11, 12, and 14]. But the effect of collimator and couch setting errors still need to be investigated in depth, especially in routine VMAT plans and in SRS/SBRT treatment based VMAT plans. The aim of our study is to evaluate the effect of couch and collimator errors and their impact on DVH and radiobiological parameters in the VMAT plans used for the SRS/SBRT treatment and in different clinical situations namely, prostate, brain and HN.

2.2 Materials and Methods

2.2.1 SRS and SBRT-VMAT planning in hypothetical PTVs

The influence of collimator and couch angular errors on the VMAT technology based SRS/SBRT treatment is assessed on different hypothetical PTVs based planning. We have generated three hypothetical PTVs with different shape and size on the brain and thoracic patient CT images. The first hypothetical PTV was generated to mimic the brain metastases (PTV_{BM}) (Figure 2.1 a), which consist of circular shaped PTVs with 1 cm, 2 cm, and 3 cm diameter to represent small, medium and large brain metastases lesions. Metastatic lesions were delineated on the same axial plane and at a minimum distance of 3.0 cm from the OARs. The second PTV was generated with a single brain lesion (PTV_{SB}), in an oval shape, with a volume of 12 cm^3 and positioned in close proximity to the OARs, which is a distance of 0.5 cm from the LT optic nerve and chiasm (Figure 2.1 b). To mimic the spinal lesion a third PTV, which is a single spine PTV (PTV_{SS}) with volume of 25 cm^3, was generated in close proximity to the cord at a distance of 0.5 cm from the spinal cord and almost wrapping it (Figure 2.2 a). In addition, to ensure a better dose conformity and to restrict the dose to the normal tissues, three ring structures with three types of avoidance structures (AVSs) were also delineated, namely, S_1 (green), S_2 (yellow), and S_3 (cyan), which formed margins of 1 cm, 2 cm, and 3 cm, respectively, around the PTVs (Figure 2.1). Further, critical structures such as brainstem, optic chiasm, right (RT) and left (LT) optic nerve, and spinal cord etc were also contoured accordingly in the three hypothetical PTVs.

The VMAT plans were generated using the Eclipse TPS (Version 10, Varian Medical Systems, Palo Alto, CA) modeled with Clinac ix (Varian Medical Systems) LINAC equipped with a Millennium 120 MLC. Two complementary full arcs (with gantry angle from 179^0 to 181^0 and collimator rotation of 30^0 and 330^0) were used for all the three PTVs. PTV_{BM}, PTV_{SB}, PTV_{SS} were planned

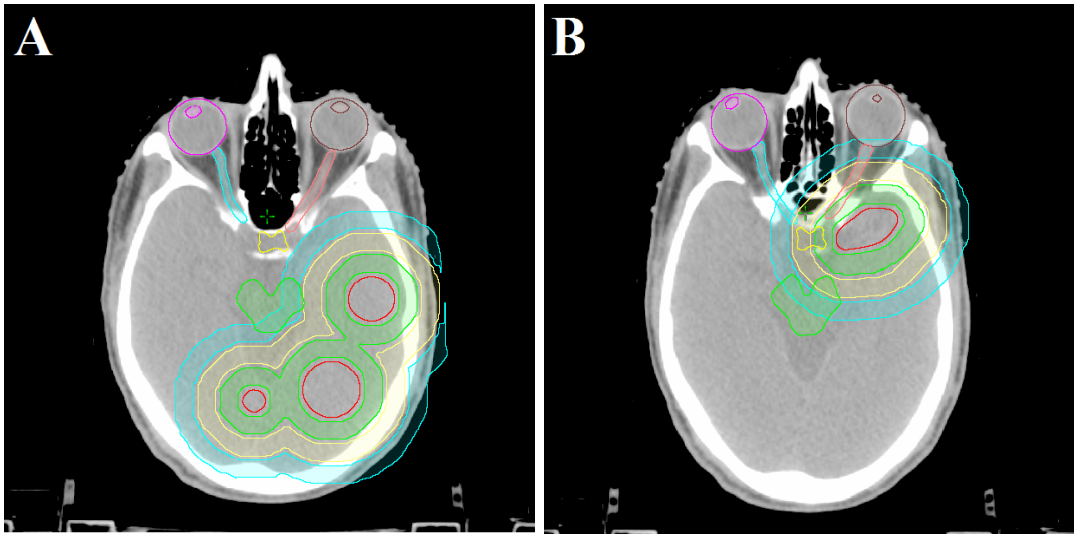

Figure 2.1: Hypothetical PTVs a) circular shaped brain metastases PTV (PTV_{BM}) with 1 cm, 2 cm, and 3 cm diameter b) oval shaped single brain PTV (PTV_{SB}) with three avoidance structures (S_1 (green), S_2 (yellow), and S_3 (cyan), forming margins of 1 cm, 2 cm, and 3 cm, respectively, around the PTVs.

in such a way that 100% of the PTV received a minimal dose of 20 Gy, 14 Gy and 16 Gy respectively in single fractions. The maximum doses to the spinal cord, chiasm, optic nerve and brain stem were limited to 10 Gy. Similarly, the maximum dose to 1% of normal brain was also restricted to 10 Gy and the dose to other OARs were kept as low as achievable. All plans, generated using a 6 MV x-ray beam, were optimized repeatedly until a better target coverage and a dose as low as the minimum goal dose at the OARs was achieved. The final dose calculation was done using Anisotropic Analytical Algorithm (AAA) with grid size of $0.25 \times 0.25 \times 0.25\ cm^3$.

To evaluate the affect of the collimator and couch angular setting variations on these hypothetical PTV based VMAT plans, three systematic couch and collimator errors each were introduced in the original optimized plan and six erroneous plans were generated by recalculating the original plan with same grid size and using AAA. The angular settings of the collimator were varied by 1^0, 2^0 and 3^0 to generate errors C-1, C-2 and C-3 and three collimator erroneous plans were created. Similarly, the couch angular settings were also varied by 1^0, 2^0 and 3^0 to generate errors CH-1, CH-2 and CH-3 to create three couch erroneous plans. To

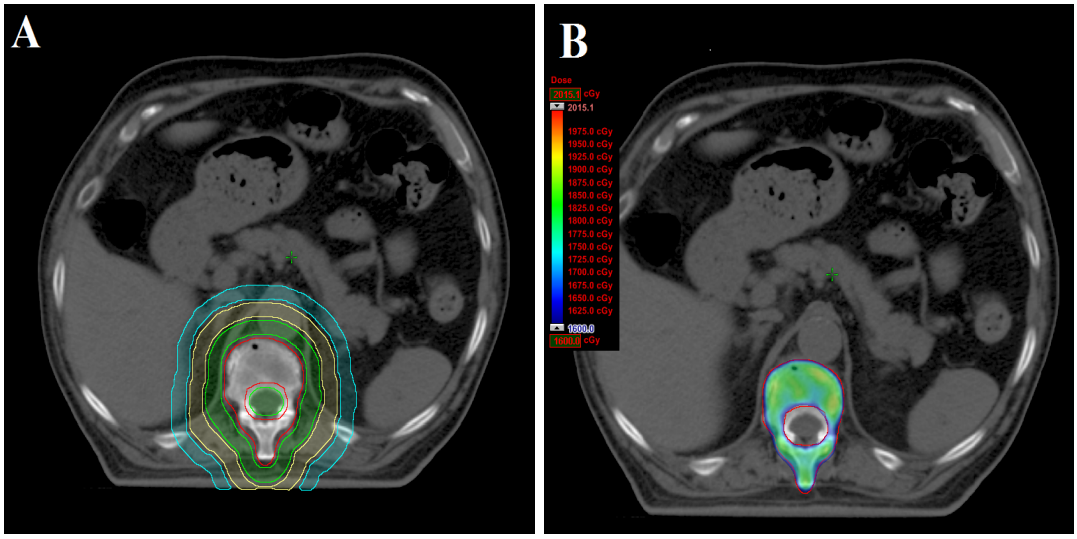

Figure 2.2: a) Hypothetical spine PTV (PTV_{SS}) with three avoidance structures (S_1 (green), S_2 (yellow), and S_3 (cyan), forming margins of 1 cm, 2 cm, and 3 cm, respectively, around the PTV. b) VMAT dose distributions for 16 Gy in PTV_{SS}

analyze the effect of different errors on the original plan, the corresponding relative percentage difference (ΔD) of the different DVH parameters were assessed. Analysis of the DVH parameters of the PTV and OAR is described in the section Analysis of the dose volume histogram and radio biological parameters. Besides, the Paddick conformity index (P_{CI}) was also assessed for all the plans [18]. This was calculated using the equation,

$$P_{CI} = \frac{(TV_{PV})^2}{TV \times PV}$$

Where TV is the target volume, TV_{PV} is the target volume within the prescription volume and PV is the prescription volume.

2.2.2 VMAT planning in patients

In order to evaluate the effect of collimator and couch errors on the routine VMAT plans, we selected 30 VMAT plans from the patients treated in our clinic. This include 10 prostate, 10 HN and 10 brain cases. CT images of the patients were acquired using a GE Light-speed CT simulator (GE Medical

Systems, Milwaukee, WI) and imported to the Eclipse TPS (Version 10, Varian Medical Systems, Palo Alto, CA). OARs, gross tumour volumes (GTV), clinical target volumes (CTV) and PTVs were contoured by a radiation oncologist on each slice of the CT images.

CT simulations of the prostate cases were done in supine position with a full bladder and empty rectum. As per the institutional protocol, the prostate plan was generated with a dose of 70 Gy in 28 fractions. The CTV 70 Gy was created by taking the whole prostate and seminal vesicles and corresponding PTV 70 Gy generated by giving an expansion of 8 mm all around, except posterior where the margin was limited to 0.4 mm, to restrict dose to the anterior rectal wall. Besides that, CTV 50.4 Gy volume was delineated to include the pelvic nodes. The corresponding PTV 50.4 Gy was generated by giving a 0.5 cm expansion to this CTV. All the critical structures such as bladder, rectum, femoral head and bowel were delineated. The volume of the bladder receiving doses more than 40 Gy (V_{40Gy}) and 70 Gy (V_{70Gy}) was kept less than 60% and 30% respectively while for the rectum, these constrains were less than 45% and 20% respectively in treatment plans. The HN cases were treated with 70 Gy in 33 fractions. Here three PTVs were delineated; 70 Gy is prescribed for the primary tumor and gross nodal diseases, 60 Gy for the high risk and 54 Gy for the low risk volumes. Here, the PTVs were generated by setting a margin of 5 mm around the corresponding CTVs. Moreover, all the critical organs such as the spinal cord, brain stem, parotid, mandible etc were delineated. In the brain tumor cases, the PTV was generated with a margin of 0.5 cm around the CTV and was treated with 60 Gy in 30 fractions with all the OARs including brain stem, chiasm, optic nerve, lens etc delineated. For both HN and brain patients, the maximum dose (D_{max}) to the spinal cord, eyes and lens were limited to less than 45 Gy, 40 Gy and 10 Gy respectively while for the Brain stem, chiasm, and optic nerve this dose was limited to less than 54 Gy. Further, in the HN cases, the mean dose (D_{mean}) to the parotid was kept less than 26 Gy.

For the clinical planning of the prostate and HN cases, two complementary

double full arcs, similar to those used in the hypothetical PTVs, are used. The brain cases used only a single full arc with a collimator rotation of 30^0. All the plans were generated with coplanar beam arrangement and zero couch angles. The plans were optimized until 95% of the prescribed dose was received by 95% of the volume of the PTV and all the OARs obtained the goal doses. All VMAT plans were planned with 6MV x-ray beam and the dose calculation was done using AAA with grid size of $0.25 \times 0.25 \times 0.25\ cm^3$. All the treated plans were delivered using Varian Clinac ix LINAC equipped with a Millennium 120 MLC. To evaluate the effect of collimator and couch angle variations, six types of systematic errors C-1, C-2, C-3, CH-1, CH-2 and CH-3 as explained in section SRS and SBRT-VMAT planning in hypothetical PTVs were introduced. The variation in the DVH and radio biological parameters of the six error plans from the treated plans were evaluated using the method described in the section Analysis of the dose volume histogram and radio biological parameters.

2.2.3 Analysis of the dose volume histogram and radio biological parameters

To quantify the effect of the collimator and couch errors on the plan quality, different DVH and radio biological parameters were analysed. Three different regions, the shoulder region ($D_{98\%}$, $D_{95\%}$), the fall of region ($D_{50\%}$) and the tail region ($D_{5\%}$, $D_{2\%}$) along with $V_{95\%}$ in the DVH of the PTV were analyzed both in the original and erroneous plans. In order to simplify the analysis process only PTVs receiving the highest dose among the various PTVs in each site were assessed. In prostate cases, the DVH indices $D_{2\%}$, $D_{5\%}$, $D_{15\%}$, $D_{25\%}$, $D_{35\%}$, $D_{50\%}$, V_{70Gy}, V_{40Gy}, V_{25Gy}, D_{min}, D_{max} and D_{mean} for the bladder and rectum were analysed. In the HN and brain cases, D_{max}, D_{1cc} and $D_{0.1cc}$ were assessed for the spinal cord and brainstem. In addition, D_{max} and $D_{0.1cc}$ for the chiasm, RT and left LT optic nerve; D_{max} for the RT and LT lens; D_{mean} and V_{30Gy} for both parotids were also evaluated. The relative dose difference ΔD for each of the DVH parameters were analysed.

In order to assess the impacts of collimator and couch errors on the radio biological parameter, we analysed the TCP and EUD for the PTVs and NTCP values for the OARs. EUD was calculated using the Niemierko phenomenological model [19] which says that, if the biologically equivalent dose is given uniformly, it will lead to the same biological effect as the actual non uniform dose distribution. It is calculated using the formula,

$$EUD = \Big(\sum_{i=1}(v_i D_i^a)\Big)^{\frac{1}{a}}$$

where v_i is a parameter which represents the i^{th}sub volume receiving dose D_i in Gy and 'a' is the model parameter which is explicitly used for the tumor and normal structures. This unitless parameter is a negative number for the tumors and is positive for the normal tissues [19]. When a = 1, EUD equals to the mean dose. The TCP is calculated from the EUD as follows,

$$TCP = \frac{1}{1 + \left(\frac{TCD_{50}}{EUD}\right)^{4\gamma_{50}}}$$

where TCD_{50} is the tumor dose required to control 50% of the tumor when the tumor is homogeneously irradiated. γ_{50} is a unitless parameter that describes the slope of the dose-response curve and is specific to both normal tissues and tumors.The NTCP values were calculated using the Lyman-Kutcher-Burman (LKB) model [20] and is obtained using the following equations.

$$NTCP = \frac{1}{\sqrt{2\Pi}} \int_{-\infty}^{t} e^{\frac{-x^2}{2}} dx$$

Where

$$t = \frac{D_{eff} - TD_{50}}{mTD_{50}}$$

and

$$D_{eff} = \Big(\sum_{i=1}(v_i D_i^{\frac{1}{n}})\Big)^n$$

where TD_{50} is the dose with which if the entire organ is uniformly irradiated, would cause a 50% chance of normal tissue complication, m is the slope parameter, and n is the volume effect parameter. All the radio biological parameters were calculated using the free available RADBIOMOD Visual Basic application based software in Micro soft excel [21]. For the TCP and EUD calculation of the tumor, the value of parameters used at different tumor sites are as follows. For prostate tumor, TCD_{50} = 70.5, γ_{50} = 2.9, and a =-24 [22, 23]. TCD_{50} = 64.9 Gy, γ_{50} = 3.2, and a =-13 for HN patients [19, 24, 25] and TCD_{50} = 27.04 Gy, γ_{50} = 0.75, and a =-8 for brain tumor patients [26]. The model parameters (α/β, m, n) for the NTCP calculations are summarized in Table 2.1. Finally, the relative percentage difference (ΔEUD, ΔTCP and ΔNTCP) for the radio biological parameters were evaluated.

In order to check the statistical significance of the difference in the dosimetric and radio biological parameters in the erroneous and original plans, one-way ANOVA was conducted using the GraphPad prism (Graphpad software, San Diego, CA, USA, version 6.07) software. The differences were considered statistically significant when $p < 0.05$.

Table 2.1: LKB model parameters used for NTCP calculations

Structure	n	m	TD_{50}	α/β	Clinical end point	Ref No
Rectum	0.09	0.13	76.9	3	Grade $\geq$ 2 rectal toxicity or rectal bleeding	27
Bladder	0.5	0.11	80	3	Symptomatic bladder contracture and volume loss	27, 28
Brainstem	0.16	0.14	65	2.5	Necrosis/infarction	27, 28
Optic nerve	0.25	0.14	65	1.6	Blindness	27, 28
Optic chiasm	0.25	0.14	65	2	Blindness	20, 21
Parotids	1	0.53	31.4	3	Xerostomia	20, 21
Spinal cord	0.05	0.175	66.5	2	Myelitis/necrosis	28, 21

2.3 Results

2.3.1 SRS and SBRT-VMAT planning in hypothetical PTVs

Figure 2.2b and Figure 2.3 depict the dose distributions of the hypothetical PTV based VMAT plans. The VMAT plans produced conformal dose distribution, and the P_{CI} were 0.653, 0.613, and 0.612 for PTV_{BM}, PTV_{SB} and PTV_{SS} VMAT plans (Figure 2.4). The results showed that the introduction of collimator and couch errors did not have a considerable effect on the P_{CI}. The largest variation was seen in PTV_{BM} where the P_{CI} reduced from 0.653 in the original plan to 0.578 for the plan with a couch angle variation of 3^0, while the other two PTVs showed no significant variation.

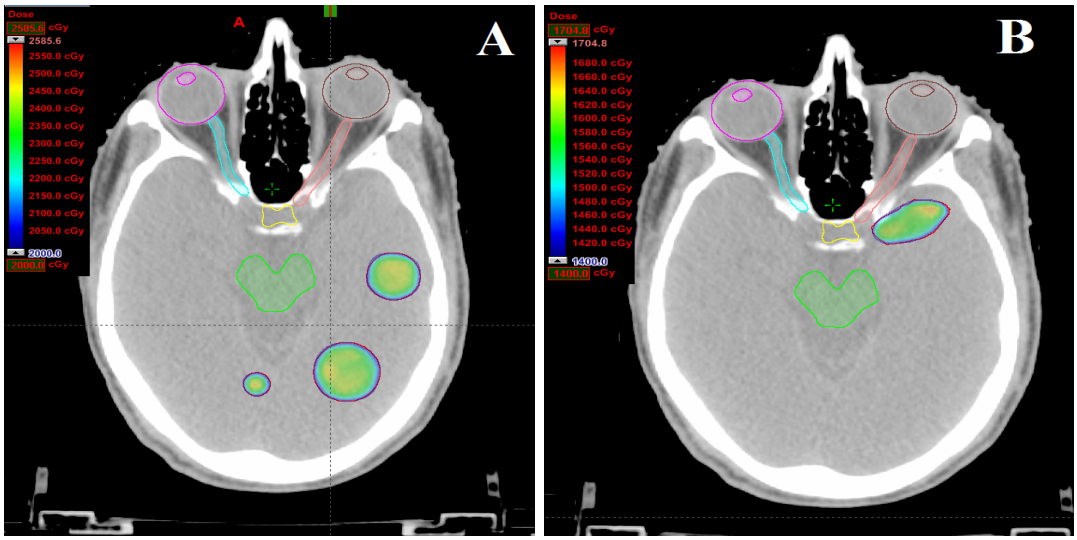

Figure 2.3: Isodose distributions for A) circular shaped brain metastases PTV (PTV_{BM}) with 1 cm, 2 cm, and 3 cm diameter and dose 20 Gy B) Single brain oval shaped PTV (PTV_{SB}) with 14 Gy

Figure 2.5 and Figure 2.6a shows the variations in the DVH parameters of the hypothetical PTV based VMAT plans. When the couch and collimator errors were introduced, the maximum variations were observed in $D_{95\%}$, $D_{98\%}$ and $V_{95\%}$. As the errors increased, there was an increase in the variations of the parameters. The variation due to collimator misplacement was observed to be larger than the

couch misplacement in these plans. The maximum variations were observed in PTV_{SS} for all types of errors. The values for $\Delta D_{95\%}$, $\Delta D_{98\%}$ and $\Delta V_{95\%}$ with C-1 error in PTV_{SS} were 2.57%, 2.62% and 2.35% respectively and these values increased to 4.9%, 6.45%, and 7.34% with C-3 error. Whereas, the variations due to couch errors were comparatively less and the maximum values for $\Delta D_{95\%}$, $\Delta D_{98\%}$ and $\Delta V_{95\%}$ were found in PTV_{SS} for CH-3, which were 4.24%, 5.52% and 6.45% respectively.

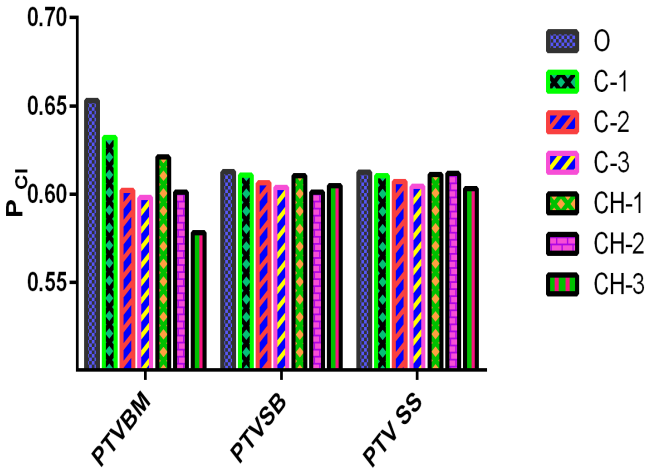

Figure 2.4: Paddick conformity index (P_{CI}) for the hypothetical PTVs in original plan (O) and when errors of 1^0, 2^0 and 3^0 were introduced in collimator (C-1, C-2 and C-3) and couch (CH-1, CH-2 and CH-3).

Figure 2.6b and Figure 2.7 shows the variations in the DVH parameters of the OARs in hypothetical spinal and brain PTV based plans respectively. Here also, the variations in the parameters were seen to be more due to the errors in collimator than the couch errors. Moreover, as we increased the degree of the errors, the variations also increased. It was also noticed that the OARs of the PTV_{SB}, which were very close to the target, showed larger variation than the distant OARs in the PTV_{BM}. In the case of chiasm, ΔD_{max} was 0.98% for PTV_{BM} in C-1 and it rose to 1.98% in C-3 whereas in PTV_{SB} these values were 1.2% and 3.4% respectively. Figure 2.6b is a scatter plot between the errors and the ΔD of OARs of the PTV_{SS} . The plot reveals that (Figure 2.6b), collimator and couch angular errors of 1^0 produces a variation of less than 1% in ΔD_{max},

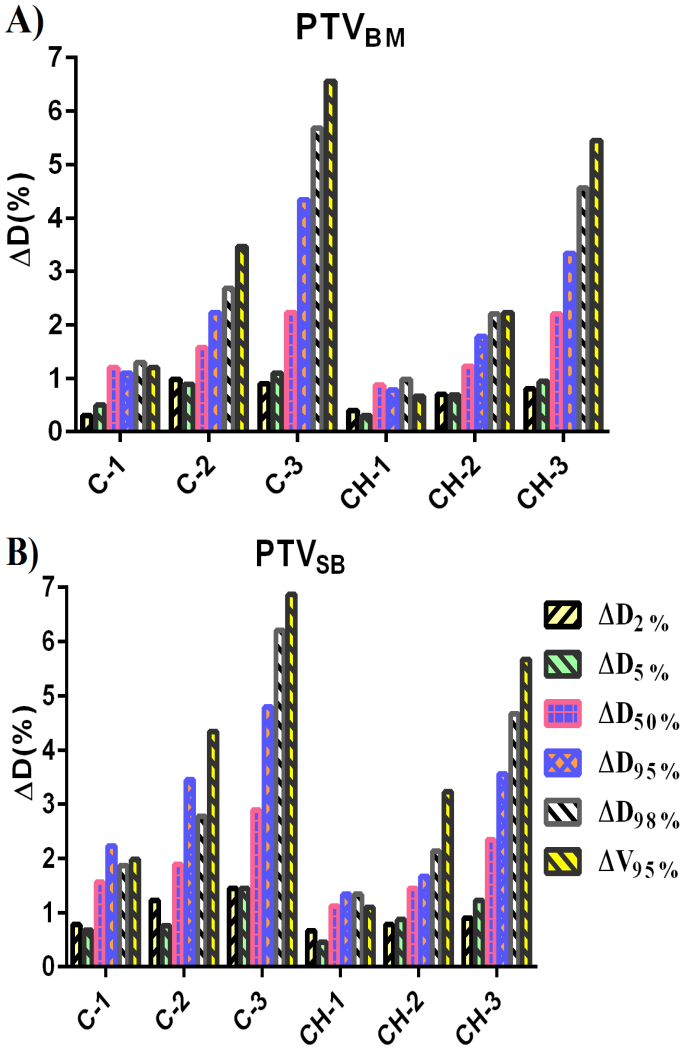

Figure 2.5: Relative percentage of variations (ΔD) in the dose volume histogram parameters of the hypothetical PTVs a) PTV_{BM} b) PTV_{SB} due to 1^0, 2^0 and 3^0 collimator (C-1, C-2 and C-3) and couch (CH-1, CH-2 and CH-3) errors.

$\Delta D_{0.1cc}$ and ΔD_{1cc} of the spinal cord. However the value of ΔD_{max} shoots to 7% due to C-3 error while the maximum variation produced by CH-3 error is 3.4% in ΔD_{max}.

2.3.2 VMAT planning in patients

Table 2.2 represents the mean and standard deviation of the variations in DVH and radiobiological parameters of the PTVs of prostate, HN and brain tumor cases. The observations were very similar to that of hypothetical PTVs. The

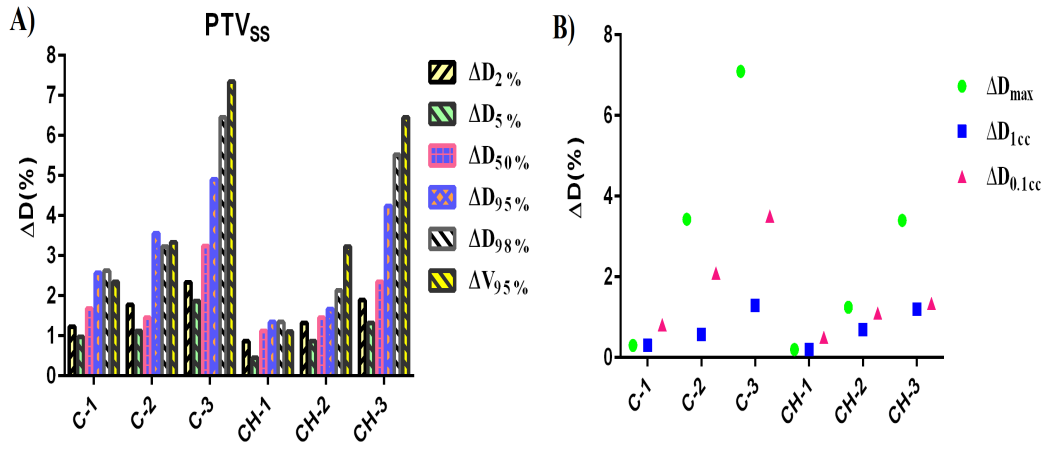

Figure 2.6: Relative percentage of variations (ΔD) in the dose volume histogram parameters of the a) hypothetical PTV_{SS} and b) spinal cord due to the 1^0, 2^0 and 3^0 collimator (C-1, C-2 and C-3) and couch (CH-1, CH-2 and CH-3) errors.

variations were more in collimator errors than couch errors and it increased with increase in the degree of errors. It is remarkable to note that the maximum variation in all the cases were seen in ΔTCP which were $3.49 \pm 2.3\%$, $3.67 \pm 1.2\%$ and $3.98 \pm 1.6\%$ respectively for prostate, HN and Brain cases with C-1 errors and rose to $10.6 \pm 4.3\%$, $11.2 \pm 5.3\%$ and $10.2 \pm 4.3\%$ correspondingly for C-3 errors. The variations in $\Delta D_{2\%}$, $\Delta D_{5\%}$ and $\Delta D_{50\%}$ were lesser compared to that in $\Delta D_{95\%}$, $\Delta D_{98\%}$, $\Delta V_{95\%}$ and ΔEUD parameters. The one-way ANOVA analysis was done to check if the values of the variations are statistically significant ($p < 0.05$). It was found that in all the cases, $\Delta D_{95\%}$, $\Delta D_{98\%}$, $\Delta V_{95\%}$, ΔEUD, ΔTCP and $\Delta D_{50\%}$ (except in the couch errors of prostate case) were statistically significant. But the p values for $\Delta D_{2\%}$ and $\Delta D_{5\%}$ (except in the collimator error of HN) were higher than 0.05, implicating that these variations are statistically insignificant.

The Tables 2.3 and 2.4 show the variation of the DVH and radio biological parameters of the bladder and rectum. It is evident from the tables that the mean variations due to C-1 errors in all the parameters, except in ΔV_{70Gy}, are less than 1%. In general the variations due to all the errors are of lesser value in bladder and rectum compared to those of the OARs in brain and HN cases. The maximum variation is seen in ΔV_{70Gy} in both OARs, which increased from

$3.0 \pm 2.3\%$ to $7.0 \pm 3.8\%$ in bladder and $1.44 \pm 2.1\%$ to $6.30 \pm 4.2\%$ in rectum. ΔNTCP in the case of bladder was not affected by any of the introduced errors but a variation is present in the case of rectum. The variations due to all the errors in both OARs gave p values greater than 0.05 and thus all the variations are statistically insignificant.

The analysis of the variations in DVH and radiobiological parameters in the OARs of the HN patients is summarized in Table 2.5. The table indicates that all the parameters are affected by the errors to a significant level. Among the various parameters, the ΔNTCP shows the maximum variation for both errors. The highest variation exhibited by the ΔNTCP is in the case of spinal cord for the collimator error. Here it varies from $2.92 \pm 2.3\%$ in C-1 error to $22.1 \pm 10\%$ in C-3. It is also noteworthy that the p values for all the parameters in the four OARs of the HN cases have a value less than 0.05 thus making all the variations statistically significant.

Table 2.6 shows the effect of couch and collimator errors on the OARs in the brain. The analysis revealed that both the errors did not have any effect on the ΔNTCP and the variations in the other parameters were also small. The maximum variations are seen in the case of RT and LT lens. In the Case of the RT lens the value of ΔD_{max} was $1.23 \pm 1.1\%$ in C-1 error and went up to $2.78 \pm 1.2\%$ in C-3 error. The values for the same parameter were $1.34 \pm 1.3\%$ and $3.34 \pm 1.9\%$ respectively for C-1 and C-3 errors in the case of LT lens. The p values for both the lenses were less than 0.1. However, none of the parameters in the critical structures of the brain were statistically significant.

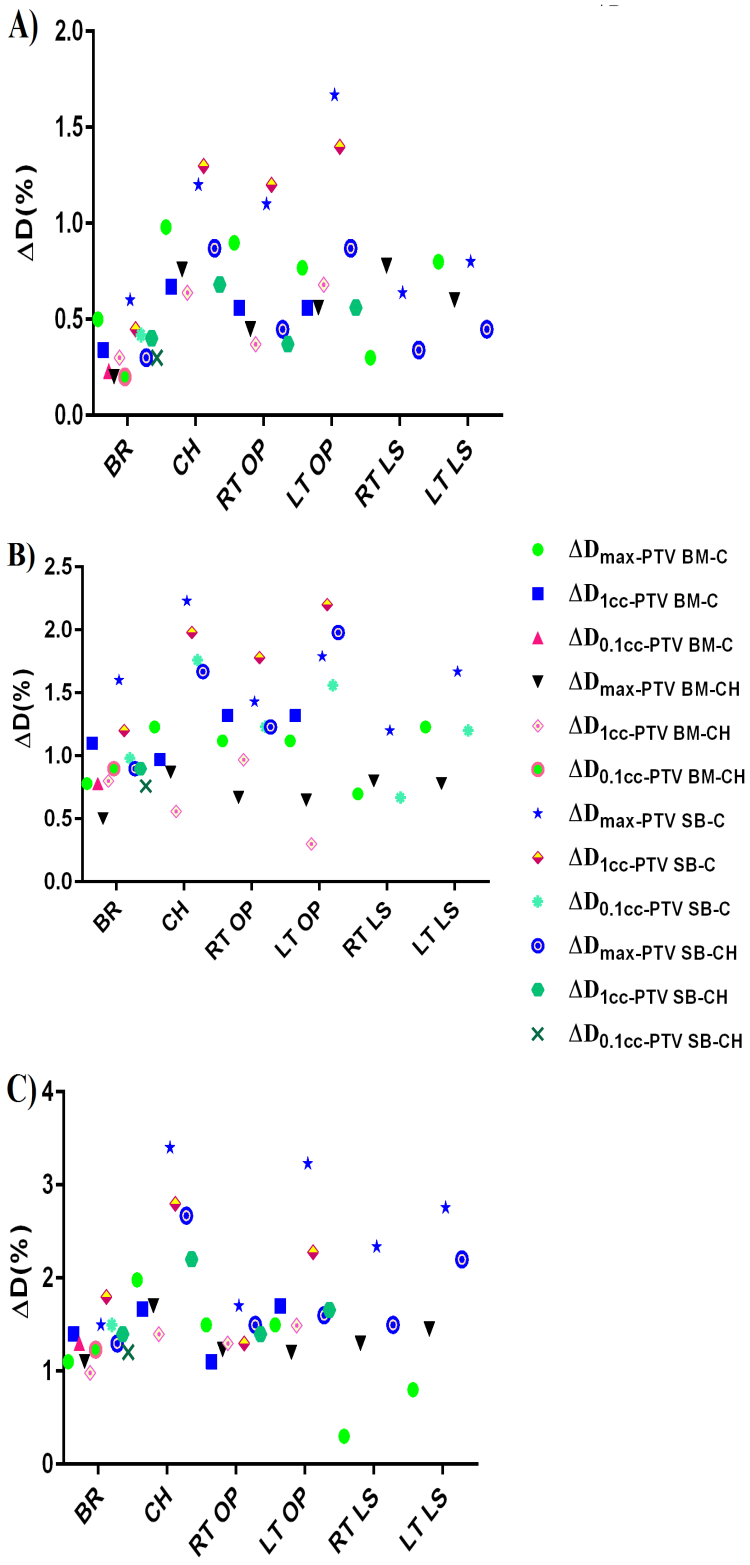

Figure 2.7: Relative percentage of variation (ΔD) in the DVH parameters (D_{max}, $D_{0.1cc}$ and D_{1cc}) of the brainstem (BR), chiasm (CH), right optic nerve (RT OP), left optic nerve (LT OP), right lens (RT LS) and left lens (LT LS) of the brain PTVs (PTV_{BM} and PTV_{SB}) when a) 1^0 anglular error in collimator (C-1) and couch (CH-1) b) 2^0 anglular error in collimator (C-2) and couch (CH-2) and c) 3^0 anglular error in collimator (C-3) and couch (CH-3) were introduced.

Table 2.2: Mean and standard deviation of the relative percentage variations in the DVH and radiobiological parameters of the PTVs in prostate, HN and brain tumor cases.

Case	DVH parameters	C-1	C-2	C-3	CH-1	CH-2	CH-3	P value collimator	P value couch
Prostate	$\Delta D_{2\%}$	$0.04 \pm 0.2\%$	$0.42 \pm 0.7\%$	$0.50 \pm 0.4\%$	$0.02 \pm 0.02\%$	$0.02 \pm 0.1\%$	$0.02 \pm 0.1\%$	0.125	0.466
	$\Delta D_{5\%}$	$0.04 \pm 0.2\%$	$0.16 \pm 0.4\%$	$0.25 \pm 0.4\%$	$0.04 \pm 0.04\%$	$0.03 \pm 0.1\%$	$0.02 \pm 0.1\%$	0.180	0.202
	$\Delta D_{50\%}$	$0.29 \pm 0.3\%$	$0.67 \pm 0.6\%$	$1.12 \pm 0.9\%$	$0.01 \pm 0.01\%$	$0.01 \pm 0.2\%$	$0.02 \pm 0.1\%$	0.039	0.357
	$\Delta D_{95\%}$	$0.63 \pm 0.3\%$	$1.98 \pm 0.8\%$	$3.85 \pm 1.4\%$	$0.19 \pm 0.12\%$	$0.80 \pm 0.5\%$	$1.72 \pm 1.1\%$	0.001	0.012
	$\Delta D_{98\%}$	$0.74 \pm 0.3\%$	$2.40 \pm 1.0\%$	$4.83 \pm 1.9\%$	$0.70 \pm 0.73\%$	$1.70 \pm 0.8\%$	$3.90 \pm 1.8\%$	0.001	0.003
	$\Delta V_{95\%}$	$1.06 \pm 0.8\%$	$3.94 \pm 2.9\%$	$8.76 \pm 5.8\%$	$0.50 \pm 0.33\%$	$1.59 \pm 0.9\%$	$2.84 \pm 1.6\%$	0.029	0.041
	ΔTCP	$3.49 \pm 2.3\%$	$5.12 \pm 3.2\%$	$10.6 \pm 4.3\%$	$1.89 \pm 1.43\%$	$2.50 \pm 3.2\%$	$6.20 \pm 3.1\%$	0.001	0.008
	ΔEUD	$0.83 \pm 0.5\%$	$2.96 \pm 1.7\%$	$6.95 \pm 3.9\%$	$0.45 \pm 0.33\%$	$2.69 \pm 1.8\%$	$5.30 \pm 2.3\%$	0.007	0.013
HN	$\Delta D_{2\%}$	$0.44 \pm 0.5\%$	$1.33 \pm 1.0\%$	$2.28 \pm 1.5\%$	$0.04 \pm 0.1\%$	$0.15 \pm 0.3\%$	$1.30 \pm 0.3\%$	0.026	0.305
	$\Delta D_{5\%}$	$0.62 \pm 0.4\%$	$0.98 \pm 0.7\%$	$1.94 \pm 1.0\%$	$0.23 \pm 0.7\%$	$0.33 \pm 0.6\%$	$0.28 \pm 0.6\%$	0.005	0.408
	$\Delta D_{50\%}$	$0.47 \pm 1.5\%$	$0.70 \pm 0.7\%$	$1.60 \pm 1.0\%$	$0.09 \pm 0.1\%$	$0.78 \pm 0.1\%$	$1.20 \pm 0.1\%$	0.023	0.034
	$\Delta D_{95\%}$	$0.82 \pm 1.7\%$	$1.78 \pm 0.7\%$	$3.01 \pm 1.5\%$	$0.38 \pm 0.3\%$	$1.39 \pm 0.8\%$	$2.99 \pm 1.6\%$	0.001	0.008
	$\Delta D_{98\%}$	$1.60 \pm 0.4\%$	$2.43 \pm 1.0\%$	$4.23 \pm 1.9\%$	$0.73 \pm 0.5\%$	$2.69 \pm 1.6\%$	$5.40 \pm 3.0\%$	0.002	0.016
	$\Delta V_{95\%}$	$1.45 \pm 0.5\%$	$3.28 \pm 1.8\%$	$7.27 \pm 3.8\%$	$1.03 \pm 0.6\%$	$2.55 \pm 1.4\%$	$4.55 \pm 2.5\%$	0.013	0.014
	ΔTCP	$3.67 \pm 1.2\%$	$7.23 \pm 3.3\%$	$11.2 \pm 5.3\%$	$1.23 \pm 1.0\%$	$2.13 \pm 1.7\%$	$6.30 \pm 6.6\%$	0.001	0.007
	ΔEUD	$1.23 \pm 0.3\%$	$3.24 \pm 3.9\%$	$7.97 \pm 3.2\%$	$1.12 \pm 0.6\%$	$2.34 \pm 3.5\%$	$6.70 \pm 3.7\%$	0.003	0.023
Brain	$\Delta D_{2\%}$	$0.27 \pm 0.3\%$	$1.32 \pm 1.6\%$	$2.23 \pm 2.4\%$	$0.08 \pm 0.1\%$	$0.12 \pm 0.4\%$	$1.34 \pm 0.7\%$	0.234	0.312
	$\Delta D_{5\%}$	$0.21 \pm 0.3\%$	$0.78 \pm 0.4\%$	$1.70 \pm 1.2\%$	$0.28 \pm 0.3\%$	$0.67 \pm 0.3\%$	$0.74 \pm 0.4\%$	0.231	0.302
	$\Delta D_{50\%}$	$0.73 \pm 0.2\%$	$1.34 \pm 0.6\%$	$1.78 \pm 0.5\%$	$0.12 \pm 0.2\%$	$1.23 \pm 0.5\%$	$1.56 \pm 0.8\%$	0.031	0.040
	$\Delta D_{95\%}$	$0.69 \pm 0.6\%$	$1.63 \pm 0.4\%$	$2.65 \pm 1.1\%$	$0.23 \pm 0.2\%$	$1.12 \pm 0.4\%$	$2.23 \pm 0.7\%$	0.001	0.008
	$\Delta D_{98\%}$	$1.23 \pm 0.8\%$	$2.23 \pm 0.9\%$	$3.23 \pm 1.3\%$	$0.67 \pm 0.3\%$	$2.12 \pm 1.2\%$	$4.23 \pm 1.2\%$	0.005	0.023
	$\Delta V_{95\%}$	$1.68 \pm 0.7\%$	$3.12 \pm 1.3\%$	$5.32 \pm 3.2\%$	$1.34 \pm 0.5\%$	$2.34 \pm 0.7\%$	$4.23 \pm 1.2\%$	0.017	0.018
	ΔTCP	$3.98 \pm 1.6\%$	$6.34 \pm 1.4\%$	$10.2 \pm 4.3\%$	$1.34 \pm 1.0\%$	$2.23 \pm 1.4\%$	$5.21 \pm 1.8\%$	0.002	0.009
	ΔEUD	$1.12 \pm 0.6\%$	$2.32 \pm 0.8\%$	$6.64 \pm 2.6\%$	$1.67 \pm 0.6\%$	$3.32 \pm 1.5\%$	$5.53 \pm 2.34\%$	0.005	0.027

Table 2.3: Mean and standard deviation of the relative percentage variations in the DVH and radiobiological parameters of the bladder.

DVH parameters	C-1	C-2	C-3	CH-1	CH-2	CH-3	P value collimator	P value couch
$\Delta D_{2\%}$	$0.20 \pm 0.2\%$	$0.41 \pm 0.5\%$	$0.69 \pm 0.7\%$	$0.04 \pm 0.2\%$	$0.06 \pm 0.2\%$	$0.08 \pm 0.2\%$	0.280	0.319
$\Delta D_{5\%}$	$0.20 \pm 0.2\%$	$0.48 \pm 0.5\%$	$0.80 \pm 0.9\%$	$0.07 \pm 0.2\%$	$0.09 \pm 0.3\%$	$0.20 \pm 0.5\%$	0.172	0.129
$\Delta D_{15\%}$	$0.01 \pm 0.3\%$	$0.03 \pm 0.7\%$	$0.04 \pm 1.1\%$	$0.00 \pm 0.2\%$	$0.03 \pm 0.5\%$	$0.06 \pm 0.8\%$	0.795	0.620
$\Delta D_{25\%}$	$0.90 \pm 0.4\%$	$1.20 \pm 0.9\%$	$1.80 \pm 1.2\%$	$0.07 \pm 0.1\%$	$0.09 \pm 0.2\%$	$0.15 \pm 0.3\%$	0.264	0.768
$\Delta D_{35\%}$	$0.10 \pm 0.2\%$	$0.26 \pm 0.4\%$	$0.60 \pm 0.5\%$	$0.02 \pm 0.0\%$	$0.03 \pm 0.1\%$	$0.05 \pm 0.1\%$	0.141	0.600
$\Delta D_{50\%}$	$0.10 \pm 0.3\%$	$0.15 \pm 0.6\%$	$0.30 \pm 0.8\%$	$0.03 \pm 0.0\%$	$0.04 \pm 0.0\%$	$0.07 \pm 0.1\%$	0.265	0.566
ΔV_{70Gy}	$3.00 \pm 2.3\%$	$5.00 \pm 3.4\%$	$7.00 \pm 3.8\%$	$0.46 \pm 2.2\%$	$1.23 \pm 3.2\%$	$3.10 \pm 3.7\%$	0.132	0.487
ΔV_{40Gy}	$0.30 \pm 0.7\%$	$0.53 \pm 1.2\%$	$0.87 \pm 2.0\%$	$0.08 \pm 0.1\%$	$0.11 \pm 0.1\%$	$0.30 \pm 0.3\%$	0.416	0.837
ΔV_{25Gy}	$0.01 \pm 0.1\%$	$0.06 \pm 0.1\%$	$0.08 \pm 0.2\%$	$0.00 \pm 0.0\%$	$0.01 \pm 0.0\%$	$0.04 \pm 0.1\%$	0.532	0.364
ΔD_{min}	$0.90 \pm 1.4\%$	$2.11 \pm 2.5\%$	$2.80 \pm 1.3\%$	$0.02 \pm 1.2\%$	$0.32 \pm 1.3\%$	$0.25 \pm 1.2\%$	0.215	0.548
ΔD_{max}	$0.10 \pm 0.4\%$	$0.31 \pm 0.7\%$	$1.00 \pm 1.4\%$	$0.21 \pm 0.1\%$	$0.20 \pm 0.2\%$	$0.19 \pm 0.2\%$	0.183	0.223
ΔD_{mean}	$0.51 \pm 1.3\%$	$0.50 \pm 1.3\%$	$0.90 \pm 1.4\%$	$0.42 \pm 1.3\%$	$0.60 \pm 1.2\%$	$0.70 \pm 1.2\%$	0.354	0.396
ΔNTCP	0.00	0.00	0.00	0.00	0.00	0.00	_	_

Table 2.4: Mean and standard deviation of the relative percentage variations in the DVH and radiobiological parameters of the rectum.

DVH parameters	C-1	C-2	C-3	CH-1	CH-2	CH-3	P value collimator	P value couch
$\Delta D_{2\%}$	$0.11 \pm 0.8\%$	$0.35 \pm 0.7\%$	$0.73 \pm 1.1\%$	$0.01 \pm 0.0\%$	$0.02 \pm 0.1\%$	$0.03 \pm 0.1\%$	0.328	0.591
$\Delta D_{5\%}$	$0.21 \pm 1.0\%$	$0.66 \pm 1.3\%$	$1.16 \pm 1.8\%$	$0.01 \pm 0.1\%$	$0.04 \pm 0.1\%$	$0.03 \pm 0.2\%$	0.106	0.183
$\Delta D_{15\%}$	$0.30 \pm 0.6\%$	$0.56 \pm 1.2\%$	$0.73 \pm 2.2\%$	$0.02 \pm 0.3\%$	$0.04 \pm 0.4\%$	$0.16 \pm 0.5\%$	0.839	0.454
$\Delta D_{25\%}$	$0.36 \pm 0.6\%$	$0.94 \pm 1.4\%$	$1.59 \pm 2.3\%$	$0.08 \pm 0.2\%$	$0.10 \pm 0.5\%$	$0.00 \pm 0.6\%$	0.158	0.646
$\Delta D_{35\%}$	$0.37 \pm 0.4\%$	$1.07 \pm 1.0\%$	$2.06 \pm 1.7\%$	$0.05 \pm 0.2\%$	$0.03 \pm 0.5\%$	$0.21 \pm 0.8\%$	0.125	0.499
$\Delta D_{50\%}$	$0.11 \pm 0.3\%$	$0.53 \pm 0.6\%$	$1.23 \pm 1.1\%$	$0.08 \pm 0.1\%$	$0.08 \pm 0.3\%$	$0.10 \pm 0.2\%$	0.220	0.624
ΔV_{70Gy}	$1.44 \pm 2.1\%$	$4.30 \pm 5.2\%$	$6.30 \pm 4.2\%$	$0.25 \pm 1.6\%$	$0.71 \pm 2.2\%$	$0.56 \pm 3.0\%$	0.152	0.461
ΔV_{40Gy}	$0.10 \pm 1.8\%$	$2.20 \pm 2.1\%$	$4.05 \pm 3.9\%$	$0.23 \pm 0.5\%$	$0.31 \pm 1.1\%$	$0.17 \pm 1.6\%$	0.641	0.430
ΔV_{25Gy}	$0.07 \pm 0.3\%$	$0.34 \pm 0.6\%$	$0.75 \pm 1.0\%$	$0.03 \pm 0.1\%$	$0.15 \pm 0.3\%$	$0.17 \pm 0.2\%$	0.264	0.232
ΔD_{min}	$0.01 \pm 0.4\%$	$1.94 \pm 3.7\%$	$2.10 \pm 1.5\%$	$0.13 \pm 0.2\%$	$0.20 \pm 0.5\%$	$0.50 \pm 0.9\%$	0.106	0.319
ΔD_{max}	$0.05 \pm 0.7\%$	$0.38 \pm 1.6\%$	$0.68 \pm 2.1\%$	$0.23 \pm 0.4\%$	$0.43 \pm 0.5\%$	$0.34 \pm 0.4\%$	0.346	0.276
ΔD_{mean}	$0.01 \pm 0.1\%$	$0.02 \pm 0.3\%$	$0.06 \pm 0.8\%$	$0.15 \pm 0.3\%$	$0.24 \pm 0.3\%$	$0.30 \pm 0.3\%$	0.178	0.533
ΔNTCP	$0.01 \pm 0.4\%$	$1.94 \pm 3.7\%$	$2.10 \pm 1.5\%$	$0.13 \pm 0.2\%$	$0.20 \pm 0.5\%$	$0.50 \pm 0.9\%$	0.323	0.534

Table 2.5: Mean and standard deviation of the relative percentage variations in the DVH and radiobiological parameters of HN and brain OARs.

Cases	Structures	DVH parameters	C-1	C-2	C-3	CH-1	CH-2	CH-3	P value collimator	P value couch
HN	Spinalcord	ΔD_{max}	$1.20 \pm 0.7\%$	$4.42 \pm 4.2\%$	$9.30 \pm 6.2\%$	$0.93 \pm 1.2\%$	$4.23 \pm 6.3\%$	$8.45 \pm 4.7\%$	0.002	0.032
		ΔD_{1cc}	$0.96 \pm 0.3\%$	$1.57 \pm 1.6\%$	$2.46 \pm 1.2\%$	$0.27 \pm 0.4\%$	$0.92 \pm 1.1\%$	$1.74 \pm 1.3\%$	0.003	0.004
		$\Delta D_{0.1cc}$	$0.89 \pm 0.2\%$	$2.53 \pm 2.5\%$	$5.12 \pm 3.6\%$	$0.50 \pm 0.5\%$	$2.05 \pm 2.1\%$	$4.53 \pm 2.3\%$	0.004	0.041
		ΔNTCP	$2.92 \pm 2.3\%$	$8.78 \pm 8.8\%$	$22.1 \pm 10\%$	$2.32 \pm 2.7\%$	$7.50 \pm 6.3\%$	$18.6 \pm 7.8\%$	0.001	0.002
	Brainstem	ΔD_{max}	$0.89 \pm 0.3\%$	$4.07 \pm 2.3\%$	$7.30 \pm 3.7\%$	$1.43 \pm 0.94\%$	$3.20 \pm 2.1\%$	$6.43 \pm 3.6\%$	0.023	0.031
		ΔD_{1cc}	$0.87 \pm 0.6\%$	$1.82 \pm 0.9\%$	$3.65 \pm 1.2\%$	$0.76 \pm 0.26\%$	$1.63 \pm 0.4\%$	$2.36 \pm 1.3\%$	0.001	0.001
		$\Delta D_{0.1cc}$	$1.23 \pm 0.7\%$	$2.70 \pm 1.9\%$	$5.53 \pm 2.9\%$	$1.10 \pm 0.87\%$	$2.45 \pm 1.4\%$	$4.94 \pm 3.6\%$	0.023	0.031
		ΔNTCP	$1.93 \pm 0.8\%$	$5.67 \pm 3.3\%$	$10.3 \pm 6.6\%$	$1.34 \pm 0.54\%$	$4.67 \pm 2.3\%$	$8.86 \pm 4.6\%$	0.001	0.001
	RT parotid	ΔD_{mean}	$0.48 \pm 1.0\%$	$1.06 \pm 1.6\%$	$1.73 \pm 1.2\%$	$0.51 \pm 0.3\%$	$1.16 \pm 1.4\%$	$2.04 \pm 1.8\%$	0.018	0.023
		ΔV_{30Gy}	$0.35 \pm 1.7\%$	$1.95 \pm 1.0\%$	$2.46 \pm 1.9\%$	$0.46 \pm 0.8\%$	$1.89 \pm 2.1\%$	$2.34 \pm 1.7\%$	0.030	0.041
		ΔNTCP	$1.76 \pm 1.5\%$	$2.61 \pm 1.9\%$	$5.89 \pm 3.2\%$	$1.54 \pm 1.8\%$	$2.34 \pm 2.4\%$	$5.67 \pm 4.2\%$	0.024	0.034
	LT parotid	ΔD_{mean}	$0.67 \pm 0.4\%$	$1.39 \pm 0.9\%$	$2.36 \pm 1.6\%$	$0.47 \pm 0.4\%$	$1.56 \pm 1.2\%$	$2.34 \pm 1.5\%$	0.017	0.031
		ΔV_{30Gy}	$0.89 \pm 0.6\%$	$2.43 \pm 1.8\%$	$4.91 \pm 2.8\%$	$1.63 \pm 1.5\%$	$2.34 \pm 1.5\%$	$3.46 \pm 2.3\%$	0.013	0.024
		ΔNTCP	$1.34 \pm 1.2\%$	$2.77 \pm 1.6\%$	$4.46 \pm 3.2\%$	$1.45 \pm 1.3\%$	$3.23 \pm 1.7\%$	$5.46 \pm 3.4\%$	0.012	0.025

Table 2.6: Mean and standard deviation of the relative percentage variations in the DVH and radiobiological parameters of brain OARs.

Cases	Structures	DVH parameters	C-1	C-2	C-3	CH-1	CH-2	CH-3	P value collimator	P value couch
Brain	Brainstem	ΔD_{max}	$0.54 \pm 0.3\%$	$1.32 \pm 0.5\%$	$1.34 \pm 1.3\%$	$0.27 \pm 0.2\%$	$0.40 \pm 0.3\%$	$0.51 \pm 0.11\%$	0.169	0.699
		ΔD_{1cc}	$0.44 \pm 0.3\%$	$1.45 \pm 0.9\%$	$1.63 \pm 1.1\%$	$0.30 \pm 0.2\%$	$0.62 \pm 0.2\%$	$0.89 \pm 0.23\%$	0.463	0.345
		$\Delta D_{0.1cc}$	$0.82 \pm 0.5\%$	$1.55 \pm 0.6\%$	$1.72 \pm 1.2\%$	$0.43 \pm 0.3\%$	$0.78 \pm 0.6\%$	$1.1 \pm 0.23\%$	0.203	0.321
		ΔNTCP	0.00	0.00	0.00	0.00	0.00	0.00	_	_
	Chaism	ΔD_{max}	$0.62 \pm 0.3\%$	$0.87 \pm 0.4\%$	$1.10 \pm 0.45\%$	$0.56 \pm 0.3\%$	$1.00 \pm 0.6\%$	$1.23 \pm 0.7\%$	0.196	0.434
		$\Delta D_{0.1cc}$	$0.45 \pm 0.2\%$	$1.10 \pm 0.6\%$	$1.65 \pm 0.8\%$	$0.65 \pm 0.4\%$	$0.93 \pm 0.5\%$	$1.21 \pm 0.8\%$	0.358	0.476
		ΔNTCP	0.0	0.0	0.0	0.0	0.0	0.0	_	_
	RT optic nerve	ΔD_{max}	$0.84 \pm 0.3\%$	$1.60 \pm 1.0\%$	$1.90 \pm 0.7\%$	$0.74 \pm 0.4\%$	$1.34 \pm 0.7\%$	$1.45 \pm 1.2\%$	0.172	0.323
		$\Delta D_{0.1cc}$	$0.66 \pm 0.4\%$	$1.20 \pm 0.7\%$	$1.93 \pm 1.2\%$	$0.63 \pm 0.7\%$	$0.87 \pm 0.5\%$	$1.83 \pm 0.8\%$	0.165	0.432
		ΔNTCP	0.00	0.00	0.00	0.00	0.00	0.00	_	_
	LT optic nerve	ΔD_{max}	$0.80 \pm 0.4\%$	$0.97 \pm 0.7\%$	$2.12 \pm 1.2\%$	$0.65 \pm 0.5\%$	$0.85 \pm 1.1\%$	$1.75 \pm 1.2\%$	0.168	0.432
		$\Delta D_{0.1cc}$	$0.78 \pm 0.2\%$	$1.76 \pm 0.5\%$	$1.96 \pm 1.3\%$	$0.65 \pm 0.8\%$	$1.23 \pm 1.2\%$	$1.32 \pm 1.1\%$	0.432	0.543
		ΔNTCP	0.00	0.00	0.00	0.00	0.00	0.00	_	_
	RT lens	ΔD_{max}	$1.23 \pm 1.1\%$	$1.87 \pm 1.2\%$	$2.78 \pm 1.2\%$	$0.78 \pm 1.4\%$	$1.23 \pm 1.4\%$	$2.45 \pm 1.3\%$	0.087	0.076
		ΔNTCP	0.00	0.00	0.00	0.00	0.00	0.00	_	_
	LT lens	ΔD_{max}	$1.34 \pm 1.3\%$	$1.67 \pm 1.5\%$	$3.34 \pm 1.9\%$	$1.45 \pm 1.4\%$	$1.90 \pm 1.4\%$	$2.98 \pm 1.7\%$	0.068	0.080
		ΔNTCP	0.00	0.00	0.00	0.00	0.00	0.00	_	_

2.4 Discussion

In this study, we have evaluated the variations in the DVH and radio biological parameters due to deviations in the collimator and couch angular settings in different types of VMAT planning situations. For this purpose, we created three hypothetical PTV based SRS/SBRT VMAT planning situations and also used 30 plans treated in our clinic which included prostate, HN and brain cases. Couch and collimator angular errors of 1^0, 2^0 and 3^0 were introduced in these plans and the variations were studied. Our study revealed that the errors introduced in collimator and couch angles produced deviations in the original plans, but the range of variations were different for different sites and parameters. Zhen et al [29] also reported similar result citing that the site of the treatment and anatomy of a patient strongly affects the predicted clinical outcome by different types of error. Deviation of 1^0 produced only a small variation in the parameters; but as we increased the angle of error, the variations also tend to increase. In all the cases, it was found that the errors due to collimator deviation produced more variation than that of couch errors. Similar finding was reported by Yang et al [30] in his study on the effect of couch and collimator angular variation in the breast IMRT plans, where they reported that the clinical target volume and the critical structures are more affected by collimator errors than the couch errors. These facts emphasize the need for maintaining mechanical accuracy of the LINAC.

American Association of Physicists in Medicine, Task Group (TG)-142 has recommended an allowable tolerance limit of 1^0 for collimator and couch mechanical indicator angles; hence it is important to look in to the dose deviation in VMAT plans due to 1^0 errors in the angular settings. In the case of hypothetical PTVs, the variations due to C-1 and CH-1 errors in all cases are less than 3% and 1.5% respectively. It is also noted from the graphs (Figure 2.5) that the variation due to C-1 and CH-1 errors is lesser in PTV_{BM} than in PTV_{SB}. The maximum variations in the parameters are seen in PTV_{SS}. This can be attributed to the fact that in PTV_{SS}, the PTV is often seen to envelope the

spinal cord cylindrically causing a steep dose gradient and calling for a tight margin. This results in a large variation even for small errors in the couch and collimator settings. This indicates that the deviations are highly dependent on the shapes, sizes and location of the PTVs. The graphs (Figure 2.5a and 2.6a) also points out that the maximum variations in the parameters for all sites in the hypothetical PTVs are in the shoulder region compared to the fall off region and tail region. Introduction of errors did not have much effect on the P_{CI}. In the case of OARs, the variation due to 1^0 errors is less than 1% in PTV_{BM} and PTV_{SS} and less than 2% in PTV_{SB}. The largest increase is seen in PTV_{SS} due to the close proximity of the spine to the PTV. Even though these variations are very small in 1^0, the value of variations increases as we increase the angle of error.

In the analysis of patient plans, a maximum decrease of 2.5% in the dose in $D_{95\%}$, $D_{98\%}$ and $V_{95\%}$ was evident in the 1^0 error, but these plans were still within the clinical acceptable target limit. That is, 95% of the volume of PTV still received a dose greater than 95% of the prescribed dose. But as the angle of error increased, the variations became more prominent. R.Holla et al [13] in their study of HN VMAT cases and Yang et al [30] in their study of breast IMRT cases reported that a collimator or couch angle variation of 1^0 does not produce any significant variations in the DVH parameters. Yang et al further quotes that when the collimator or couch angle error is more than 4^0, bigger hotspots can be seen in some patients. Their findings are similar to our results. The value of ΔTCP was the highest among all the parameters. Both the radiobiological parameters were statistically significant in the overall variation of clinical cases, while only $\Delta D_{95\%}$, $\Delta D_{98\%}$, $\Delta V_{95\%}$ and $\Delta D_{50\%}$ (except in the couch errors of prostate case) were statistically significant among the DVH parameters.

In the case of prostate and brain OARs, it can be seen that none of the DVH or radio biological parameters were statistically significant. A larger variation was seen in the case of ΔV_{70Gy} in the bladder and rectum than in other parameters. Additionally, the value of ΔNTCP for the bladder and for the OARs in brain

was found to be zero. Among the four OARs of the HN cases, the spinal cord and the brain stem show the maximum variation. Here the maximum variation was seen in the ΔNTCP and all the DVH and radio biological parameters were statistically significant. This could be due to the complex dose distribution in the HN case and also due to the positions of the OARs like spinal cord and brain stem which are very close to the target or parotid which is partially included in the target. The sharp dose gradient existing near these OARs may potentially change the planned dose due to these errors. R Holla et al [13] studied the effect on the 1^0 collimator and gantry errors on the dosimetric parameters in the VMAT plans of the five HN patients. They have observed that the effect of C-1 error was more significant compared to 1^0 Gantry error because the former increased the maximum dose to the spinal cord and mean dose to the parotid.

It is observed from the evaluation of clinical cases that, in PTVs the TCP and in some of the OARs NTCP is the most varying parameters. Even these parameters vary differently in different sites. Zhen et al [29] studied the variations in the NTCP and TCP values by introduction of errors in MLC and machine output in IMRT and they reported that the values for NTCP and TCP were different for different errors and also these values were effected differently for differerent organs when a same type of error was induced. This is same in the case of DVH parameters also. This shows that couch and collimator error affected the VMAT plans in different way. This necessitates the testing of the mechanical accuracy of the LINAC before each delivery, to determine the angular variations. But in clinical situations, usually overall uncertainties before delivery are tested using advanced quality assurance devices. But it is a questionable issue whether the detection of such small errors in the collimator, gantry or couch is possible by using the most common 3%/3mm gamma index criteria [31] in the QA device. The investigation done by Alaei [32] on the IBA MatriXX ion chamber array for the IMRT QA reported that couch and collimator errors produced significant variation on planar dose distributions and to detect these errors during evaluation a more stringent gamma evaluation criteria of 2%/2mm has to be

used. Vieillevigne et al [33] studied the sensitivity of QA devices towards the induced errors and found that a 3^0 error in gantry, collimator and couch rotation was detected only by stringent evaluation criteria of 2%/2mm. We have limited our study to the effect of systematic couch and collimator errors, while there are other errors like gantry and MLC errors which need to be investigated in detail in different clinical scenarios. Besides, we have studied the effects of these errors on SRS/SBRT plans by creating hypothetical PTV based planning situation and more clinical investigation is needed in the future.

2.5 Conclusion

The collimator and couch angular variations have different effects in different planning situations. The errors due to collimator were observed to produce more variations, both in DVH and radiobiological parameters, than the couch errors. Variations due to 1^0 errors were less; but as the degree of error increased there was a steady increase in the variations. The effects of errors are different in the DVH and radiobiological parameters as well. In the OARs which are in close proximity to the PTVs, variations were high. The parameter TCP showed more variations than the DVH parameters in PTVs. The NCTP of the bladder and the brain OARs were zero, while in the HN OARs, its value was significant. Our study shows that the treatment site and the patient anatomy effects the outcome produced by different types of errors. Our study emphasis on the need for maintaining the mechanical accuracy of the LINAC.

References

[1] Otto K. (2008). Volumetric modulated arc therapy: IMRT in a single gantry arc. Med Phys 35, 310-7.

[2] Vanetti E, Clivio A, & Nicolini G, et al. (2009). Volumetric modulated arc radiotherapy for carcinomas of the oro-pharynx, hypo-pharynx and larynx: a treatment planning comparison with fixed field IMRT. Radiother Oncol 92, 111-17.

[3] Cozzi L, Dinshaw KA, & Shrivastava SK, et al. (2008). A treatment planning study comparing volumetric arc modulation with RapidArc and fixed field IMRT for cervix uteri radiotherapy. Radiother Oncol 89, 180-91.

[4] Fogliata A, Clivio A, Nicolini G, Vanetti E, & Cozzi L. (2008). Intensity modulation with photons for benign intracranial tumours: a planning comparison of volumetric single arc, helical arc and fixed gantry techniques. Radiother Oncol 89, 254-62.

[5] Zhang P, Happersett L, Hunt M, Jackson A, Zelefsky M, & Mageras G. (2010). Volumetric modulated arc therapy: planning and evaluation for prostate cancer cases. Int J Radiat Oncol Biol Phys 76, 1456-62.

[6] Pardo Montero J & Fenwick J D. (2011). The effect of different control point sampling sequences on convergence of VMAT inverse planning. Phys. Med. Biol 56, 2569-83.

[7] Mu G, Ludlum E & Xia P. (2008). Impact of MLC leaf position errors on simple and complex IMRT plans for head and neck cancer. Phys. Med. Biol 53, 77-88.

[8] H. Parsai, P. S. Cho, M. H. Phillips, R. S. Giansiracusa, & D. Axen. (2003). Random and systematic beam modulator errors in dynamic intensity modulated radiotherapy. Phys.Med. Biol 48, 1109-1121.

[9] RangelA & Dunscombe P. (2009). Tolerances on MLC leaf position accuracy for IMRT delivery with a dynamic MLC. Med. Phys 36, 3304-9.

[10] Xing L, Lin Z, Donaldson SS, Le QT, Tate D, Goffinet DR, Wolden S, Ma L, & Boyer AL. (2000). Dosimetric effects of patient displacement and collimator and gantry angle misalignment on intensity modulated radiation therapy. Radiother Oncol 56, 97-108.

[11] M. Oliver, I. Gagne, K. Bush, S. Zavgorodni, W. Ansbacher, & W. Beckham. (2010). Clinical significance of multi-leaf collimator positional errors for volumetric modulated arc therapy. Radiother. Oncol. 97, 554-560.

[12] M. Oliver, K. Bush, S. Zavgorodni, W. Ansbacher, & W. A. Beckham. (2011). Understanding the impact of RapidArc therapy delivery errors for prostate cancer. J. Appl. Clin. Med. Phys 12, 32-43.

[13] R Holla, V & Anand Ravikumar and B Pillai. (2013). Effect of Gantry and Collimator Positional Errors On Volumetric Modulated Arc Therapy (VMAT). Med. Phys. 40, 368 [abstract].

[14] Betzel GT, Yi BY, Niu Y, & Yu CX. (2012). Is RapidArc more susceptible to delivery uncertainties than dynamic IMRT?. Med Phys 39, 5882-90.

[15] Wolff HA, Wagner DM, Christiansen H, Hess CF, & Vorwerk H. (2010). Single fraction radiosurgery using Rapid Arc for treatment of intracranial targets. Radiat Oncol 5, 77.

[16] Wu QJ, Yoo S, Kirkpatrick JP, Thongphiew D, & Yin FF. (2009). Volumetric arc intensity-modulated therapy for spine body radiotherapy: comparison with static intensity-modulated treatment. Int J Radiat Oncol Biol Phys. 75:1596-604.

[17] Kuijper IT, Dahele M, Senan S, & Verbakel WF. (2010). Volumetric modulated arc therapy versus conventional intensity modulated radiation therapy for stereotactic spine radiotherapy: A planning study and early clinical data. Ingrid Radiotherapy and Oncology 94, 224-228.

[18] Paddick I. (2000). A simple scoring ratio to index the conformity of radiosurgical treatment plans. Technical note. J Neurosurg 93, 219-222.

[19] Gay HA, & Niemierko A. (2007). A free program for calculating EUD-based NTCP and TCP in external beam radiotherapy. Phys Med 23,115-25.

[20] Semenenko VA, & Li XA. (2008). Lyman-Kutcher-Burman NTCP model parameters for radiation pneumonitis and xerostomia based on combined analysis of published clinical data. Phys Med Biol,53:737-55.

[21] Chang JH, Gehrke C, Prabhakar R, Gill S, Wada M, Lim Joon D, & Khoo V. (2016). RADBIOMOD: A simple program for utilising biological modelling in radiotherapy plan evaluation. Phys Med. 32, 248-54.

[22] Levegrun S, Jackson A, Zelefsky MJ, Venkatraman ES, Skwarchuk MW, & Schlegel W, et al. (2002). Risk group dependence of dose-response for biopsy outcome after three-dimensional conformal radiation therapy of prostate cancer. Radiother Oncol 63,11-26.

[23] Sovik A, Ovrum J, Olsen DR, & Malinen E. (2007). On the parameter describing the generalised equivalent uniform dose (gEUD) for tumours. Phys Med;23:100-6.

[24] Stuschke M, & Thames HD. (1999). Fractionation sensitivities and dose-control relations of head and neck carcinomas: analysis of the randomized hyper fractionation trials. Radiother Oncol 51,113-21.

[25] Withers HR, Taylor JM, & Maciejewski B. (1988). The hazard of accelerated tumor clonogen repopulation during radiotherapy. Acta Oncol 27, 131-46.

[26] Jaganathan A, Tiwari M, Phansekar R, Panta R, & Huilgol N.(2011).Intensity-modulated radiation to spare neural stem cells in brain tumors: a computational platform for evaluation of physical and biological dose metrics. J Cancer Res Ther. 7:58-63.

[27] Marks LB, Yorke ED, Jackson A, Ten Haken RK, Constine LS, & Eisbruch A, et al. (2010). Use of normal tissue complication probability models in the clinic. Int J Radiat Oncol Biol Phys 76,S10-19.

[28] Burman C, Kutcher GJ, Emami B, & Goitein M. (1991). Fitting of normal tissue tolerance data to an analytic function. Int J Radiat Oncol Biol Phys 21,123-35.

[29] Zhen H, Nelms BE, & Tom WA. (2013). On the use of biomathematical models in patient-specific IMRT dose QA. Med Phys 40,071702.

[30] Yang J, Ma C, Wang L, Chen L, & Li J. (2009). Effect of collimator and couch angle change on breast IMRT dose distributions. J Appl Clin Med Phys.10, 3058.

[31] Low DA, Harms WB, Mutic S, & Purdy JA. (1998). A technique for the quantitative evaluation of dose distributions. Med Phys. 25, 656-61.

[32] P Alaei. (2015). Sensitivity of Routine IMRT QA Metrics to Couch and Collimator Rotations Med. Phys. 42, 3554.

[33] Vieillevigne L, Molinier J, Brun T, & Ferrand R. (2015). Gamma index comparison of three VMAT QA systems and evaluation of their sensitivity to delivery errors. Phys Med. 31,720-5.

Chapter 3

Effect of translational couch shifts and predicting it's impact on daily dose delivery.

3.1 Introduction

Radiotherapy aims at providing maximum dose to the tumor while minimising the exposure to the normal tissue. Various developments and advances are happening in the field of radiotherapy to achieve this goal. The volumetric modulated arc therapy (VMAT) is one of the new techniques used to produce highly conformal dose distribution around the tumor, sparing critical structures. VMAT has the ability to produce complex dose distribution in a single rotation of gantry within a short time by modulating gantry speed, dose rate and the position of multileaf collimator (MLC) [1]. Therefore, this technique is attaining wide acceptance and is being used to treat several sites [2-5]. The treatment planning is done based on the assumption that patient anatomy is static over the course of treatment. But during treatment delivery, patient repositioning and motion of internal organs give rise to uncertainties [6-8]. In addition, MLC positional errors or small calibration errors in the angular settings of the collimator, couch

or gantry may create difference in dose [9-11]. In combination, the patient set up variations and the machine delivery errors produce a delivered dose different from that of the planned dose. These effects are especially significant in VMAT techniques, where there is a steep dose gradient between the tumor and the organ at risk (OAR).

The uncertainties in the patient set up and internal organ motions are inevitable part of radio therapy. Several reports reveal that there are variations in the delivered dose from that of the planned dose, received by the tumor and OARs, due to set up errors. Fu et al [6] investigated the effect of set up errors in head and neck (HN) cases treated with intensity modulated radiotherapy (IMRT) and reported that for some fractions, the dose that covers 98% of target volume ($D_{98\%}$) was reduced by 5.5% for the clinical target volume (CTV) and the dose that covers 95% of target volume ($D_{95\%}$) decreased by 13.2% for planning target volume (PTV). They also reported a significant increase in the dose to the spinal cord. Wertz1 et al [7] reported that there was a -24% decrease in the volume of prostate receiving 95% of prescribed dose ($V_{95\%}$) and the mean dose to the rectum was increased by up to 41%, due to set up uncertainty. They noticed an increase in $V_{95\%}$ of the prostate by up to 17% and up to -23% reduction in the mean dose to rectum, after linear translational correction was applied. Unlike the translational set up errors, rotational set up errors have lesser impact on dose variation in prostate plans [8]. Fu et al [8] reported a variation within 1.5% in Equivalent uniform dose (EUD) and only a 1% decline in tumor control probability (TCP) due to a 3^0 rotational error. These variations, however, can be minimized by proper adoption of the image guided radiotherapy (IGRT) method [12-13].

In order to take these uncertainties into account, margins are always given around the CTV, either based on the recommendation of the International Commission on radiation units and measurements [14] or following the formula recommended by the van Herk et al[15], based on the analysis of dose-population histograms. A wider margin around the CTV increases the dose to normal tissue,

therefore different online correction methods are being proposed to reduce the margin between the CTV and PTV so as to minimize the exposure [16-17]. Wen et al [16] studied the effect of margin reduction on the radio biological parameters around the prostate CTV and reported that there is decline in the value of NTCP of the rectum when the posterior margin was reduced; but there also is an average reduction in the predicted TCP of the treated plan. Gill et al [17] had tried to find an optimal PTV margin based on the daily CBCT dose calculation in prostate IMRT plans and they reported that the increase in the margin around the CTV have increased the CTV dose coverage and at the same time the dose to the rectum and the variations in the bladder dose were also found to increase on a daily basis. This implies that, due to positional variations, a smaller margin may result in an under dose to the CTV while a larger margin can increase the dose received by the normal tissue or OARs. This calls for an optimal margin around the PTV and a careful evaluation of treated dose on a daily basis.

The imaging techniques allow us to verify patient position on a daily basis and monitor the tumor positional changes. Using this technique, the right-left (R-L), anterior-posterior (A-P), and superior-inferior (S-I) shifts from the planned iso-centre (IC) positions can be obtained. The plan can be executed as such, if the shifts are within certain tolerance limits. But otherwise, either shift should be applied on the couch positions; or repositioning of the patient is required if the shift is larger. But different plans have different levels of complexity and different dose gradient. In prostate tumor patients, in order to reduce rectal complications, the margin is reduced in the posterior part of the CTV. In such cases, due to set up variations in A-P direction in the rectal volume, a part of the anterior rectum may regularly receive full prescription dose [17]. This will change depending upon the magnitude of the shifts accepted and the dose gradient in the posterior direction, and may lead to rectal complexity [16]. Due to the variations in the set up, the dose volume histogram (DVH) of the accepted base plan may not exactly correspond to the actual treated dose. The exact effect

of these variations on the DVH and the radio biological parameters need to be found on a daily basis for applying couch translational corrections. Our aim is to study the effect of systematic couch translational shifts in R-L, S-I and A-P directions, in the DVH and radio biological parameters in prostate cases and to develop a simple and swift method to predict the same online, on a daily basis.

3.2 Materials and Methods

3.2.1 Impacts of systematic translational couch shifts on DVH parameters in prostate VMAT plans

Ten prostate patients treated with VMAT technology were taken for this study. The simulation was done in the supine position with a full bladder and empty rectum. CT images were acquired using a GE Light-speed CT simulator (GE Medical Systems, Milwaukee, WI) with a 3 mm slice thickness and were then transferred into the treatment planning system (TPS) (Version 10, Varian Medical Systems, Palo Alto, CA). After that, a radiation oncologist contours the CTVs, PTVs and the OARs on each slice of the CT images. The prostate plan was generated with a dose of 70 Gy in 28 fractions. The whole prostate, along with seminal vesicles were taken to create the CTV 70 Gy and an 8 mm margin was added around it to create the corresponding PTV. The margin was limited to 6 mm in the posterior to restrict the dose to the anterior rectal wall. OARs such as rectum, bladder, bowel and femoral head were contoured. The volumes receiving doses more than 40 Gy (V_{40Gy}) and 70 Gy (V_{70Gy}) were kept less than 60% and 30% respectively in bladder and less than 45% and 20% respectively in the case of rectum.

The VMAT plans were generated using the Eclipse TPS modeled with Clinac ix (Varian Medical Systems, Palo Alto, CA) equipped with a Millennium 120 MLC. The plans were generated using two complementary full arcs with gantry angle from 179^0 to 181^0 and collimator rotation of 30^0 and 330^0. The plans were

optimized until a minimum 95% of the volume of the PTV received at least 95% of the prescribed dose and all the OARs dose constraints were met. All VMAT plans were planned with 6MV x-ray beam and the dose calculation was done using Anisotropic Analytical Algorithm with grid size of $0.25 \times 0.25 \times 0.25\ cm^3$.

In order to find the effect of systematic translational couch shifts on the DVH parameters, errors were introduced in the clinically accepted base plan. Errors were introduced with an increment of 1 mm and up to 5 mm from the IC in both positive and negative directions on each of the three axis, x (R-L), y (S-I) and z (A-P). Thus for each patient, 30 plans with introduced errors were generated by simply recalculating the base plan, without changing any other parameter. As a result, a total of 300 error plans were generated for 10 patients. The variations in the DVH parameters at $D_{98\%}$ and $D_{95\%}$ of the PTV and CTV and at V_{70Gy}, V_{60Gy} and V_{40Gy} of the bladder and rectum were analysed, both for the base plan and the error plans. The percentage of difference in dose (ΔD) was calculated for each error plan from the base plan.

3.2.2 Impacts of the systematic translational couch shifts on radio biological parameters in prostate VMAT plans.

In order to assess the impacts of systematic translational couch shifts on the radio biological parameter such as the TCP, NTCP and EUD, DVHs of the error induced plans described in the section Impacts of systematic translational couch shifts on DVH parameters in prostate VMAT plans were used. The DVHs of the base plan and the error plans were imported into the MATLAB software (R2013a, The MathWorks, Natick, MA). All the radio biological parameters were calculated using the in house program written in MATLAB and the percentage of variation in the EUD and TCP of the PTV (ΔEUD_{PTV} and ΔTCP_{PTV}) and CTV (ΔEUD_{CTV} and ΔTCP_{CTV}) were calculated. In the case of OARs, NTCP and EUD of the bladder ($\Delta NTCP_{bladder}$, $\Delta EUD_{bladder}$) and rectum ($\Delta NTCP_{rectum}$,

ΔEUD_{rectum}) were calculated.

EUD is calculated using the Niemierko model [18], according to which a uniform equivalent dose will produce the same biological effect as the actual non uniform dose distribution. It is found by the formula,

$$EUD = \Big(\sum_{i=1} (v_i D_i^a) \Big)^{\frac{1}{a}}$$

where, D_i is the dose in Gy, received by the i^{th} sub volume represented by the parameter and 'a' is a unitless model parameter which is a negative number for the tumors and is positive for the normal tissues [17]. When a = 1, EUD becomes the mean dose. TCP can be calculated from EUD using the following equation,

$$TCP = \frac{1}{1 + \left(\frac{TCD_{50}}{EUD} \right)^{4\gamma_{50}}}$$

where TCD_{50} is the tumor dose required to control 50% of the tumor when the tumor is homogeneously irradiated. γ_{50} is a unitless parameter that describes the slope of the dose-response curve and is specific to both normal tissues and tumors.The NTCP values were calculated using the Lyman-Kutcher-Burman (LKB) model [19] and is obtained using the following equations.

$$NTCP = \frac{1}{\sqrt{2\Pi}} \int_{-\infty}^{t} e^{\frac{-x^2}{2}} dx$$

Where

$$t = \frac{D_{eff} - TD_{50}}{mTD_{50}}$$

and

$$D_{eff} = \Big(\sum_{i=1} (v_i D_i^{\frac{1}{n}}) \Big)^n$$

where TD_{50} is the dose with which if the entire organ is uniformly irradiated, would cause a 50% chance of normal tissue complication, m is the slope parameter

and n is the volume effect parameter.

For the calculation of TCP and EUD, the values of parameters used are as given below. TCD_{50}=70.5, γ_{50}=2.9, and a=-24 [20, 21]. For NTCP calculation in the bladder using the LKB model, n=0.0099, m=0.022, and TD_{50}=77.60 Gy for late genitor urinary toxicity [22] and for the calculation of NTCP in the rectum, n=0.09, m=0.13, and TD_{50}=76.9 Gy for Grade $\geq$ 2 rectal toxicity [23].

3.2.3 Generating DVH for random translational couch shifted plans and calculating radio biological parameters.

A cumulative DVH is a plot between the dose in Gy or percentage along the horizontal axis and the volume of structure receiving that dose in CC or in percentage along the vertical axis. Let $D_j(x_0, y_0, z_0)$ is the dose received by V_j^{th} volume of a structure in the DVH of base plan, planned with an IC (x_0, y_0, z_0) (Figure 3.1a). When there is a translational couch shift of 'i' on either side of the IC position (x_{0+i} in the right or positive x direction and x_{0-i} in the left or negative x direction), the dose received by the V_j^{th} volume due to translational couch shift will now become $D_j(x_{0+i}, y_0, z_0)$ and $D_j(x_{0-i}, y_0, z_0)$ provided, there is no positional shift in the y and z axis (Figure 3.1a). Thus the variations in $D_j(x_0, y_0, z_0)$ along the x direction can be represented by the polynomial function f(x, v_j) (Figure 3.1b). Similarly variation in $D_j(x_0, y_0, z_0)$ along the y and z axis can be represented by polynomial functions f(y, v_j) and f(z, v_j) respectively.

DVHs of error plans described in section 3.2.1 was imported to MATLAB and an in-house MATLAB code was written to find best fitted polynomials f(x, v_j), f(y, v_j) and f(z, v_j) for each target and OAR at every points on the DVH. These functions can be used to find the variations in the dose points on the DVH due to the daily translation couch shifts in the three directions. If x_1, y_1 and z_1 are the translation shifts in R-L, S-I and A-P directions and ΔD_{jx}, ΔD_{jy} and ΔD_{jz} is the dose difference in $D_j(x_0, y_0, z_0)$ due to these shifts, then the variations in

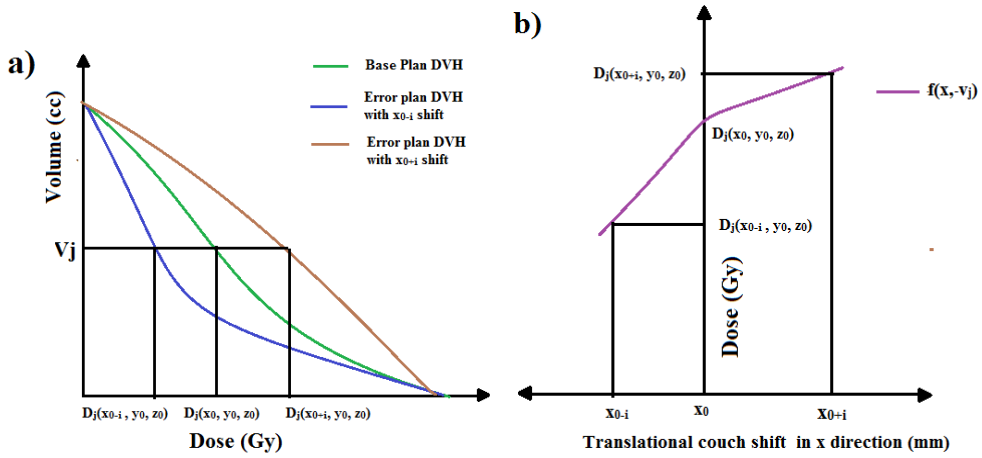

Figure 3.1: (a) Plot of cumulative DVH when planned at iso centre (IC) (x_0, y_0, z_0) and with translational couch shift of 'i' in the positive and negative x direction, with no errors in y and z axis. (b) Function f(x, v_j) which represent the variations in dose due to translational couch shifts along the x direction.

the dose can be calculated as follows ΔD_{jx} = f(x_0, v_j)- f(x_1, v_j), ΔD_{jy} = f(y_0, v_j)- f(y_1, v_j) and ΔD_{jz} = f(z_0, v_j)- f(x_1, v_j). Then the total deviation in dose, ΔD_T can be given by, $\Delta D_T = \Delta D_{jx} \pm \Delta D_{jy} \pm \Delta D_{jz}$ and the new dose point D_j for the translational couch shifts of x_1, y_1 and z_1 will become, $D_j(x_1, y_1, z_1) = D_j(x_0, y_0, z_0) \pm \Delta D_T$

Using this methodology, we are able to generate dose points corresponding to each volume by generating predicted DVH of the daily translational couch variations. This predicted DVH is then used to find the daily radio biological parameters such as EUD, TCP and NTCP as per the method described in section 3.2.1. In order to validate the above method, 10 plans with random translational couch shifts were generated from the base plan in the TPS for each of the 10 patients. Shifts were applied in R-L, S-I and A-P directions with magnitude as shown in Figure 3.2. The TPS generated DVH is then compared with the MATLAB generated predicted DVH and the percentage of deviation between the two and the radio-biological parameters were analysed. Based on the above concepts a Graphical user interphase tool (GUI) was created for user can enter the data and verify the effect on the DVH on daily basis.

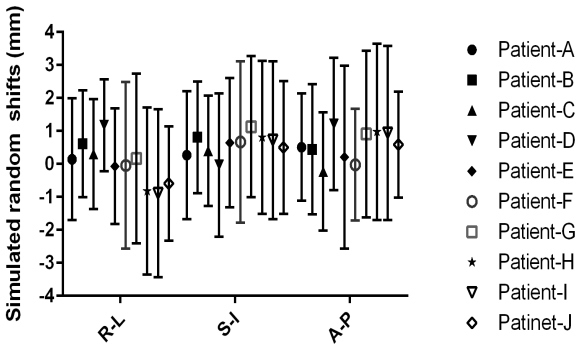

Figure 3.2: Mean and standard deviations of the simulated random shifts in the right-left (R-L), superior-Inferior (S-I) and anterior-posterior (A-P) directions in 10 patients.

3.3 Result

3.3.1 Impacts of systematic translational couch shifts on DVH parameters in prostate VMAT plans.

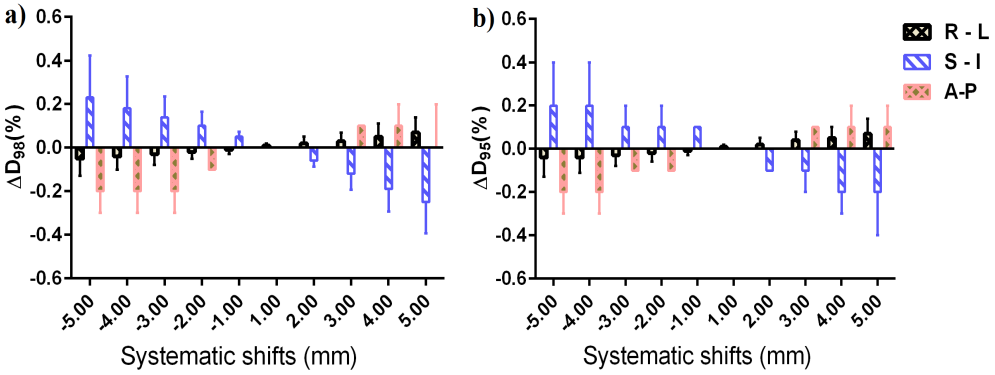

Figure 3.3: Mean and standard deviations of (a) $\Delta D_{98\%}$ and (b) $\Delta D_{95\%}$ of CTV due to systematic translational couch shifts in the right-left (R-L), superior-Inferior (S-I) and anterior-posterior (A-P) directions.

Figure 3.3 and 3.4 shows the mean and standard deviations in $D_{98\%}$ and $D_{95\%}$ of PTV and CTV due to systematic translational couch shifts in the R-L, S-I and A-P directions. In both the cases, these parameters are seen to decrease after applying the shifts. In CTV, the positional errors made no significant impact in the dose as the variations in any of the three directions were less than 1%. The maximum variations were observed in the S-I direction than in the A-P or R-L

directions, both for CTV and PTV. In the case of PTV, it can be seen that the maximum variations is in $D_{98\%}$ than that in $D_{95\%}$. It is also noted that as the magnitude of the systematic shifts increased, variations in the parameters also increased. The maximum variations in S-I direction in the PTV were found to be -12.6±8.6% and -6.2±3.26% for $D_{98\%}$ and $D_{95\%}$ respectively, when a 5 mm shift was applied in the superior direction. Similarly, the maximum variations for $D_{98\%}$ and $D_{95\%}$ were -7.2±1.9% and -3.8±2.3% in the R-L direction and -7.7±4.5% and -4.2±3.7% in the A-P direction, when the 5 mm shift was applied.

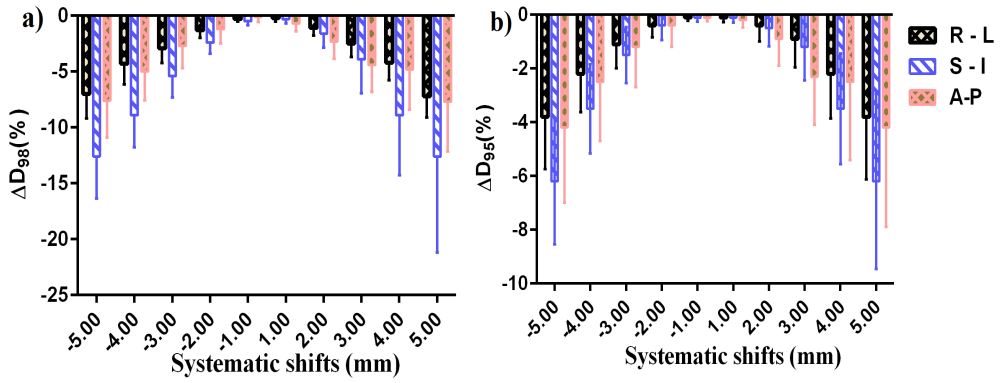

Figure 3.4: Mean and standard deviations of (a) $\Delta D_{98\%}$ and (b) $\Delta D_{95\%}$ of PTV due to systematic translational couch shifts in the right-left (R-L), superior-Inferior (S-I) and anterior-posterior (A-P) directions.

The variations in V_{70Gy}, V_{60Gy} and V_{40Gy} of the bladder due to systematic translational couch shifts in the R-L, S-I and A-P directions is shown in Figure 3.5 and 3.6. It was noted that the maximum variation was in V_{70Gy} due to the S-I shift. While the variations were more due to S-I shift in V_{70Gy} and V_{60Gy}, in the V_{40Gy}, A-P shift caused higher variation. The R-L shifts produced very small changes in the parameters compared to the other two shifts. It can be observed that in the right, superior and anterior directions of couch shifts, the percentage of deviation is along the positive direction, which means that the bladder dose is more than the base plan dose. While in the left, inferior and posterior couch shifts, the dose received by the bladder seem to decrease compared to the planned dose. A 5 mm shift in superior direction caused a variation of 58.5±9.9% in V_{70Gy} and 42.6±7.4% in V_{60Gy}, while the same amount of shift in the inferior direction

showed a variation of -54±5.1% and -38.4±4.8% in V_{70Gy} and V_{60Gy} respectively.

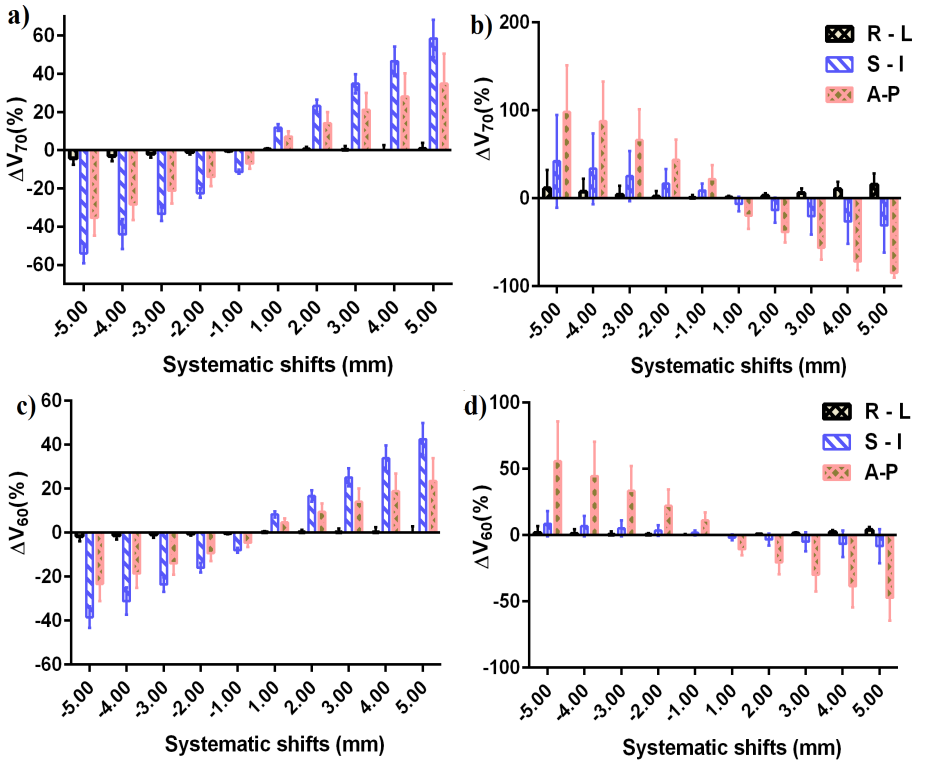

Figure 3.5: Mean and standard deviations of ΔV_{70Gy} of (a) bladder and (b) rectum and ΔV_{60Gy} of (c) bladder and (d) rectum due to systematic translational couch shifts in the right-left (R-L), superior-Inferior (S-I) and anterior-posterior (A-P) directions.

Figure 3.5 and 3.6 shows the variations in V_{70Gy}, V_{60Gy} and V_{40Gy} parameters of the rectum. The shifts in the A-P direction show the highest variations in all the three parameters. The highest variation is observed in V_{70Gy} when a posterior shift of 5 mm was applied and the magnitude of variation was 98±53%, while in the anterior direction, a 5 mm shift produced a variation of -84.7±5.7%. Similarly, a shift of 5 mm in anterior direction produced a variation of 55.7±30% and 16.6±11.95% in V_{60Gy} and V_{40Gy} respectively. A 5 mm shift in the right direction causes variations of 15.6±12.73%, 3.9±2.4%, 4.21±4.7% in V_{70Gy}, V_{60Gy} and V_{40Gy} respectively and a shift of same magnitude in the inferior direction creates variations of 42.1±52.8%, 8.6±9.6% and 3.48±6.3% in the V_{70Gy}, V_{60Gy} and V_{40Gy} respectively. Unlike the bladder cases, in the rectum, the inferior and posterior shifts produce positive variation in the percentage dose, implying

the dose received by rectum is more than the planned dose. While the shifts in superior and anterior direction produced rectum dose less than the planned dose. However, in the R-L shifts, the rectum dose remained more than the base plan dose, irrespective of the direction. It can also be noted that, in the case of rectum, when the magnitude of shifts was increased in any of the direction, the magnitude of variation also increased for all the three parameters.

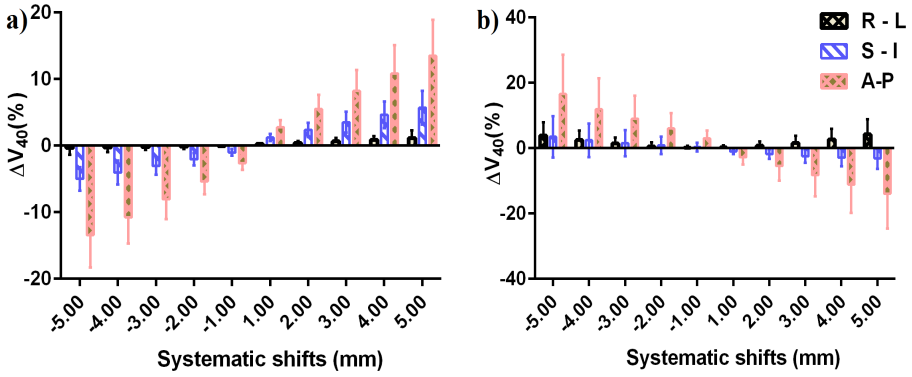

Figure 3.6: Mean and standard deviations of ΔV_{40Gy} of (a) bladder and (b) rectum due to systematic translational couch shifts in the right-left (R-L), superior-Inferior (S-I) and anterior-posterior (A-P) directions.

3.3.2 Impacts of systematic translational couch shifts on radio biological parameters in the prostate VMAT plans

Table 3.1 shows the percentage of variation in EUD, TCP and NTCP values of the PTV, CTV, bladder and rectum due to systematic translational couch shifts in different directions. It can be noticed that, when the couch shifts were applied, the variations in EUD is more, compared to that of TCP for PTV and CTV. The magnitude of variations increases with increase in the magnitude of shifts. The variations observed were highest when superior-inferior shifts were applied. When a 5 mm shift was applied in the superior direction, the variation in EUD and TCP were -43.4±25.8% and -37.99±22% respectively for the PTV and -0.29±0.30 and -0.03±0.03 for CTV respectively. It is also noted that, in

the case of PTV, the target dose is less than the planned dose for the shifts in R-L, S-I and A-P directions. The variations in EUD and TCP were less than 1% for all the shifts in CTV.

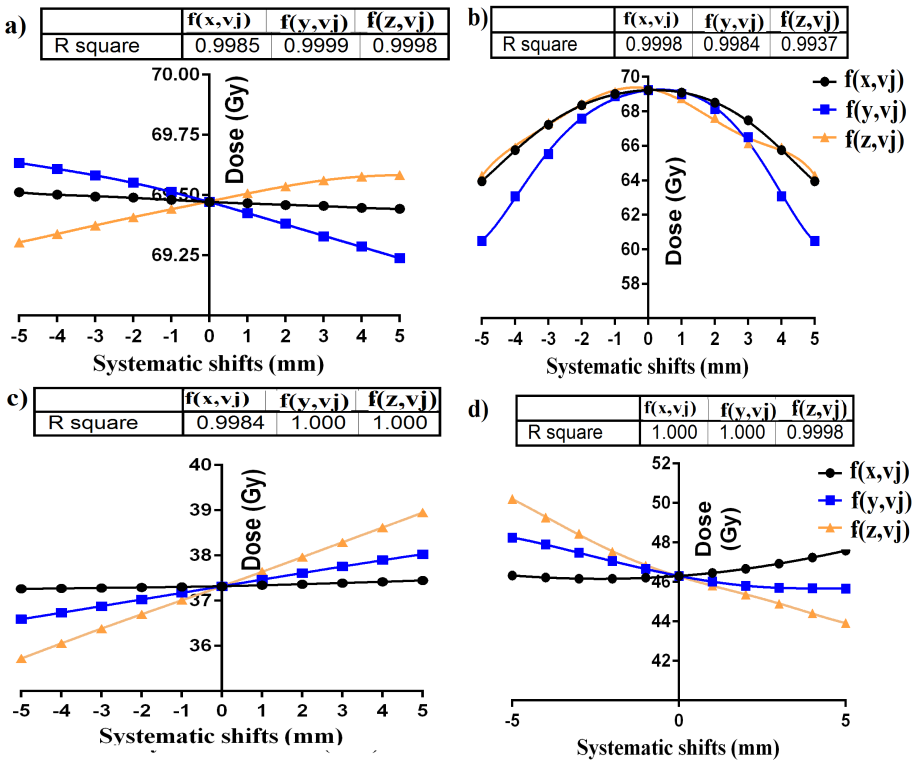

Figure 3.7: Fitted polynomial curves values of R^2 for (a)$D_{98\%}$ of CTV, (b) $D_{98\%}$ of PTV, (c) $D_{50\%}$ of bladder and (d) $D_{50\%}$ of the rectum in the right-left (R-L), superior-Inferior (S-I) and anterior-posterior (A-P) directions.

For bladder, the variation in NTCP is much more compared to that of EUD. It is also seen that the couch shifts in the A-P direction produced maximum variations in the radiobiological parameters while the shifts in R-L direction produced very small variations compared to the other two directional shifts. An error of 5 mm in the anterior direction increase the EUD and NTCP by 5.97±1.73% and 24.80±17.81%, while the same shift in the posterior direction decrease these parameters by -5.67±1.49% and -10.29±4.88% respectively. The table also shows that the variations in EUD and NTCP tend to increase as we move towards the anterior, superior and right direction while it shows a decrease when shifts in posterior, inferior and left direction occur.

It is noted that the radio biological parameters in the rectum are also most

affected by the shifts in the A-P direction and the magnitude of variations is very small in the R-L direction compared to the other two directions. It can also be noted that the shifts in anterior and superior direction always result in a lower EUD and NTCP values compared to that of base plan, while the posterior and inferior shifts cause a higher parameter values. However, when errors in the R-L direction were applied, the values of the parameter remained higher than that of the base plan throughout the shifts. The maximum variations for EUD were -14.9±6.60% and 9.98±8.6% when errors of 5 mm were introduced in the anterior and posterior directions respectively. Similarly, the maximum variations in NTCP for a 5 mm error in anterior and posterior direction were -12.90±8.6% and 45.29±30.51% respectively.

3.3.3 Generating DVH for random translational couch shifted plans and calculating radio biological parameters.

Figure 3.7 illustrate the functions f(x, v_j), f(y, v_j) and f(z, v_j) of the $D_{98\%}$ of the CTV and PTV and $D_{50\%}$ of the bladder and rectum, which is represented by three 6^{th} order polynomial curves. In all the cases, it can be noted from the graph that, the values of R^2 is close to 1. Figure 3.8 comprises of two DVH plots, which showed maximum variation when the T.P.S calculated and MATLAB predicted DVHs were compared. From the figure, it is clear that both DVH curves almost overlap with each other and the maximum variation between the two curves at any point is less than 0.5% in CTV, PTV, rectum and bladder (Figure 3.8b).

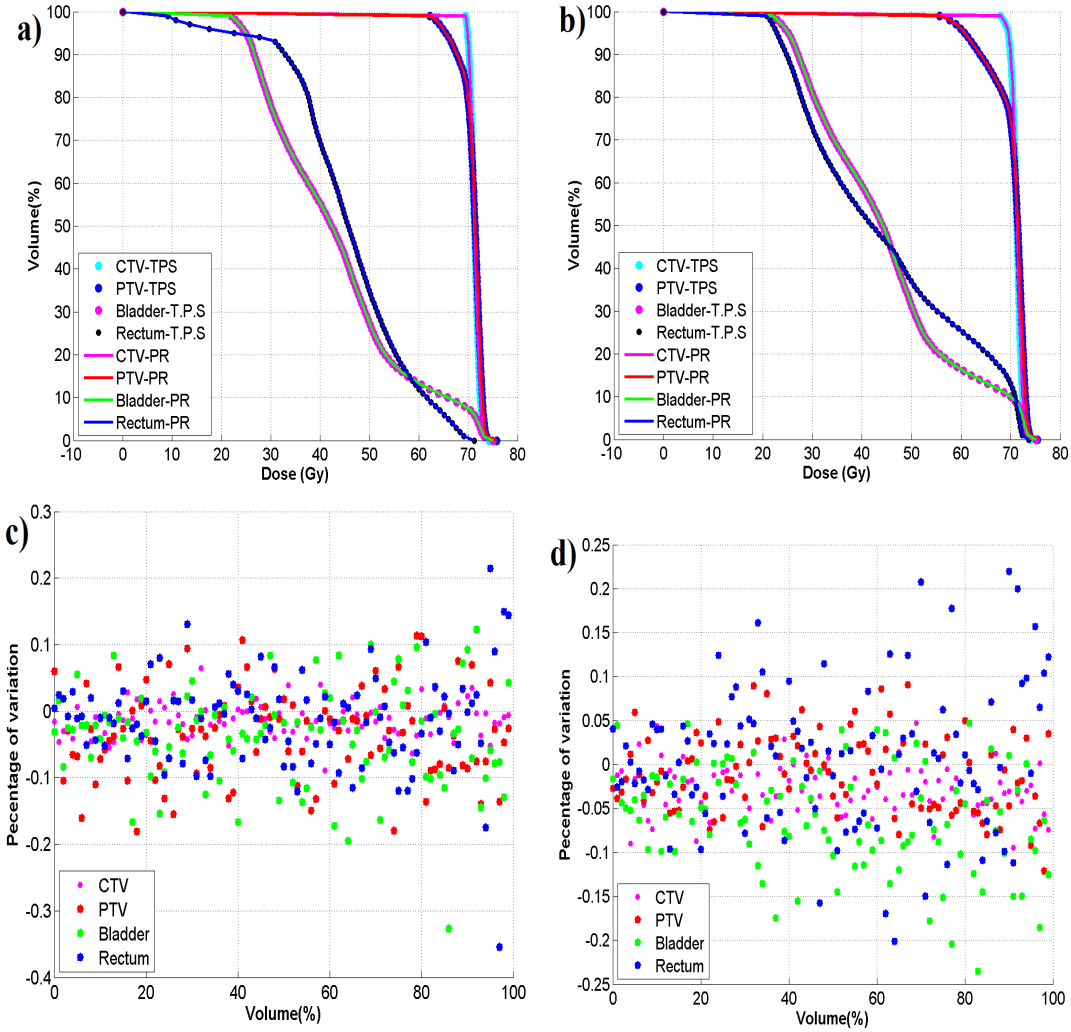

Figure 3.8: a) and b) Comparing treatment planning system (TPS) calculated DVH of the CTV (CTV-T.P.S), PTV (PTV-T.P.S), bladder (Bladder-T.P.S) and the rectum (Rectum-T.P.S) with the MATLAB predicted (PR) DVH of the CTV(CTV-P.R), PTV(PTV-PR), bladder (Bladder-PR) and rectum (Rectum-PR), when random translational couch shifts were applied. c) and d) Corresponding percentage of deviation at each point of the TPS calculated and the MATLAB predicted DVH.

Table 3.1: Mean and standard deviation of the percentage variations in EUD, TCP and NTCP values of the PTV, CTV, bladder and rectum due to systematic translational couch shifts in different directions.

structure	Directions	-5 mm (%)	-4 mm (%)	-3 mm (%)	-2 mm (%)	-1 mm (%)	1 mm (%)	2 mm (%)	3 mm (%)	4 mm (%)	5 mm (%)
ΔEUD_{PTV}	R-L	-6.00 ± 3.2	-3.47 ± 2.0	-1.74 ± 1.0	-0.70 ± 0.4	-0.16 ± 0.1	-0.13 ± 0.1	-0.64 ± 0.5	-1.68 ± 1.2	-3.48 ± 2.3	-6.24 ± 3.5
	S-I	-11.9 ± 6.4	-6.90 ± 4.0	-3.10 ± 1.8	-1.10 ± 0.6	-0.20 ± 0.1	-0.30 ± 0.2	-2.50 ± 1.4	-13.1 ± 7.4	-29.2 ± 18.4	-43.4 ± 25.8
	A-P	-6.06 ± 3.6	-3.72 ± 2.4	-1.96 ± 1.3	-0.80 ± 0.5	-0.16 ± 0.1	-0.29 ± 0.2	-1.15 ± 1.0	-2.80 ± 2.3	-5.37 ± 4.2	-8.69 ± 6.5
ΔTCP_{PTV}	R-L	-0.85 ± 0.5	-0.45 ± 0.3	-0.21 ± 0.1	-0.08 ± 0.1	-0.01 ± 0.1	-0.02 ± 0.1	-0.08 ± 0.1	-0.213 ± 0.1	-0.468 ± 0.3	-0.912 ± 0.6
	S-I	-1.90 ± 1.2	-0.95 ± 0.6	-0.39 ± 0.2	-0.13 ± 0.1	-0.22 ± 0.1	-0.04 ± 0.1	-0.32 ± 0.2	-2.57 ± 1.3	-12.70 ± 7.7	-37.99 ± 22.2
	A-P	-0.86 ± 0.6	-0.49 ± 0.3	-0.24 ± 0.2	-0.09 ± 0.1	-0.02 ± 0.1	-0.03 ± 0.1	-0.14 ± 0.1	-0.37 ± 0.3	-0.780 ± 0.7	-1.45 ± 1.3
ΔEUD_{CTV}	R-L	0.04 ± 0.1	0.03 ± 0.1	0.02 ± 0.1	0.01 ± 0.06	0.00 ± 0.0	0.02 ± 0.0	0.05 ± 0.0	0.08 ± 0.0	0.12 ± 0.0	0.16 ± 0.1
	S-I	0.53 ± 0.3	0.41 ± 0.2	0.30 ± 0.2	0.19 ± 0.1	0.10 ± 0.0	-0.08 ± 0.0	-0.15 ± 0.1	-0.21 ± 0.1	-0.26 ± 0.2	-0.29 ± 0.3
	A-P	-0.22 ± 0.1	-0.18 ± 0.1	-0.13 ± 0.1	-0.09 ± 0.0	-0.04 ± 0.0	0.06 ± 0.0	0.09 ± 0.0	0.11 ± 0.1	-0.09 ± 0.2	-0.01 ± 0.3
ΔTCP_{CTV}	R-L	0.00 ± 0.02	0.00 ± 0.01	0.00 ± 0.01	0.00 ± 0.01	0.00 ± 0.00	0.00 ± 0.00	0.00 ± 0.00	0.01 ± 0.01	0.01 ± 0.01	0.02 ± 0.01
	S-I	0.05 ± 0.03	0.04 ± 0.02	0.03 ± 0.02	0.02 ± 0.01	0.01 ± 0.01	-0.01 ± 0.01	-0.01 ± 0.01	-0.02 ± 0.02	-0.02 ± 0.02	-0.03 ± 0.03
	A-P	-0.02 ± 0.02	-0.02 ± 0.01	-0.01 ± 0.01	-0.01 ± 0.01	0.00 ± 0.00	0.01 ± 0.00	0.01 ± 0.01	0.01 ± 0.01	40.01 ± 0.02	0.00 ± 0.03
$\Delta EUD_{Bladder}$	R-L	0.00 ± 0.21	-0.02 ± 0.16	-0.02 ± 0.1	-0.02 ± 0.07	-0.01 ± 0.04	0.04 ± 0.04	0.07 ± 0.07	0.12 ± 0.11	0.16 ± 0.16	0.23 ± 0.21
	S-I	-4.68 ± 1.0	-4.05 ± 1.12	-2.92 ± 0.67	-1.94 ± 0.45	-0.96 ± 0.22	1.01 ± 0.26	1.99 ± 0.52	2.96 ± 0.77	2.71 ± 3.25	3.37 ± 4.05
	A-P	-5.67 ± 1.4	-4.54 ± 1.21	-3.40 ± 0.92	-2.27 ± 0.62	-1.13 ± 0.32	1.14 ± 0.32	2.14 ± 0.80	3.26 ± 1.10	4.37 ± 1.41	5.97 ± 1.73
$\Delta NTCP_{Bladder}$	R-L	0.00 ± 0.6	-0.06 ± 0.50	-0.07 ± 0.34	-0.08 ± 0.23	-0.04 ± 0.1	0.12 ± 0.13	0.24 ± 0.24	0.39 ± 0.37	0.54 ± 0.52	0.77 ± 0.70
	S-I	-9.32 ± 4.3	-8.45 ± 4.07	-6.63 ± 3.16	-4.75 ± 2.30	-2.54 ± 1.24	3.14 ± 1.64	6.73 ± 3.59	10.91 ± 5.96	15.31 ± 9.62	20.77 ± 13.43
	A-P	-10.29 ± 4.8	-8.92 ± 4.31	-7.26 ± 3.59	-5.26 ± 2.68	-2.86 ± 1.51	3.50 ± 1.96	7.12 ± 4.78	712.01 ± 8.04	17.84 ± 12.30	24.80 ± 17.81
ΔEUD_{Rectum}	R-L	0.32 ± 0.72	0.16 ± 0.56	0.06 ± 0.39	0.00 ± 0.24	0.02 ± 0.11	0.09 ± 0.06	0.22 ± 0.14	0.40 ± 0.23	0.62 ± 0.32	0.88 ± 0.51
	S-I	1.83 ± 1.54	1.48 ± 1.26	1.11 ± 0.96	0.75 ± 0.64	0.37 ± 0.32	-0.38 ± 0.39	-0.74 ± 0.78	-1.08 ± 1.22	$-1.39 \pm 1,69$	-1.66 ± 2.21
	A-P	9.98 ± 3.25	8.33 ± 2.80	6.55 ± 2.27	4.58 ± 1.65	2.42 ± 0.90	-2.61 ± 1.02	-5.22 ± 2.61	-8.30 ± 3.90	-11.56 ± 5.27	-14.9 ± 6.60
$\Delta NTCP_{Rectum}$	R-L	2.17 ± 4.47	1.15 ± 3.18	0.45 ± 2.13	0.04 ± 1.30	0.10 ± 0.64	0.52 ± 0.47	1.26 ± 1.08	2.32 ± 1.87	3.71 ± 2.92	5.46 ± 4.28
	S-I	14.29 ± 10.6	10.99 ± 11.05	7.94 ± 7.82	5.07 ± 4.88	2.42 ± 2.24	-2.22 ± 2.40	-4.12 ± 4.50	-5.68 ± 6.57	-6.85 ± 8.66	-7.63 ± 10.8
	A-P	45.29 ± 30.51	32.44 ± 21.46	21.64 ± 14.08	12.72 ± 8.20	5.57 ± 3.60	-4.94 ± 2.90	-7.24 ± 3.68	-9.88 ± 5.34	-11.71 ± 7.05	-12.90 ± 8.6

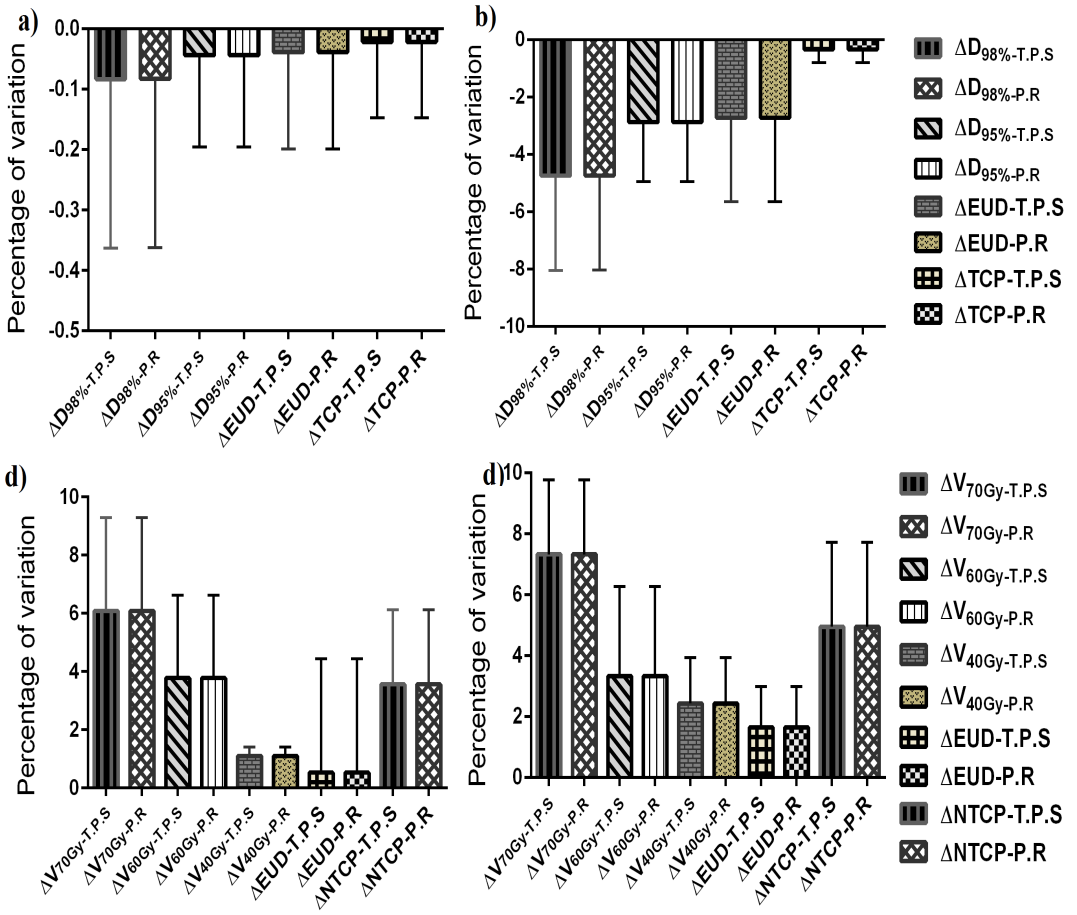

Figure 3.9: The comparison of treatment planning system calculated and MATLAB predicted values of mean percentage of variation in the DVH and radio biological parameters of a)CTV, b)P.T.V, c)Bladder, d)Rectum, when the random couch shift plans.

The mean standard deviations of the variations, due to random shifts, in the DVH and radio biological parameters for the targets and OARs calculated by T.P.S and MATLAB are shown in Figure 3.9. The graph shows a good correlation between the parameters calculated by both the methods. The mean and standard deviation of $D_{98\%}$ for PTV, when calculated by T.P.S and MATLAB were -4.75±3.3% and -4.74±3.29% respectively. Similarly, the mean and standard deviation of EUD and TCP for PTV when calculated in T.P.S were -2.73±2.92% and -0.344±0.46% which exactly matched with the MATLAB predicted values. Likewise, in the case of CTV, the variations calculated using the two methods were in line with each other in all the parameters. In the case of OARs the

maximum variation was found in the V_{70Gy} which were 6.09±3.2% and 7.32±2.5% respectively for bladder and rectum. Here also, the variations in the DVH and radiobiological parameters due to the couch shifts calculated using both the methods were in par with each other.

3.4 Generating Graphical user interphase tool in MATLAB for daily treatment analysis

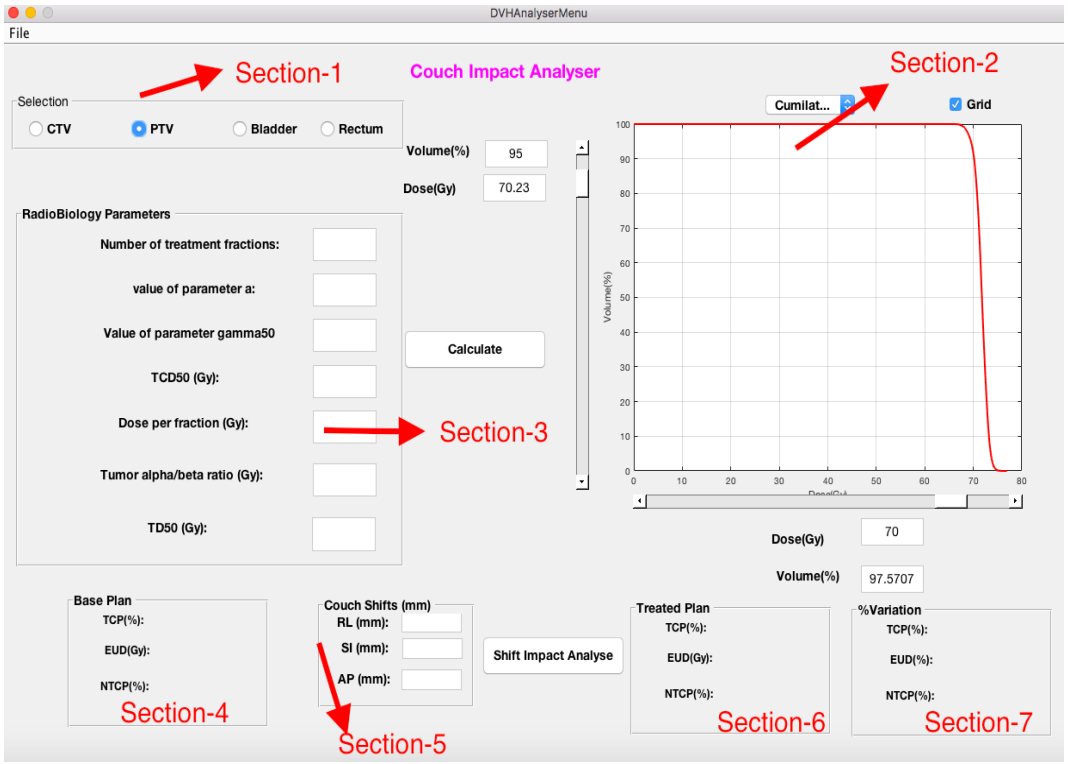

Figure 3.10: The graphical user interphase tool for the analysis of the daily DVH impacts with different calculation module sections.

A GUI tool was created (named Couch Impact Analyser, Figure 3.10), which allows the user to predict the effect of daily transition shifts on DVH before the daily treatment. The GUI consist of seven different sections (Figure 3.10). Section-1 allows the user to select the type of the structure such as PTV, CTV or OARs. Analysis and viewing tool can be done in the section-2. Here user can select a differential or cumulative DVH using a pop up menu set in the

upper corner and with grid on off button. Section-4 is generated to enter the radiobiological model parameters such as TD50,TCD50 etc, and analyse the EUD and TCP or NTCP values of the base plan. Section-5 will be used to enter the couch translational shifts in the x, y and z direction in mm. The corresponding impact on the radiobiological parameter can be assed from the section 6 and section 7 of the software and the deviations in the radiobiological parameter from the base plan can be calculated.

3.5 Discussion

VMAT plans produce highly conformal dose distributions around the target with a sharp dose gradient between the PTV and OARs. The level of dose gradient may differ depending upon the beam arrangement and planning constraints given during the optimization, thus varying the impacts of the set up deviation on the final treatment plans. In routine clinical situation the set up errors are analysed based on modern imaging technology. Analysis of errors for each patient set up and then applying the correction process may result in an increased workload and treatment time. There are also chances of errors arising during the correction procedure. So, if we analyze potential dose delivery errors in advance and incorporate the corrections, the efficiency of the treatment can be improved at the same time as achieving the preferred dose coverage. A tolerance level for set up errors needs to be established on the basis of target site and institutional protocol. Since every plan is different, we need to analyze the effect of accepted tolerance level in couch shifts on the parameters, preferably in the treatment position itself. In our study, we extensively examined the effect of systematic translational couch shifts in the prostate VMAT plans on the DVH and radiobiological parameters and developed a method to predict these effects on a daily basis.

After evaluating the effects of systematic translational couch shifts from the error plans generated for the ten patients, we observed that the variations in

the parameters depend upon the direction and magnitude of the shift. Our study revealed that in the case of PTV and CTV both DVH and radiobiological parameters are affected most due to S-I shifts than the shifts in A-P and R-L directions. Since the inferior and superior field borders are common for the field segments, the dose gradient will be highest in the inferior and/or superior direction. The higher dose gradient, compared to the R-L and A-P direction, thus results in higher dose difference due to S-I shifts. Lo et al [24] have studied the effect of systematic and random shifts on DVH parameters and they reported that the effect was insignificant on the prostate CTV, as the $D_{95\%}$ of prostate was more than 99.95% of the prescribed dose. Our study matched with their observation as we could not find any significant changes in the dose to the CTV, due to both systematic and random shifts. We found the value for $\Delta D_{95\%}$ was less than 1%. This can be attributed to the fact that the margin given around the CTV was adequate enough to sustain the shifts applied. Whereas, in the case of PTV, systematic shifts caused significant variation in the parameters, while the variations due to random shifts were comparatively less. Algan O et al [25] studied the effect of daily set up errors on the prostate IMRT by moving the iso-centre in the opposite direction of the shift, thus mathematically negating the shift. They found significant variations between the planned and delivered dose to the PTV. They reported that The mean value for V_{95} before correcting the patient setup and after were 87.3% and 99.9%, respectively.

It was noted that, in the case of bladder and rectum, most of the parameters are affected by the A-P shifts than the shifts in other two directions. C Lo et al [24] had reported similar findings as they had noted larger variations in rectum volume due to A-P shifts, that is, more than 6% volume changes due to a 1.0 mm shift in anterior direction. We had found that V_{70Gy} and V_{60Gy} of the bladder were more effected by S-I shifts while, the shifts in R-L direction produced comparatively less variations in the parameters. Our results matched with those of C Lo et al, as they too reported more than 3% change in the bladder volume due to 3.0 mm S-I shift and that the changes in volume in the $V_{90\%}$ and

$V_{70\%}$ of bladder and rectum due to systematic errors were within 3.0 mm in the R-L direction. The shifts in A-P direction produced the largest variations in the radiobiological parameters in both the critical structures. This may be due to the position of bladder and rectum, which borders the anterior and posterior walls of the target respectively. As we try to minimize the dose to the critical structures a sharp dose gradient exists in this region, which leads to high dose variations even for small shifts. For instance, whenever there is a shift in the posterior direction, the rectum enters the high dose area of the target.

DVH is a potential tool used in evaluating the treatment plans. The shape of the DVH curve and the area under it plays an important role in determining the adequacy and the homogeneity of dose coverage in the tumor volume and also in deciding the acceptable dose to the OARs. The DVH can also be used to calculate the radio biological parameters. But patient set up errors causes the planned dose to be different from the delivered dose which leads to changes in the daily DVH and in turn causes variations in the radiobiological parameters. So, we have introduced a method for calculating the daily DVH incorporating the random translational couch shifts and using this, the changes in the radio biological parameters can be monitored on a daily basis.

In order to predict the effect of shifts on the DVH and the radio biological parameters on a daily basis, we have introduced a method using the polynomial curve fitting method. For this, we found three polynomial functions f(x, v_j), f(y, v_j)in three direction using the data from the DVHs of systematic translational shifts. A program was written to find these functions using the curve fitting tools available in the MATLAB in such a way that the best fitted polynomials are found. This function is then used to find the variation in the dose points of the DVH due to random couch shifts. The validation of the MATLAB predicted and the T.P.S calculated DVHs was done and the values showed good correlation, with maximum variation being less than 0.5%. These DVHs were then used to calculate the variation in radio biological parameters and it was found that the predicted and T.P.S calculated radio biological parameters were in accordance

with each other.

We observed that the daily simulated random shifts produced lesser effect on the DVH and radio biological parameters than the systematic shifts. The variations due to random couch shifts were less than 0.5% for all the parameters in the CTV. We had observed larger variations in the $V_{70\%}$ and $V_{60\%}$ of the bladder and rectum due to the systematic shifts whereas; the variations were less when the random shifts were applied. This can be attributed to the fact that the introduction of random errors resulted in dose smearing [26]. Lo et al [24] reported that in the DVH parameters of prostate IMRT cases, random set up errors produced lesser volume changes than the systematic errors, which was in agreement with our findings. S Arumugam et al [26] have analysed the effect of random errors in IMRT and VMAT prostate plans and they reported that the variations in the dose to the CTV between the base plan and the error simulated plans were less than 1%. But they observed a higher difference in the dose in VMAT than IMRT for the PTV and concluded that in the case of dose to the PTV, the VMAT plans are relatively more sensitive than the IMRT to the random errors.

In this context, our method of predicting the effect of couch shifts on the DVH and radiobiological parameters can be utilized on a daily basis to determine the uncertainties in the dose delivery and to enhance the quality of the treatment. As this method does not require any further re-calculation of the plans, it can be considered as an online tool to predict the variations in the clinics. But, our method uses the data from the DVHs of systematically shifted plans. Hence this method does not consider any organ deformation or organ motion. Therefore, further investigation is needed before implementing this method clinically. In our future study, we are planning to incorporate the daily information obtained from the CBCT into this method and predict the effects of shifts on the DVH and radio biological parameters on a daily basis, more realistically.

3.6 Conclusion

In our study, we have evaluated the effects of couch shifts on DVH and radiobiological parameters of prostate VMAT plans and found that the variations in the parameters depend upon the direction and magnitude of the shift. It was noted that the variations in the dose to the CTV, due to both systematic and random shifts, were very small. Further, for CTV and PTV, the maximum variations were observed in the S-I direction than in the A-P or R-L directions. But it was found that the parameters in rectum and most of the parameters in the bladder were affected by the A-P shifts than the shifts in other two directions due to the sharp dose gradient that exist in this region. We also checked the feasibility of applying daily translational couch shifts using the MATLAB predicted DVH and was found to be in good correlation with the TPS generated DVH. Further studies are required before clinical implementation of this method so as to incorporate organ motions and deformation.

References

[1] Otto K. (2008). Volumetric modulated arc therapy: IMRT in a single gantry arc. Med Phys 35,310-7.

[2] Zhang P, Happersett L, Hunt M, Jackson A, Zelefsky M, & Mageras G. (2010). Volumetric modulated arc therapy: planning and evaluation for prostate cancer cases. Int J Radiat Oncol Biol Phys 76,1456-62.

[3] Vanetti E, Clivio A, & Nicolini G, et al. (2009). Volumetric modulated arc radiotherapy for carcinomas of the oro-pharynx, hypo-pharynx and larynx: a treatment planning comparison with fixed field IMRT. Radiother Oncol 92,111-17.

[4] Cozzi L, Dinshaw KA, & Shrivastava SK, et al. (2008) A treatment planning study comparing volumetric arc modulation with RapidArc and fixed field IMRT for cervix uteri radiotherapy. Radiother Oncol. 89,180-91.

[5] Fogliata A, Clivio A, Nicolini G, Vanetti E, & Cozzi L. (2008). Intensity modulation with photons for benign intracranial tumours: a planning comparison of volumetric single arc, helical arc and fixed gantry techniques. Radiother Oncol. 89,254-62.

[6] Fu W, Yang Y, Yue NJ, Heron DE, & Saiful Huq M. (2013). Dosimetric influences of rotational setup errors on head and neck carcinoma intensity-modulated radiation therapy treatments. Med Dosim.Summer;38(2),125-32.

[7] Wertz H, Lohr F, Dobler B, Mai S, Welzel G, Boda-Heggemann J, & Wenz F. (2007). Dosimetric consequences of a translational isocenter correction

based on image guidance for intensity modulated radiotherapy (IMRT) of the prostate. Phys Med Biol.Sep 21;52(18),5655-65.

[8] Fu W, Yang Y, Li X, Heron DE, Huq MS, & Yue NJ. (2006). Dosimetric effects of patient rotational setup errors on prostate IMRT treatments. Phys Med Biol. 51(20),5321-31.

[9] M. Oliver, I. Gagne, K. Bush, S. Zavgorodni, W. Ansbacher, & W. Beckham. (2010). Clinical significance of multi-leaf collimator positional errors for volumetric modulated arc therapy. Radiother. Oncol. 97, 554-560.

[10] M. Oliver, K. Bush, S. Zavgorodni, W. Ansbacher, & W. A. Beckham. (2011). Understanding the impact of RapidArc therapy delivery errors for prostate cancer. J. Appl. Clin. Med. Phys. 12,32-43.

[11] Noufal M P, Abdullah K K, Niyas P, & Nambiar VR. (2017). Analysis of Influence of Errors in Angular Settings of Couch and Collimator on the Dosimetric and Radiobiological Parameters in VMAT Plans. J. Med. Imaging Radiat. Sci. 48(2),166-177.

[12] Becker-Schiebe M , Abaci A , Ahmad T, & Hoffmann W et al. (2016). Reducing radiation-associated toxicity using online image guidance (IGRT) in prostate cancer patients undergoing dose-escalated radiation therapy. Rep Pract Oncol Radiother. 21(3),188-94.

[13] Park SS , Yan D, McGrath S, & Dilworth JT et al. (2012). Adaptive Image-Guided Radiotherapy (IGRT) Eliminates the Risk of Biochemical Failure Caused by the Bias of Rectal Distension in Prostate Cancer Treatment Planning: Clinical Evidence. Int J Radiat Oncol Biol Phys. 83(3):947-52.

[14] ICRU. (1993). Prescribing, Recording and Reporting Photon Beam Therapy ICRU Report No 50. ICRU; Bethesda, MD.

[15] M. van Herk, P. Remeijer, C. Rasch, & J. V. Lebesque, (2000). "The probability of correct target dosage: Dose-population histograms for deriving

treatment margins in radiotherapy," Int. J. Radiat. Oncol., Biol., Phys. 47,1121-1135.

[16] Wen N , Kumarasiri A, Nurushev T, Burmeister J, Xing L, Liu D, Glide-Hurst C, & Kim J, et. (2013). An assessment of PTV margin based on actual accumulated dose for prostate cancer radiotherapy. Phys Med Biol. Nov 7;58(21),7733-44.

[17] Gill SK, Reddy K, Campbell N, & Chen C. (2015) Determination of optimal PTV margin for patients receiving CBCT-guided prostate IMRT: comparative analysis based on CBCT dose calculation with four different margins. J Appl Clin Med Phys. Nov 8;16(6):,5691.

[18] Gay HA, & Niemierko A. (2007). A free program for calculating EUD-based NTCP and TCP in external beam radiotherapy. Phys Med. 23,115-25.

[19] Semenenko VA, & Li XA. (2008). Lyman-Kutcher-Burman NTCP model parameters for radiation pneumonitis and xerostomia based on combined analysis of published clinical data. Phys Med Biol. 53,737-55.

[20] Levegrun S, Jackson A, Zelefsky MJ, Venkatraman ES, Skwarchuk MW, & Schlegel W, et al. (2002) Risk group dependence of dose-response for biopsy outcome after three-dimensional conformal radiation therapy of prostate cancer. Radiother Oncol. 63,11-26.

[21] Sovik A, Ovrum J, Olsen DR, & Malinen E. (2007). On the parameter describing the generalised equivalent uniform dose (gEUD) for tumours. Phys Med. 23,100-6.

[22] M. R. Cheung, S. L. Tucker, L. Dong, R. de Crevoisier, A. K. Lee, S. Frank, R. J. Kudchadker, H. Thames, R. Mohan, & D. Kuban. (2007). Investigation of bladder dose and volume factors influencing late urinary toxicity after external beam radiotherapy for prostate cancer. Int. J. Radiat. Oncol., Biol., Phys. 67,1059-1065.

[23] J. M. Michalski, H. Gay, A. Jackson, S. L. Tucker, & J. O. Deasy. (2010). Radiation dose-volume effects in radiation-induced rectal injury. Int. J. Radiat. Oncol., Biol., Phys. 76,S123-S129.

[24] C Lo, D Huang & J Hong. (2007). The Dose-Volume Differences by Set-Up Error for Prostate. Med. Phys. 34,2494.

[25] Algan O , Jamgade A, Ali I, Christie A, Thompson JS, Thompson D, Ahmad S, & Herman T. (2012). The dosimetric impact of daily setup error on target volumes and surrounding normal tissue in the treatment of prostate cancer with intensity-modulated radiation therapy. Med Dosim. Winter;37(4):406-11.

[26] S Arumugam, A Xing, L Holloway and G Goozee. (2011). A Study on the Sensitivity of VMAT and IMRT Prostate Plans Considering Uncertainties in Treatment Delivery and Patient Positioning. Med. Phys. 38,3672.

Chapter 4

Analysis of dosimetric impacts of cone beam CT based volumetric modulated Arc therapy planning

4.1 Introduction

In the new era of radiotherapy, the kilo voltage Cone Beam Computed Tomography (CBCT) has become a potential tool for evaluating the deviations in the positioning set up and the changes in the organ dimensions of the patient during the course of treatment. These images provide the necessary anatomical information needed for correcting the set up deviations [1-5]. The CBCT images offer a better picture of the soft tissues by providing sufficient soft tissue contrast thus enabling to visualize the target on the daily basis, compared to the traditional method using the megavoltage (MV) portal images. Positioning of the patients is confirmed after matching the soft tissues and bony structures in CBCT images to those in planning CT, which is not possible in the MV imaging systems. Further, it helps to assess the anatomical changes in the patients due to weight loss, tumour shrinkage and soft tissue changes [6, 7]. The changes in anatomy and organ motion can lead to variations in the dose distributions calculated based on

planning Computed Tomography (CT). These changes may end up with a daily dose which does not match with the prescribed dose. Therefore, the CBCT data acquired prior to the treatment can be used as a potential tool for recalculating the daily treatment plans based on the daily patient anatomy [8-16]. This adaptive planning allows us to modify the radiation therapy course based on the delivered dose. However, due to the scattering artifacts and limitation in the reconstruction of CBCT images, it shows deviations in the HU from that of the planning CT [9, 11, 12, 15, and 17].

There are several efforts described in the literature for correcting the HU variations in the CBCT images. The simplest method is creating a HU-relative electron density curve specific to CBCT [13]. Another common method is correcting the CBCT by mapping it with the planning CT information [9]. Also there is a projection scatter correction method, which reduces the scatter before the CBCT image reconstruction [18-20]. However, studies of Yoo and Yin and that of Lee et al showed that, HU variation in CBCT images acquired using Varian On-Board Imager (OBI) system showed only a small variation (less than 10HU) [8,14]. Therefore, they tried to recalculate the CT based plan directly on the CBCT, without any correction. Their investigations revealed that Intensity Modulated Radiotherapy (IMRT) dose variation between the CT and CBCT based dose calculations are within 3%. There was a good correlation between the CT and CBCT based IMRT plans. In contrast, the Elekta Synergy CBCT system-XVI showed larger deviations in HU which makes correction strategy necessary [11, 15].

Most of the studies dealing with dose reconstruction on the CT and CBCT images are done on Three Dimensional Conformal Radiotherapy (3DCRT) and IMRT [9, 11, 12, 13, 14, and 16]. There are other techniques like volumetric Modulated Arc Therapy (VMAT) which is getting very popular these days and hence needed to be evaluated on the CT and CBCT based dose calculations. RapidArc (Varian, Palo Alto, California, USA) is a VMAT technique based on the simultaneous optimisation of Multi Leaf Collimator (MLC) shapes, dose rate

and gantry rotation speed [21]. The VMAT plan relates to delivery of a single or double arc which moves around the patient's body. In this work, the effect of the dosimetric difference between CT based and CBCT based VMAT planning in three different patient scenarios, namely brain, prostate (pelvic region) and head and neck (HN) were studied.

4.2 Materials and Methods

4.2.1 Hounsfield unit (HU) comparison between CT and CBCT images

For the comparison of HU between CT and CBCT images a Catphan 504 phantom (The Phantom Laboratory, Salem, NY) was used. The Catphan contains seven different materials which are: air (0 gm/cm^3), polymethylpentene (PMP) (0.83 gm/cm^3), low density polyethylene (LDPE) (0.92 gm/ cm^3), Polystyrene (1.05 gm/cm^3), Acrylic (1.18 gm/cm^3), Delrin (1.41 gm/cm^3) and Teflon (2.16 gm/cm^3) [22]. The HU values of these materials approximately range from -1000HU to +1000HU. CT images of the Catphan were acquired using a GE Light-speed CT simulator (GE Medical Systems, Milwaukee, WI). These images were imported to Eclipse (Varian Medical Systems, Palo Alto, CA, Version-10) treatment planning system. CBCT images for this study were generated using a kV X-ray tube and an amorphous silicon detector (aSi500, PortalVi-sion, Varian Medical systems) mounted on Varian Clinac iX linear accelerator, called OBI. The system is attached to the machine through a robotically controlled arm. Using this system, CBCT can be acquired in two modes: full-fan mode and half-fan mode. As per the manufacturer's suggestion, an additional filter called 'Bow-Tie' filter is used to increase the image quality. There are two filters, namely full Bow-Tie and half Bow-Tie, used for the full-fan mode and half-fan mode respectively. CBCT images of the Catphan were acquired for half-fan mode (CBCT_{HF}) and full-fan mode (CBCT_{FF}) with appropriate filters.

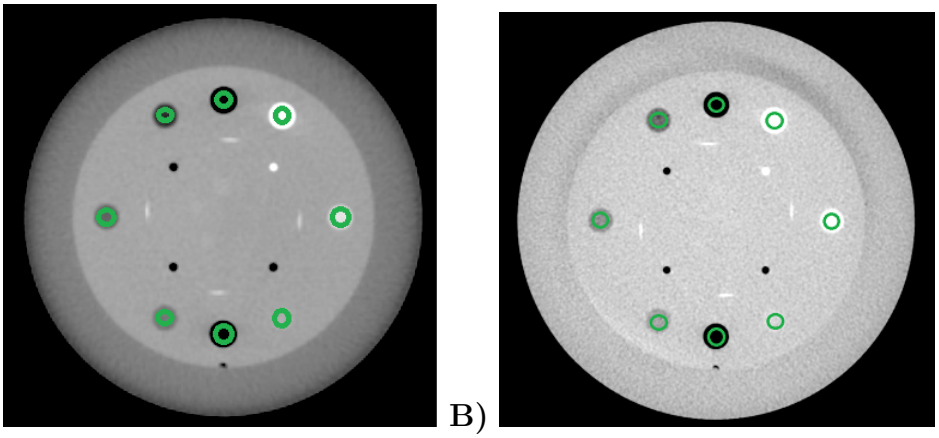

Figure 4.1: A) Axial slice of Catphan acquired with the full-fan and B) half-fan mode CBCT with area of interest for each of the seven material inserts

The HU values for the CT and CBCT images of the Catphan were analysed at different areas of interest (AOI) defined on the seven materials (Figure 4.1). The mean HU of CT and CBCT for these materials were measured and compared. Then, new HU-relative electron density curves were generated for CBCT_{HF} and CBCT_{FF}. The differences in the HU of CT and CBCT were analysed using these curves. After that, the HU variations along the horizontal and vertical axes of the phantom were evaluated.

4.2.2 Validation of the CT and CBCT based VMAT plans using Catphan

The dosimetric variations of the CT and CBCT based VMAT plans were assessed by using Catphan. Using the Eclipse treatment planning system, the different hypothetical structures were delineated on the CT images of the Catphan (Figure 4.2). These structures mimic the organs at risk (OAR) in a brain tumour patient. Here eight hypothetical OARs were contoured, which included Right (RT) Eye (magenta), RT Lens (cyan), Left (LT) Eye (yellow), LT Lens (orange), RT optic nerve (blue), LT optic nerve (green), Chiasm (pink) and Brainstem (brown). In addition a 2 cm radius ring R_1 (red) was contoured on this image to indicate the planning target volume (PTV). To study the dose variations outside the PTV, a

A) 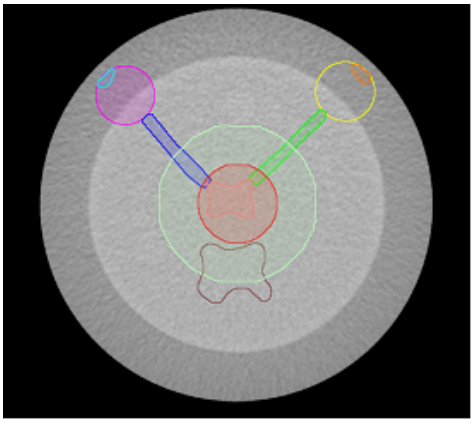 B) 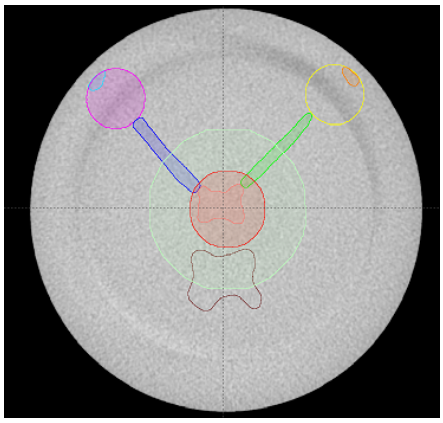

Figure 4.2: A) CT B) CBCT images of the Catphan with hypothetical structures RT Eye (magenta), RT Lens (cyan), LT Eye (yellow), LT Lens (orange), RT optic nerve (blue), LT optic nerve (green), Chiasm (pink) Brainstem (brown) , R_1(red) and R_2 (light green).

4 cm radius ring R_2 (light green) around the ring R_1 was generated. Whole CT structure set is copied onto the CBCT images to generate the same hypothetical structures.

Barker JL Jr. et al. reported that over the course of treatment, the relative median loss in gross tumor volume was about 69.5% and hence significant anatomic changes were found throughout the fractionated radiotherapy in HN patients [6]. These types of changes potentially affect the delivered dose, and the variation in VMAT plans due to them can be evaluated using the Catphan. Body of the Catphan was reduced by 0.5 cm ($CBCT_{SH0.5cm}$, $CT_{SH0.5cm}$) and then by 1 cm ($CBCT_{SH1cm}$, CT_{SH1cm}) using Eclipse treatment planning system and new CT and CBCT images were created (Figure 4.3). The percentage variations of the dosimetric parameters in VMAT plans on these images were evaluated.

A single arc VMAT plan was generated for PTV R_1 using Eclipse treatment planning system with a full arc (6MV photon beam) from gantry angle 179^0 to 181^0 and a collimator rotation of 30^0. The plan was optimized using Progressive Resolution Optimizer (PRO) algorithm with a prescription dose of 54Gy in 30 fractions. The Anisotropic Analytical Algorithm (AAA), which is a photon dose calculation algorithm, was used for the dose calculations with voxel resolution of $0.25 \times 0.25 \times 0.25\ cm^3$. Initially a VMAT plan was created on the CT images of

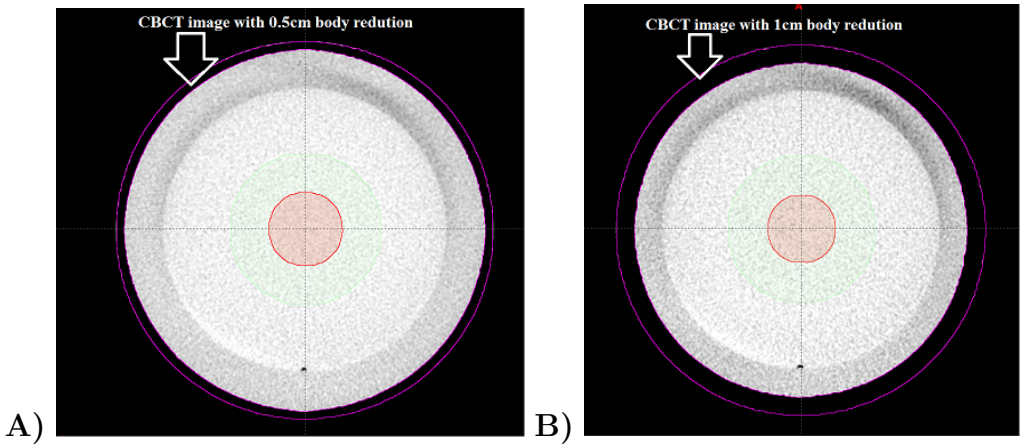

Figure 4.3: A) Axail CBCT images of the Catphan with 0.5 cm body reduction and B) with 1 cm body reduction

the Catphan and this same plan was transferred to CBCT images of the phantom iso-centrically. For the dose calculation in CBCT, the same HU-relative electron density curve generated for the commissioning of the Eclipse planning system was used.

Three points on the Dose volume histogram (DVH) - $D_{5\%}$ (dose to 5% of the volume), $D_{50\%}$ (dose to 50% of the volume) and $D_{95\%}$ (dose to 95% of the volume) were evaluated for structures R_1 and R_2. The relative percentage of difference (ΔD(%)) between CT and CBCT based VMAT plans were examined. The hypothetical critical structures were also analyzed based on the DVH data. $D_{1\%}$ (dose to 1% of the volume), D_{max} (maximum dose to the critical structure) and D_{mean} (mean dose to the critical structure) of these structures were studied and corresponding ΔD(%)s were calculated. Low et al introduced a method which compares the measured and calculated dose distributions using the gamma quality index [23]. It uses the distance to agreement (Δd_M) and the dose difference (ΔD_M) dose comparison criteria. The same evaluation criteria can be used to compare the variations in the dose distributions between CT and CBCT VMAT plans in our study. If the CT dose is D_{CT} and CBCT dose is D_{CBCT} then gamma quality index (γ) at each point of the CBCT dose distribution is

given by

$$\gamma(r_{CBCT}) = min\{\Gamma(r_{CBCT}, r_{CT})\}\forall\{r_{CT}\}$$

$$\Gamma(r_{CBCT}, r_{CT}) = \sqrt{\frac{r^2(r_{CBCT}, r_{CT})}{\Delta d_M^2} + \frac{\delta^2(r_{CBCT}, r_{CT})}{\Delta D_M^2}}$$

Where,

$$r(r_{CBCT}, r_{CT}) = |r_{CT} - r_{CBCT}|$$

and

$$\delta(r_{CBCT}, r_{CT}) = D_{CT}(r_{CT}) - D_{CBCT}(r_{CBCT})$$

.

When $\gamma(r_{CBCT}) \leq 1$, the calculation is considered as passed whereas if $\gamma(r_{CBCT}) \geq 1$, then it is failed. Here, we use three gamma criterions for the evaluation purpose: ΔD_M=3% dose in Δd_M=3mm distance (3mm-3%), ΔD_M=2% dose in Δd_M=2mm distance (2mm-2%) and ΔD_M=1% dose in Δd_M=1mm distance (1mm-1%) on three consecutive axial, sagittal and coronal iso-centric planes of the CT and CBCT based VMAT plans. The gamma evaluation of the the VMAT plans were done using the Omnipro-I'mRT software (IBA Dosimetry, Germany).

4.2.3 Study of CT and CBCT based VMAT plans using Patient's image

In order to assess the VMAT dose calculation accuracy of the CBCT and CT images, 27 patients treated in our clinic were selected. These included 10 prostate, 10 brain and 7 HN tumour patients. The patients, whose data set of the body contour exceeded the field of view (FOV) of the CBCT, were excluded from the study. For treatment planning, CT images of the patients were acquired from the GE CT simulator using either of the two protocols: the "head scan" mode with 140 kVp, 120 mA and 2.5 mm slice thickness was used for the brain and HN patients, while the "pelvis for fracture" mode with 120 kVp, 550 mA and 2.5 mm slice thickness was used for the prostate patients. For the CBCT image acquisition in HN and brain cancer cases, full-fan mode with full-bowtie filter (100 kVp, 20 mA) was used. While in the prostate cancer patients, the half-fan mode with half-bowtie filter (110 kVp, 20 mA) was used. Weekly CBCT images of these patients were acquired for the set up purpose. The CBCT images of those patients with minimal anatomical and organ volume variations in comparison with planning CT were selected. This is because, this method of study concentrates on the dose difference comparison in the use of CT and CBCT images due to HU variations rather than on volumetric changes. For the treatment purposes, the VMAT plans were generated using Eclipse planning system as described in the section 4.2.2.

The prostate cancer patients were treated with 70 Gy in 28 fractions, while the brain and HN patients were treated with 60 Gy in 30 fractions and 70 Gy in 33 fractions respectively. For the prostate and HN patients, VMAT plans were generated with two complimentary full arcs with gantry rotation from 179^0 to 181^0 and collimator rotations of 30^0 and 330^0 whereas only single arc plans were used for the brain cases. In the case of prostate patients, two PTVs were delineated on planning CT: PTV-70Gy for the whole prostate and PTV-50.4Gy for the nodal regions. Further, OARs like bladder, rectum, bowel etc. were contoured. The brain tumour patients were planned with PTV-60Gy and the

OARs (RT Eye, RT Lens, LT Eye, LT Lens, RT optic nerve, LT optic nerve, Chiasm and Brainstem) were countered. Three PTVs (PTV-70Gy, PTV-60Gy and PTV-54Gy) with OARs (RT Parotid, LT Parotid, Spinal cord and mandible etc) were delineated for the HN patients. In all the cases, both the VMAT based plans and the contours were transferred to the CBCT images and the dose was recalculated using AAA algorithm. The dosimetric differences between the CT and CBCT based plans were assessed using DVH. The ΔD(%) at $D_{5\%}$, $D_{50\%}$ and $D_{95\%}$ of the PTVs for the two VMAT plans were evaluated using DVH comparisons. Further, ΔD(%) at different dosimetric parameters ($D_{5\%}$, $D_{50\%}$ and D_{mean}) were evaluated for critical organs like bladder and rectum of the prostate patients, while ΔD(%) at $D_{1\%}$, D_{max}, and D_{mean} were assessed for critical structures of the brain and HN patients. Those OARs coming outside the FOV of the CBCT were excluded from the study. For further validation of the dose calculations performed on CBCT, a quantitative evaluation was done in the region of interest (enclosing PTV and OAR, excluding border areas) using OmniPro I'mRT. Gamma criteria, as mentioned in section 4.2.2, was used to evaluate the VMAT plans in patients also.

4.3 Results

4.3.1 Hounsfield unit comparison between CT and CBCT images

The comparison between HU-relative electron density calibration curves for the CT and CBCT half-fan and full-fan modes is depicted in figure 4.4. No significant differences in the calibrations were noted over the considered range of HUs. The variations in the HUs of the inserts for the two modes of CBCT were less than 20 HU, except in the cases of Air, Delrin and Teflon inserts. The maximum relative differences were 6%, 7% and 8% for Air, Delrin and Teflon inserts respectively among which the maximum variation was observed in Teflon which was 74 HU

in $CBCT_{FF}$ and 69 HU in the $CBCT_{HF}$. Similarly, the HU variation in Delrin was 20 HU to 26 HU in the two modes. The HU difference in the case of Acrylic varied from 7 HU to 10 HU while that for the Polystyrene was almost a constant for the two modes. The relative percentage difference was less than 5% for LDPE and PMP. Figure 4.5 shows the line profile comparison between CT and CBCT images. A vertical line and a horizontal line were plotted and HU variations along these lines, between CT and CBCT, were as shown in the figure 4.5. The line comparison shows that there is a good correlation between the CT and CBCT in terms of HU values. However there were some significant discrepancies in the values near the edges of the phantom.

4.3.2 Validation of the CT and CBCT based VMAT plans using Catphan

Figures 4.6A and 4.6B show the VMAT isodose distributions on a homogenous section of the Catphan phantom, calculated using the CT and CBCT (Half-fan) images. The hypothetical structures are visible in the figures. A good correlation at higher and lower isodose lines can be visualized from these figure. The maximum dose was observed to be 102% in CT and 103% in CBCT. By analyzing the DVH of the hypothetical structures (Figure 4.7), it can be seen that the dosimetric parameters are nearly identical in both cases. The corresponding DVH curves for the rings R_1 and R_2 and for the critical structures were nearly overlapping. The dosimetric comparisons between CT and CBCT are shown in Table 4.1. The three dosimetric points on the DVH, $D_{5\%}$, $D_{50\%}$, and $D_{95\%}$, are seen to be in good agreements for the rings R_1 and R_2. The maximum difference between CT and CBCT images was observed at $D_{50\%}$ of the R_2, which was 1.3%. For the same structures, when the body of the Catphan was reduced by 0.5 cm ($CBCT_{SH0.5cm}$), the maximum ΔD(%) became 2.2%. This dose difference was quite matching with the results of the comparison of the CT and reduced body CT ($CT_{SH0.5cm}$), which shows that CBCT image dose calculations are reproducible even if the body size is reduced. When the body of the CBCT

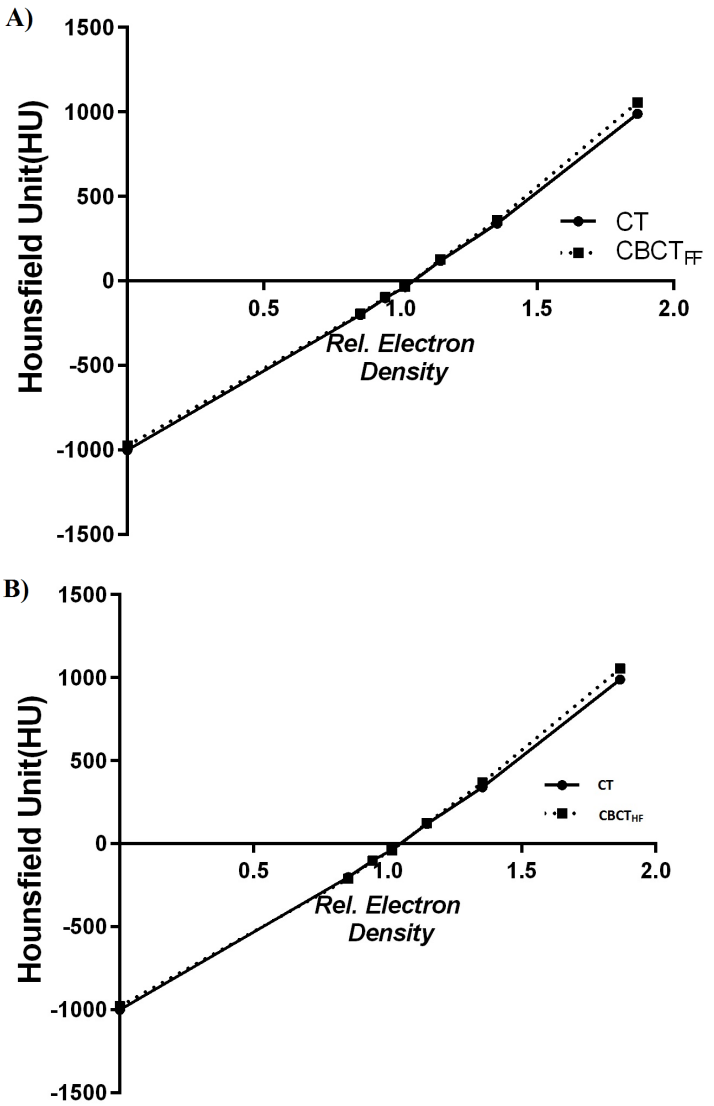

Figure 4.4: The Hounsfield Unit (HU)- relative electron density curves for the CT compared with A) CBCT full-fan mode ($CBCT_{FF}$) and B) CBCT half-fan mode ($CBCT_{HF}$).

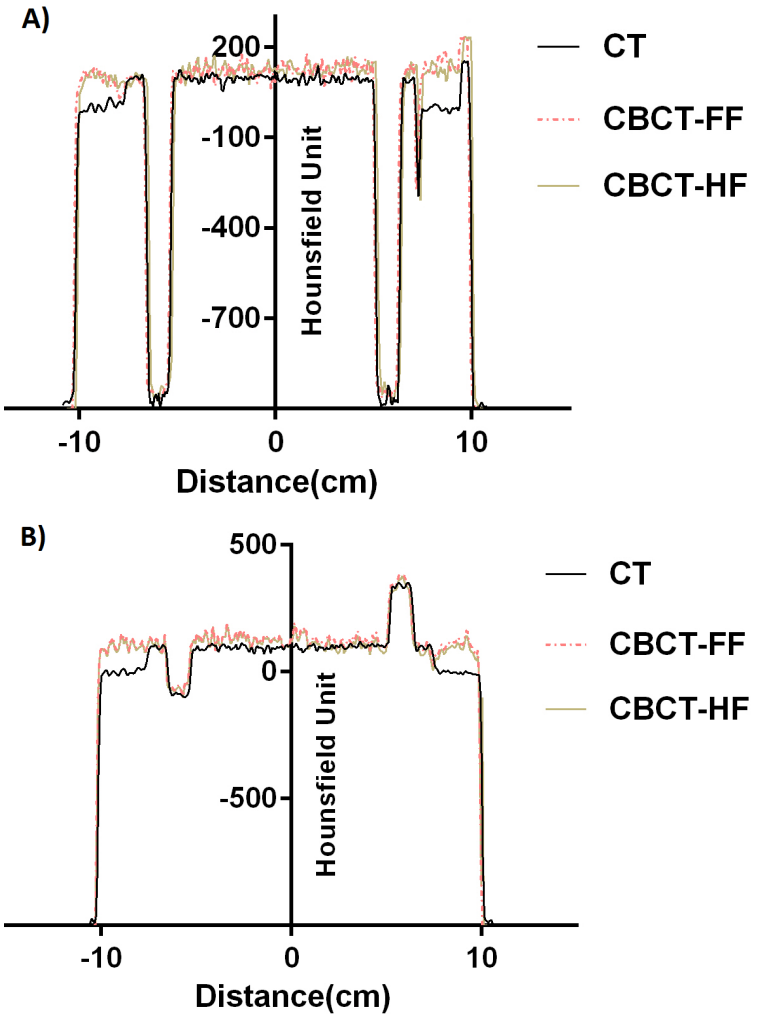

Figure 4.5: A) The vertical Hounsfield Unit (HU) profiles along the lines top to bottom for the $CBCT_{HF}$, $CBCT_{FF}$ and CT. B) The horizontal Hounsfield unit (HU) profiles along the lines right to left for the $CBCT_{HF}$, $CBCT_{FF}$ and CT.

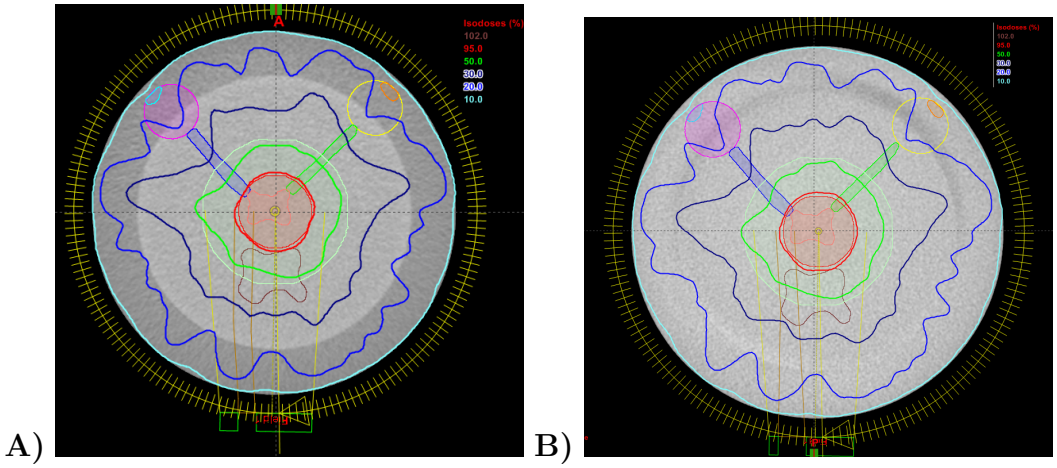

Figure 4.6: Single VMAT dose distributions on the axial slice with A) CT-based and B) the planning CBCT-based dose calculations.

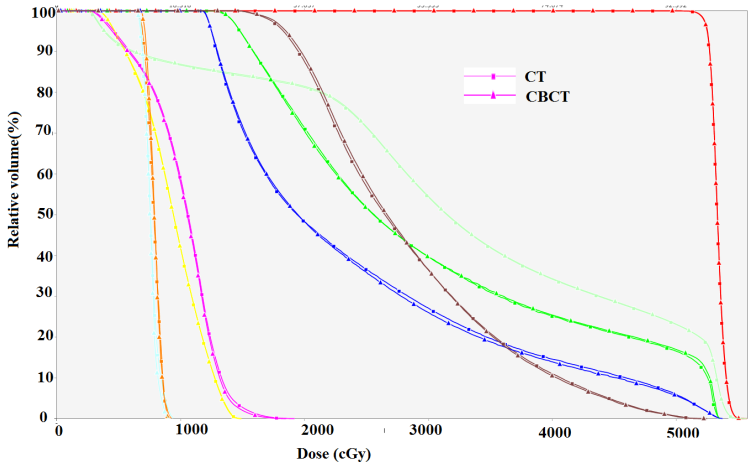

Figure 4.7: Dose volume histograms of the hypothetical structures for CT and CBCT based VMAT plans on the Catphan

was reduced by 1 cm ($CBCT_{SH1cm}$), the maximum ΔD(%) was noticed at $D_{5\%}$ (4.6%). As above, the results matched with ΔD(%) of CT and CT_{SH1cm}.

The dosimetric parameters of the hypothetical critical structures are summarized in Tables 4.2 and 4.3. The ΔD(%) between CT and CBCT at three points, namely $D_{1\%}$, D_{max} and D_{mean}, of the hypothetical critical structures were less than 1.9%. The ΔD(%) between CT and $CBCT_{SH0.5cm}$ for these structures was less than 2.6%. This ΔD(%) was comparable with that of CT and $CT_{SH0.5cm}$. The ΔD(%) between CT and $CBCT_{SH1cm}$ was less than 4.9%. Dosimetric parameters of the RT and LT lenses were not evaluated in reduced CT and CBCT

Comparison of VMAT Plans	ΔD(%) of $RingR_1$			ΔD(%) of $RingR_2$		
	$D_{5\%}$	$D_{95\%}$	$D_{50\%}$	$D_{5\%}$	$D_{95\%}$	$D_{50\%}$
CT and CBCT	0.06	0.03	0.04	0.04	0.16	1.31
CT and $CBCT_{SH0.5cm}$	2.2	2.1	2.1	2.2	2.1	2.2
CT and $CT_{SH0.5cm}$	2.1	2.1	2.0	2.1	1.9	2.0
CT and $CBCT_{SH1cm}$	4.6	4.5	4.5	4.6	4.5	4.3
CT and CT_{SH1cm}	4.5	4.3	4.4	4.4	4.4	4.1

Table 4.1: The percentage of dose differences in the dosimetric parameters of rings R_1 and R_2 in VMAT plans calculated using CT, CBCT and reduced body images.

Comparison of VMAT Plans	ΔD(%) of Brainstem			ΔD(%) of Chaism		
	$D_{1\%}$	D_{max}	D_{mean}	$D_{1\%}$	D_{max}	D_{mean}
CT and CBCT	0.4	1.9	0.2	0.3	0.2	0.1
CT and $CBCT_{SH0.5cm}$	2.1	2.6	2.3	2.1	2.1	2.2
CT and $CT_{SH0.5cm}$	2.1	2.6	2.1	2.0	2.1	2.1
CT and $CBCT_{SH1cm}$	4.4	4.9	4.2	4.5	4.3	4.6
CT and CT_{SH1cm}	4.6	4.7	4.1	4.4	4.4	4.5

Table 4.2: The percentage of dose differences in the dosimetric parameters of the hypothetical Brainstem and Chaism in VMAT plans, calculated using CT, CBCT and reduced body images of Catphan.

images because in this case, the positions of these structures extend beyond the reduced body. The 3mm-3% gamma pass rates of the dose calculation on the axial, sagittal and coronal iso-centric plans were 99%, 98% and 97% respectively, while the 2mm-2% gamma for the same planes were reduced to 97%, 96% and 95% respectively. The 1mm-1% pass rates were less than 90% in the three planes.

4.3.3 Study of CT and CBCT based VMAT plans using Patient's image

Table 4.4 shows the mean and standard deviation (SD) in ΔD(%) of the PTVs in the prostate, brain and HN patients calculated on the CT and CBCT images. The ΔD(%) of the three parameters $D_{5\%}$, $D_{50\%}$ and $D_{95\%}$ are with in 3.2% for PTV-70Gy and 2.6% for PTV-50.4Gy in the prostate patients. However, the ΔD(%) of the above three parameters are with in 2.2% in brain patients. The

Comparison of VMAT Plans	ΔD(%) of RT optic nerve			ΔD(%) of LT optic nerve		
	$D_{1\%}$	D_{max}	D_{mean}	$D_{1\%}$	D_{max}	D_{mean}
CT and CBCT	0.1	0.5	0.8	0.17	0.0	0.2
CT and $CBCT_{SH0.5cm}$	2.2	2.1	1.8	2.4	2.4	2.2
CT and $CT_{SH0.5cm}$	2.3	2.3	2.0	2.2	2.4	1.9
CT and $CBCT_{SH1cm}$	4.8	4.3	3.9	4.6	4.6	4.3
CT and CT_{SH1cm}	4.6	4.4	4.0	4.6	4.7	4.4

Table 4.3: The percentage of dose differences in the dosimetric parameters of the hypothetical RT optic nerve and LT optic nerve in VMAT plans, calculated using CT, CBCT and reduced body images of Catphan.

maximum variation in ΔD(%) at PTV-70Gy, PTV-60Gy and PTV-50.4Gy are found to be 7% ($D_{50\%}$), 6% ($D_{50\%}$) and 4% ($D_{5\%}$) respectively in HN patients. Figure 4.8 shows the mean and the SD in ΔD(%) of different dosimetric parameters ($D_{5\%}$, $D_{50\%}$ and D_{mean}) for the bladder and rectum in the prostate patients. The maximum dose difference is observed in the D_{mean} of the rectum which is $2.3\% \pm 0.2\%$. Similarly, the mean and SD of the ΔD(%) at different dosimetric parameters ($D_{1\%}$, D_{mean} and D_{max}) in the CT and CBCT images of the critical structures in the brain and HN patients are shown in figures 4.9A and 4.9B. The maximum mean dose difference observed for the $D_{1\%}$, D_{max} and D_{mean} is $1.5\% \pm 0.4\%$ in RT optic nerve, $1.6\% \pm 0.8\%$ in RT optic nerve and $1.8\% \pm 0.7\%$ in LT optic nerve respectively in brain patients while the maximum variation in HN cases are seen for the spinal cord and mandible which are above 6%.

The average gamma pass rate with VMAT dose comparison on the CT and CBTC images in the three iso-centric planes for the 10 prostate, 10 brain and 7 HN patients are depicted in figures 4.10A, 4.10B and 4.10C respectively. The average 3mm-3% gamma pass rate for the prostate patients was found to be 96%±0.06%, while that of 2mm-2% gamma is reduced by 5% and the 1mm-1% gamma is $75.2\% \pm 0.5\%$. The 3mm-3%, 2mm-2% and 1mm-1% gamma was 97%±0.2%, 88.8%±0.06% and 76.6%±0.09% respectively for the brain patients and $93.3\% \pm 1.1\%$, $79\% \pm 6\%$ and $60\% \pm 6\%$ respectively for the HN patients.

Dosimetric parameters	Mean and standard deviations of ΔD(%)					
	PR PTV-70Gy	PR PTV-50.4Gy	BR PTV-60Gy	HN PTV-70Gy	HN PTV-60Gy	HN PTV-54Gy
$D_{5\%}$	$1.5\% \pm 1.0\%$	$1.0\% \pm 0.6\%$	$0.7\% \pm 0.76\%$	$2.7\% \pm 3.0\%$	$2.6\% \pm 2.2\%$	$1.8\% \pm 1.5\%$
$D_{50\%}$	$1.3\% \pm 0.7\%$	$1.6\% \pm 0.7\%$	$1.1\% \pm 0.58\%$	$2.2\% \pm 2.4\%$	$2.0\% \pm 1.9\%$	$1.1\% \pm 0.3\%$
$D_{95\%}$	$1.4\% \pm 0.9\%$	$1.4\% \pm 0.8\%$	$0.9\% \pm 0.58\%$	$2.9\% \pm 3.2\%$	$2.9\% \pm 1.3\%$	$1.4\% \pm 1.0\%$

Table 4.4: The mean and standard deviations of the ΔD(%) in PTVs of the prostate (PR), brain (BR), Head and neck (HN) patients

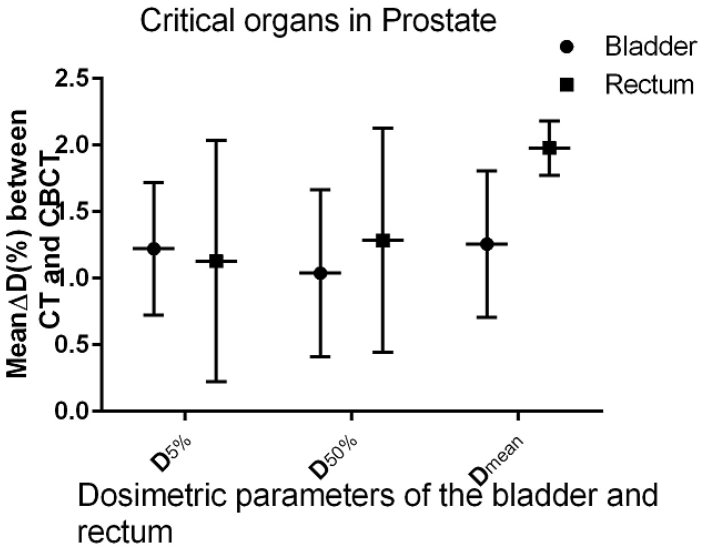

Figure 4.8: Mean and standard deviations of the ΔD(%) between CT and CBCT at $D_{5\%}$, $D_{50\%}$ and D_{mean} of Bladder and Rectum.

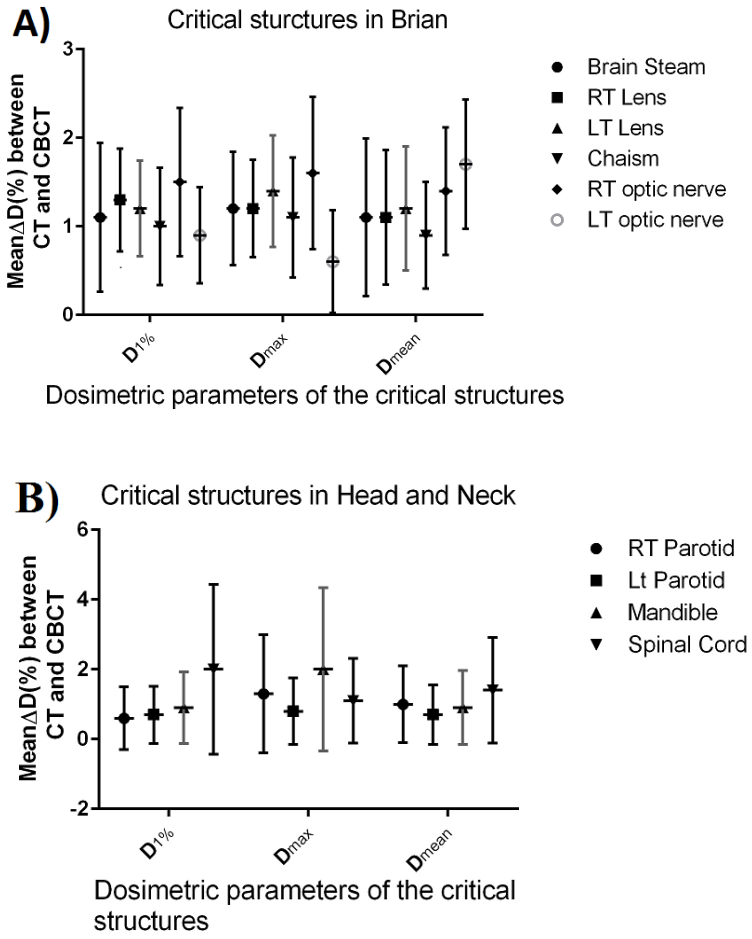

Figure 4.9: A) Mean and standard deviations of the ΔD(%) between CT and CBCT at $D_{1\%}$, D_{mean} and D_{max} of different critical structures in Brian B)Head and neck cases.

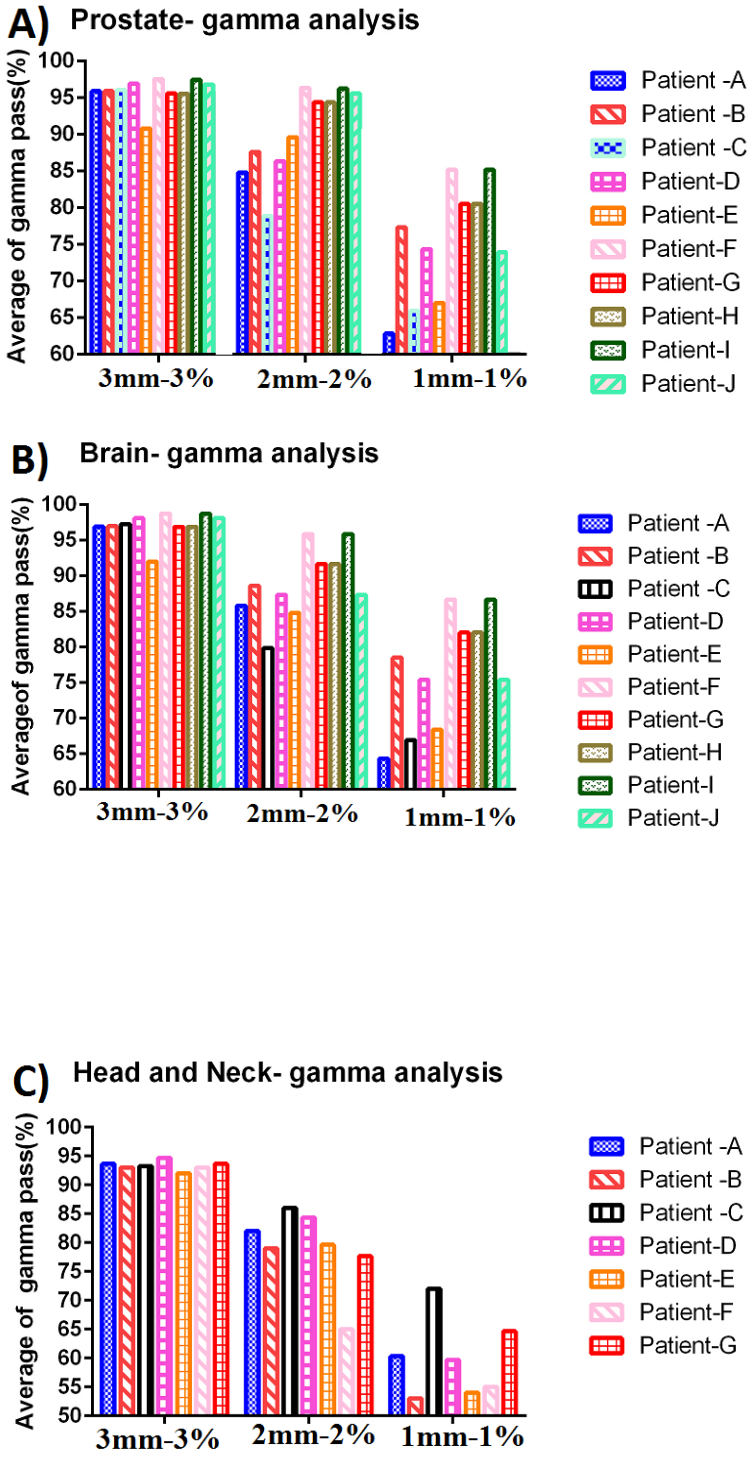

Figure 4.10: Average gamma pass rates for A) prostate, B) brain, and C) Head and neck patients.

4.4 Discussion

The adaptive radiotherapy has now become a main area for discussion due to the large number of recent research activities in the field of imaging and treatment planning. The CBCT images have become an important tool for the adaptive planning process and it also helps the physician to evaluate the dosimetric changes due to organ deformation or tumor shrinkage. A large dose gradient always exists between the tumor site and the critical structure in the VMAT plans and so volumetric changes as mentioned above in turn create a potential change in the dose received on the critical structure. Jin et al studied the usefulness of the CBCT images based VMAT plan adaptation in nasopharyngeal tumor patients and found that there was a reduction of 4.5 cm^3 in parotid volume during the course of treatment and as a result, the dose received was increased up to 8.8% than the planned value [24]. CBCT can be used to monitor such changes on a daily basis and reconstruct the dose apart from providing actual set up information of the patient. Overall, it helps the physicians to decide whether re-planning CT is required or not. In this work, we use the pre-treatment CBCT images acquired during the course of treatment for the VMAT planning and try to compare the dosimetric parameters obtained with that of the original planning CT images. A Catphan phantom was used to assess the HU variation in the CBCT images.

Several authors have studied HU variations in the CBCT images generated from the Varian OBI using the Catphan phantom [8, 12, 14, 16, 25]. Yoo and Yin had found that the maximum relative HU difference in the CBCT images of the Catphan was observed in Teflon [8]. Similarly, the studies of Lee et al also showed that maximum difference was in air and Teflon [14]. Our findings also matched with their results. The line profile comparison in our study revealed that the maximum variation was observed in the peripheral regions of the phantom, which was also confirmed by the studies of Ding et al [16]. Yang et al also noted some significant inaccuracies near the edges of the phantom [12]. They also noticed considerable HU variation in the CBCT images when increasing the

size of the phantom which was due to the increased magnitude of the scatter radiations. But our studies on the phantom reveal that, the variation in the HU of the CBCT has only a very negligible effect on the VMAT dose calculation. This fact is supported by Thomas in his study stating that 8% difference in electron density results only in 1% difference in dose calculation [26]. Lee et al conducted a similar testing with the IMRT dose calculation on the Catphan CBCT images and found a dose difference of less than 1%. We have used the same approach as Lee et al for the VMAT dose calculation on the CBCT without applying any correction factor on the images.

The dosimetric parameters of the hypothetical structures in the two plans also showed a good correlation. DVHs of the hypothetical targets were also in concurrence (Figure 4.7). Qian et al performed a similar VMAT dose calculation on the Catphan and found that the difference in the maximum dose of the PTV was 1.3% and that in the mean dose was 0.7% [25] which was in accordance with our result. The 3mm-3% gamma pass rates of the CBCT and CT based VMAT dose calculation in phantom plans were within 97%. However, it is noteworthy that when the stringent gamma criterion (1mm-1%) was used, the pass rate dropped to 90%. The ΔD(%) between $CBCT_{SH0.5cm}$ and $CBCT_{SH1cm}$ when compared with CT gave almost the same results when $CT_{SH0.5cm}$ and CT_{SH1cm} were compared with the normal CT. Evaluations of these results show that, CBCT could be directly used in the dose reconstruction of VMAT plans.

After the study on phantom, the CBCT images based VMAT dose calculation in different clinical situations was evaluated. For our study, we have selected 10 brain, 10 prostate and 7 HN patients from our clinic and investigated the viability and accuracy of using CBCT to do dosimetry in VMAT treatments. In contrast to the phantom study, there was a notable variation between CT and CBCT images of the patient because of various reasons like organ deformation, difference in patient position from the CT simulation position and discrepancies while copying the contoured structures from CT to CBCT [16]. The dose calculation also showed more divergence when greater inhomogeneity was involved

[8, 15], especially in HN and lung cases where the effect of scatter significantly influence the quality of the image. These issues make it difficult to assess the accuracy of the CBCT based dose calculation. However, we have found that in the brain and prostate cases, the CBCT based doses agree with CT based calculation to within 3% and here the 3mm-3% gamma pass rates were above 95%. Hence, in most of the brain and prostate cases, the CBCT images can be used directly for dosimetric validation. Yang et al [12] also reported a comparable result for the prostates, as their variation in dose calculated on the unmodified and modified CBCT agreed within 2%.

In HN cases, we have found the difference in dosimetric parameters has gone up to 7%. Here the average 3mm-3% gamma pass rates also reduced to 93%. Similar findings can be observed in the recent analysis of CBCT based treatment panning by Chen et al.[27]. They have analyzed the dose calculation accuracy on CT-based and CBCT-based IMRT and VMAT plans for four types of treatment sites which included HN, lung, pancreas and pelvis and a lower gamma pass rate was found in the HN region. Rong et al, in their study, noted that the maximum HU variation appeared in the lungs and dense bone regions compared to those closer to tissue [28]. We have also found large deviations in the dose in the mandible and spinal cord regions, which was above 6%. This points out that, in the HN regions with large inhomogeneities, the dose calculation accuracies clearly deteriorate compared to other sites. VMAT plans use AAA algorithm for dose calculations which have a lower gamma pass rate than the pencil beam convolution (PBC) algorithm, as reported by Ali et al [29]. These facts necessitate the correction process in HU variations before it is used for dose calculation when inhomogeneous regions are involved. van Zijtveld et al used a mapping method where the HU of the CT was mapped to the CBCT in the HN patients and they achieved a dose accuracy of 1% and attained a pass rate of 92% to 95% in the 2mm-2%. As the HU number greatly depends on the acquisition techniques in Elekta XVI system, the use of patient specific HU to electron density table for pelvis, thorax and head reduces the inaccuracies in the

CBCT based plans [11].

The inferior quality of CBCT images, as compared to the conventional CT and Magnetic resonance imaging (MRI) where the critical structures are better visualized, may affect the delineation of the tumor. This can be especially seen in small critical structures like optic nerve and optic chiasm where a small change in the delineation drastically changes the organ dose. There are other factors like scatter, beam hardening and organ motions which affect the quality of the CBCT images. Moreover, the changes in shape and location of anatomical structures in the patient's body, such as the changes caused by tumor shrinkage or weight loss, also affect the accuracy of the image. This makes the usage of CBCT images directly for dose calculation a questionable issue in all sites especially in HN cases where greater inhomogeneity is involved. Another major limitation was because of the restricted FOV in the CBCT, due to which it was difficult to analyze more number of patients. This restricted our study to the dose calculation for certain types of patients. Some authors have tried to improve the FOV of the CBCT by taking the CBCT image acquisitions at different table positions [16, 25].

There are several methods to improve the quality of the CBCT images in which deformable image registration (DIR) technique is an important one. It attains an association between voxels in the CT and CBCT there by transferring the organ contours from the planning CT to daily CBCT. But it requires a robust DIR algorithm to achieve a greater accuracy. Even though DIR is said to be a clinically practical method for automatic contour propagation in adaptive radiotherapy, a thorough review by the physician is required [30, 31]. Another method to map the HU from CT to CBCT is by employing deformable electron density mapping (DEDM) using B-Spline deformable mode to produce modified CBCT images [12]. There is a different approach using DIR which modifies the CT image closely replicating the CBCT image, and using it for adaptive planning and calculating the "dose of the day" [32]. More detailed studies are required before implementing these techniques clinically. Further research is also needed to obtain a more reliable CBCT image with consideration for organ

motion. However, our study emphasizes the usefulness of using CBCT images obtained prior to treatment and at intervals during the prescribed course to simultaneously evaluate the dosimetric changes caused by changes in body cross sections, position and size of internal organs and structures and help in overall monitoring during the full course of treatment. In near future, information from the CBCT can be used for online treatment planning technique and to modify the daily dose delivered.

4.5 Conclusion

The accuracy of CBCT based VMAT plans was tested on the phantom and the patients. The results confirm that, the CBCT images can be used as a tool for assessing the daily dose variations. A small difference in HU was seen between the conventional CT and CBCT in the test phantom, especially at or near the edges. But the study proves that, this difference in HU has a negligible effect on the dose calculation. The study also indicates that the dosimetric accuracy of CBCT based VMAT dose calculation in prostate and brain patients is acceptable for the purpose of dosimetric evaluations, while that in HN patients needed to be corrected. It may be concluded that, the CBCT is reliable for reconstructing dose for assessing dosimetric variation for certain sites only.

References

[1] van Mourik A, van Kranen S, den Hollander S, Sonke JJ, van Herk M, van Vliet-Vroegindeweij C. (2011). Effects of setup errors and shape changes on breast radiotherapy. Int J Radiat Oncol Biol Phys, 79:1557-1564.

[2] Letourneau D, Martinez AA, Lockman D, et al. (2005). Assessment of residual error for online cone-beam CT-guided treatment of prostate cancer patients. Int J Radiat Oncol Biol Phys, 62:1239-1246.

[3] Polat B, Wilbert J, Baier K, et al. (2007). Nonrigid patient setup errors in the head-and-neck region. Strahlenther Onkol, 183:506-511.

[4] Bernchou U, Hansen O, Schytte T, Bertelsen A, Hope A, Moseley D, Brink C. (2015). Prediction of lung density changes after radiotherapy by cone beam computed tomography response markers and pre-treatment factors for non-small cell lung cancer patients. Radiother Oncol, 117(1):17-22.

[5] Boda-Heggemann J, Lohr F, Wenz F, Flentje M, Guckenberger M. (2011). kV cone-beam CT-based IGRT: a clinical review. Strahlenther Onkol, 187:284-291.

[6] Barker JL Jr, Garden AS, Ang KK, O'Daniel JC, Wang H, Court LE, Morrison WH, Rosenthal DI, Chao KS, Tucker SL, Mohan R, Dong L. (2004). Quantification of volumetric and geometric changes occurring during fractionated radiotherapy for head-and-neck cancer using an integrated CT/linear accelerator system. Int J Radiat Oncol Biol Phys, 59:960-970.

[7] Kreppel M, Drebber U, Eich HT, Dreiseidler T, Zoller JE, Muller RP, Scheer M. (2011). Combined-modality treatment in advanced oral squamous cell carcinoma: primary surgery followed by adjuvant concomitant radio chemotherapy. Strahlenther Onkol, 187:555-560.

[8] Yoo S, Yin FF. (2006). Dosimetric feasibility of cone-beam CT-based treatment planning compared to CT-based treatment planning. Int J Radiat Oncol Biol Phys, 66:1553-1561.

[9] van Zijtveld M, Dirkx M, Heijmen B. (2007). Correction of conebeam CT values using a planning CT for derivation of the "dose of the day". Radiother Oncol, 85:195-200.

[10] Hu W, Ye J, Wang J, Ma X, Zhang Z. (2010). Use of kilo voltage X-ray volume imaging in patient dose calculation for head-and-neck and partial brain radiation therapy. Radiat Oncol, 5:29.

[11] Richter A, Hu Q, Steglich D, Baier K, Wilbert J, Guckenberger M, Flentje M.(2008).Investigation of the usability of cone beam CT data sets for dose calculation. Radiat Oncol, 3:42.

[12] Yang Y, Schreibmann E, Li T, Wang C, Xing L. (2007). Evaluation of onboard kV cone beam CT (CBCT)-based dose calculation. Phys Med Biol, 52:685-705.

[13] Rong Y, Smilowitz J, Tewatia D, Tome WA, Paliwal B. (2010). Dose calculation on kV cone beam CT images: an investigation of the Hu-density conversion stability and dose accuracy using the site-specific calibration. Med Dosim, 35:195-207.

[14] Lee L, Le QT, Xing L. (2008). Retrospective IMRT Dose Reconstruction Based on Cone-Beam CT and MLC Log-File. Int J Radiat Oncol Biol Phys, 70:634-644

[15] Houser C, Nawaz AO, Galvin J, et al. (2006). Quantative Evaluation of Cone Beam CT Data Used for Treatment Planning. Medical Physics, 33:2285-2286.

[16] George X. Ding, Dennis M. Duggan, Charles W. Coffey, Matthew Deeley, Dennis E. Hallahan, Anthony Cmelak, Arnold Malcolm. (2007). A study on adaptive IMRT treatment planning using kV cone-beam CT. Radiotherapy and Oncology, 85:116-125.

[17] Lei Zhu, Yaoqin Xie, Jing Wang, Lei Xing. (2009). Scatter correction for cone-beam CT in radiation therapy. Med Phys, 36: 2258- 2268.

[18] Ruhrnschopf EP, Klingenbeck K. (2011). A general framework and review of scatter correction methods in x-ray cone-beam computerized tomography. Part 1: scatter compensation approaches. Med Phys, 38:4296-4311.

[19] Niu T, Sun M, Star-Lack J, Gao H, Fan Q, Zhu L. (2010). Shading correction for on- board cone-beam CT in radiation therapy using planning MDCT images. Med Phys, 37:5395-5406.

[20] Niu T, Al-Basheer A, Zhu L. (2012). Quantitative cone-beam CT imaging in radiation therapy using planning CT as a prior: first patient studies. Med Phys, 39:1991-2000.

[21] Otto K. (2008). Volumetric modulated arc therapy IMRT in a single gantry arc. Med Phys, 35:310-7.

[22] Phantom Laboratory Catphan 504 Manual. (2006). Green- wish, NY, The Phantom Laboratory, Inc.

[23] Low D A, Harms W B, Mutic S, Purdy J A. (1998). A technique for the quantitative evaluation of dose distributions Med. Phys, 25:65661

[24] Jin X, Hu W, Shang H, Han C, Yi J, Zhou Y and Xie C. (2013). CBCT-based volumetric and dosimetric variation evaluation of volumetric modu-

lated arc radiotherapy in the treatment of nasopharyngeal. Radiation Oncology, 8:279.

[25] Qian J, Lee L, Liu W, et al. (2010). Dose reconstruction for volumetric modulated arc therapy (VMAT) using cone-beam CT and dynamic log files. Phys.Med. Biol, 55:3597-3610.

[26] Thomas S J. (1999). Relative electron density calibration of CT scanners for radiotherapy treatment planning Br. J. Radiol, 72:7816.

[27] S Chen, Q Le, Y Mutaf, B Yi, W D'Souza. (2015). Dosimetric Study of Cone-Beam CT-Based Radiation Treatment Planning Using a Patient-Specific Stepwise CT-Density Table Med. Phys, 42:3280.

[28] Y Rong, D Tewatia B Paliwal. (2007). Evaluation of Kilo-Voltage Cone Beam CT Image Quality in Context to Dose Re-Computation. Med. Phys, 34:2334.

[29] I Ali, S Oyewale S Ahmad. (2011). Quantitative Assessment of Dose Differences Between CT and Cone-Beam CT Using Pencil Beam Convolution and Analytical Anisotropic Algorithms. Med. Phys, 38:3500.

[30] Hardcastle N, Elmpt W Van, Ruysscher D De, Bzdusek K and Tom WA. (2013). Accuracy of deformable image registration for contour propagation in adaptive lung. Radiation Oncology, 8:243.

[31] Zhang T, Chi Y, Meldolesi E and Yan D. (2007). Automatic delineation of on-line head and neck computed tomography images: toward on-line adaptive radiotherapy. Int J Radiat Oncol Biol Phys, 68:522-530.

[32] C.Veiga, J. Mcclelland, S. Moinuddin, A. Loureno, K. Ricketts, J. Annkah, M. Modat, S. Ourselin, D. D'souza, and G. Royle. (2014). Toward adaptive radiotherapy for head and neck patients: Feasibility study on using CT-to-CBCT deformable registration for "dose of the day" calculations. Med Physics, 41:031703-12

Chapter 5

Study of impacts of different evaluation criteria on gamma pass rates in VMAT QA using MatriXX and EPID

5.1 Introduction

Recently, the volumetric-modulated arc therapy (VMAT) has become a widely accepted technique for treatment delivery in radiotherapy as it produces highly conformal plans and delivers it in a short time [1-2]. VMAT is a complex delivery technique that produces the dose distribution by the real-time variation of three parameters: dose rate, the gantry speed and the positions of the multi-leaf collimator (MLC) [3]. In intensity-modulated radiotherapy (IMRT), MLC is the only varying parameter; however the level of complexity in VMAT is increased because the gantry speed and the dose rate also change during treatment delivery. The real-time correlation between these parameters is inevitable during VMAT delivery because any variation generates a potential error [4]. The MLC plays a vital role in VMAT delivery and thus, any error in the MLC position creates

an over- or under-dose during treatment [5]. Considerable differences also exist between the optimization processes of VMAT and IMRT, which complicates VMAT plans. In VMAT, the treatment planning system (TPS) uses a series of discrete control points during the optimization process and a continuous real-time interpolation between these control points is required during the delivery [6]. These factors necessitate stringent quality assurance (QA) to be performed before treatment delivery.

Among the several commercially available devices employed for the VMAT QA, two-dimensional (2D) arrays are the most widely used. The diode-detector-based MapCHECK (Sun Nuclear Corporation, US) [7], the ion-chamber based Seven29 2D array (PTW, Germany) [8, 9], and MatriXX (IBA Dosimetry, Germany) [10-14] are commonly used commercial 2D detector arrays. The MatriXX array has a linear response with dose and it is independent of energy [12]. Additionally, the system provides results comparable with those of the film and various point dose detectors [15, 16]. However, it has the major limitation of angular dependence; specifically, a 7%-11% dose discrepancy was reported by Wolfsberger et al. for beam incidence in the perpendicular and oblique directions [11]. This necessitates the application of correction factors, especially in VMAT delivery in which the beam rotates by 360^0. The use of correction factors resulted in an improvement in the measurement accuracy of the composite dose verification [17, 18]. Additionally, some uncertainties have been reported in dose measurements in the low-dose or peripheral regions, which are due to four types of errors: namely, positive bias, over-response to scattered dose, round-off errors, and angular dependence [14].

Another tool used for VMAT QA is the electronic portal imaging device (EPID) [10, 19]. EPID as a QA tool is preferred for its large detector density, high contrast, linear response to the dose, and excellent online capabilities. EPID does not require any additional phantoms or cables for QA [19, 20]. The advantage of EPID over MatriXX is that the resolution limit of the amorphous silicon flat-panel detector of EPID is significantly better than that of the ion chamber

detector of MatriXX [21]. However, because the detector in EPID is mounted to a rotating gantry, there is a risk of angle-dependent detector sag due to the gravitational force, therefore EPID obtains different results for VMAT plans performed using fixed and rotating gantry configurations [10, 20]. Despite their many merits, both MatriXX and EPID are unable to measure large dimension radiation fields because of the smaller sensitive area and lower spatial resolution of both systems compared to those of film dosimetry.

The gamma index (γ) is the most widely accepted method for the evaluation of 2D distributions, The measured and calculated 2D dose distributions in both systems were compared using this method, as recommended by Low et al [22]. This method combines two important dose comparison criteria: the dose difference (ΔD_M) and the distance to agreement (Δd_M). According to this method, when γ<1, the pixels are regarded as pass points. There different gamma evaluation criteria have been using depending upon institutional protocols. The gamma pass rates can be assessed using the 3%/3mm (Δd_M =3% and Δd_M=3 mm), 2%/2mm (Δd_M =2% and Δd_M =2 mm) and 1%/1mm (Δd_M =1% and Δd_M =1 mm) criteria. Besides that, to eliminate the low-dose areas and those outside the field, threshold (TH) values were set, in combination with gamma criteria and TH value determine the QA pass rates. The American Association of Physicists in Medicine (AAPM) Task Group (TG)-119 has recommended the use of either a 10% dose threshold or a region of interest determined by the jaw setting for 2D dose analysis. In our clinic, we used the 3%/3mm gamma criterion at $TH_{10\%}$ for this evaluation and consider all points, including those above 95%, as acceptable.

The pass rates of gamma analysis highly depend upon its normalization. The normalization of the ΔD_M determines whether the gamma analysis is done locally or globally. In local normalization, ΔD_M is calculated by normalizing the percentage difference between the measured dose and calculated dose to the calculated dose at that point. While in global normalization, the ΔD_M is normalized to the maximum calculated dose [23]. Although the 3%/3 mm

criterion is the most commonly used condition in, it is not sufficient to detect clinically relevant errors. Hussein et al. reported that small errors introduced in the collimator rotation and the MLC were not detected when the 3%/3mm criterion was used and it requires more stringent gamma evaluation criteria to be adopted [9]. Hence, in addition to the 3%/3 mm criterion, we used the 2%/2mm and the 1%/1mm criteria for the analysis of VMAT QA. However, the gamma index method is sensitive to the spatial resolution of the measured and calculated dose distribution system [24]. Low and Dempsey [24] recommend the minimum ratio between the spatial resolution of the evaluated distribution and the Δd_M criterion to be 1:3. This makes the use of stringent gamma criteria with Δd_M values less than the detector spacing and the calculation grid size a questionable issue. These facts demand a careful approach when using the 1%/1 mm criterion. It is important to identify the limitations imposed by the combined effects of the gamma index and the equipment in use. The aim of our study is to evaluate the gamma pass rates in VMAT QA, using MatriXX and EPID in planning situations involving complex hypothetical planning target volumes (PTVs) and different clinical conditions, namely, prostate, brain, and head and neck (HN) cases, when different evaluation criteria and TH settings are used.

5.2 Materials and Methods

5.2.1 VMAT planning in hypothetical PTVs

VMAT plans can produce highly conformal dose distributions around a PTV and simultaneously protect the organs at risk (OARs). These distributions are produced by the sophisticated dose optimization algorithms incorporated within the TPS and the plans are generated based on constraints and objectives specified by the user during the optimization process. This is achieved by using MLC modulations of different shapes and sizes, along with the modulation of gantry speed and dose rate. But, even advanced clinical dose calculation algorithms are not able to determine a correct dose distribution for small and irregular MLC

patterns where there is lack of charged particle equilibrium, which makes the dosimetry of such patterns a challenge [25]. It is essential to test non clinical plans having different MLC sizes and shapes and with different modulation of the MLC. Evaluation of the VMAT plans using MatriXX and EPID, especially in the above situation, is important to understand the limitation of these devices and how the different MLC shapes affect the quality assurance results. To produce MLC patterns with varying shapes, we have randomly selected four complex hypothetical 3D PTVs which resemble the English alphabet letters X (X-PTV), U (U-PTV), Z (Z-PTV) and O which is a ring shaped PTV (O-PTV)(Figure 5.1).

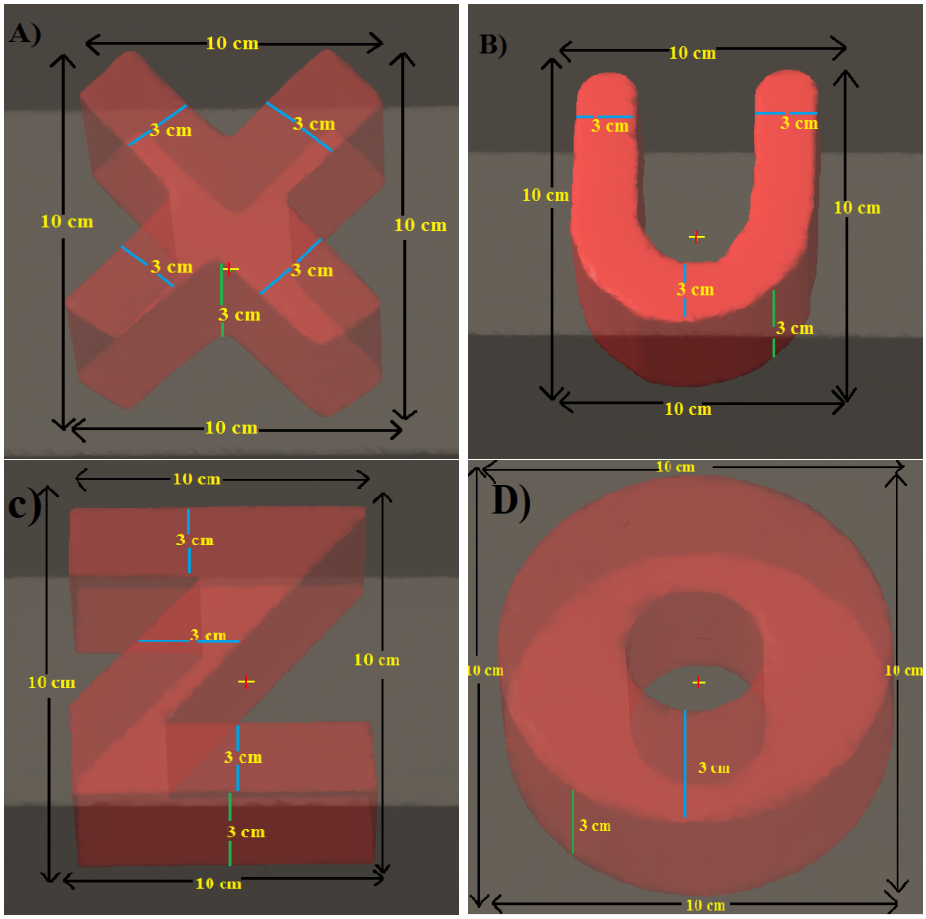

Figure 5.1: Three dimensional view of the hypothetical PTVs a) X-PTV, b) U-PTV, c) Z-PTV, and d) O-PTV on a homogeneous phantom with height (green) and thickness (blue) of 3 cm each.

The 2D detector array measuring device has a major drawback of limited

spatial resolution. This affects the sensitivity of the detectors to errors and hence, the effectiveness of dose evaluation. So, it is important to know how the spacing of detectors in the device affects the measurement especially when the size of PTV varies. This can be assessed by varying the diameter of the inner and outer rings of O-PTV. Three O-PTVs were countered for this purpose. A small O-PTV with inner diameter of 0.25 cm and outer diameter of 0.5 cm ($O - PTV_{0.5cm}$), an intermediate-size O-PTV with inner diameter 1 cm and outer diameter 2 cm ($O - PTV_{2cm}$), and a large one with inner and outer diameter of 2 cm and 4 cm respectively ($O - PTV_{4cm}$).

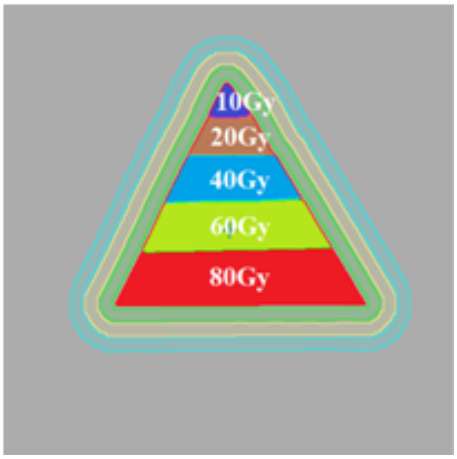

Figure 5.2: Hypothetical Δ-PTV with five segmented PTVs of thickness 3 cm and with a dose of 80 Gy (segment-1, red), 60 Gy (segment-2, yellow), 40 Gy (segment-3, cyan), 20 Gy (segment-4, brown) and 10 Gy (segment-4, blue) and avoidance structures S1 (green), S2 (yellow) and S3 (cyan).

High organ sparing in VMAT results in a steep dose gradient between the PTV and OAR regions. This produce a large difference between the calculated and the measured dose in highly complex MLC shapes, even for small changes in the position of the dose measuring device [24]. This necessitates testing of the devices in different dose gradient situations. In order to produce different dose gradient regions within the PTV, we have generated a pyramid shaped PTV (Δ-PTV) with a combination of five segmented PTVs with a dose of 80 Gy (segment-1, red), 60 Gy (segment-2, yellow), 40 Gy (segment-3, cyan), 20 Gy (segment-4, brown) and 10 Gy (segment-4, blue) (Figure 5.2).

All the PTVs were delineated on a homogeneous phantom (30 × 30 × 30 cm) generated using the Eclipse TPS system (Varian Medical Systems, Palo Alto, CA, Version 10). Each of the PTVs is set in coronal plane of size 10×10 cm and has a height and thickness of 3 cm each (Figure 4.1), except in the case of size varying O-PTVs where the thickness is varying in accordance with inner and outer diameter. To control the dose spillage outside the PTVs, and thus generate a highly conformal dose distribution during the plan optimization, three types of avoidance structures (AVSs) were also delineated; namely, S1 (green), S2 (yellow) and S3 (cyan) which formed margins of 1 cm, 2 cm, and 3 cm respectively around the PTVs (Figure 5.2).

Two VMAT plans were generated using Eclipse TPS: one with a single arc (gantry angle 179^0-181^0, collimator rotation of 30^0) and one with double complementary arcs (gantry angles 179^0-181^0 and 181^0-179^0, collimator rotations of 30^0 and 330^0). The plans were inversely optimized using the progressive resolution optimizer (PRO-II). The hypothetical PTVs (X-PTV, U-PTV, Z-PTV, O-PTV, $O - PTV_{0.5cm}$, $O - PTV_{2cm}$, and $O - PTV_{4cm}$) were planned with a dose of 50 Gy and the maximum dose to the AVS was restricted to 40 Gy, 30 Gy and 20 Gy for S1, S2, and S3 respectively. The Δ-PTV was optimized for five dose regions: 80 Gy, 60 Gy, 40 Gy, 20 Gy and 10 Gy along with the AVS structures to produce a conformal plan. The optimization was repeated until the desired dose distributions and constraints were achieved. Finally, the doses were calculated using an AAA with a voxel resolution of 0.25×0.25×0.25 cm^3.

5.2.2 VMAT planning in patients

We have selected 30 patient plans of three different sites, which included 10 prostate, 10 brain and 10 HN cancer cases. The prostate cancer patients were treated with 70 Gy in 28 fractions. The VMAT plans were generated with two complementary full arcs and with collimator rotations of 30^0 and 330^0. Here, two PTVs were delineated on planning computed tomography (CT): PTV-70Gy for the whole prostate and PTV-50.4Gy for the nodal regions. The plans of the

brain tumor patients were created with 60 Gy in 30 fractions with a single full arc and collimator rotations of 30. The HN patients were treated with 70 Gy in 33 fractions, with three PTVs, PTV-70Gy, PTV-60Gy and PTV-54Gy, with two complementary full arcs. The VMAT plans were generated using Eclipse, as described in Section 5.2.1.

5.2.3 Verification of plans using MatriXX and EPID

The pre-treatment verification of both the patient plans and the hypothetical PTV-based plans were conducted using two QA systems: a MatriXX system embedded inside a MultiCube phantom (hereafter named IM) and a Varian EPID dosimetric system attached to a Clinac iX (Varian Medical Systems, Palo Alto, CA). All the plans were delivered using the Clinac iX with a Millennium 120-leaf MLC.

The MatriXX is an ionization chamber array consisting of 1020 single air-vented plane-parallel cylindric ionization chambers (0.55 cm height, 0.4 cm diameter, centre-to-centre distance 0.76 cm) arranged in a 32 $\times$ 32 matrix (there are no chambers in the corners of the array). A maximum field of view of 24 $\times$ 24 cm^2 can be achieved. A The Multicube phantom, in which the MatriXX was embedded, had an 11 cm thick buildup block and a 7 cm thick backscatter block. The centre of the MatriXX chamber had a source axis distance of 100 cm during the measurement. All the VMAT plans were projected onto the CT images of the IM system to generate the verification plans. The array calibration and absolute dose calibration of the ionization chamber were performed using the manufacturer recommended methods. Before each measurement, a 1-h stable time was set and a 10 Gy pre-dose radiation was provided. Background signals were collected for 20 ms and corrections were performed in the temperature and pressure. The QA was conducted in the planned position with planned gantry angles. A gantry angle sensor was used to detect the gantry positions during VMAT delivery and the corresponding angular correction factors were applied for each measurement. Images of the dose were acquired every 0.5 s using the movie mode and were

then converted into an integral dose distribution. The planned full arcs were independently verified using the IM system. The measured and calculated 2D dose distributions were analysed with the OmniPro-I'mRT (Version 1.7, IBA Dosimetry) analysis software and were subsequently compared using the gamma index method.

The second method for the verification of the plans employed a Varian EPID dosimetric system attached to the Clinac iX (hereafter named EP). The EP system used in our study had amorphous-silicon (aSi 1000) photodiodes arranged in a 40 $\times$ 30 cm^2 active detector area (1024 $\times$768 pixels, 0.039 $\times$ 0.034 cm pixel pitch) [21]. The commissioning of the portal dose image prediction (PDIP) algorithm and the calibration of EPID were performed according to the manufacturer's recommendations. The calibration was conducted at a source to detector distance of 100 cm for a 6-MV beam to achieve the relationship between the calibration unit and monitor units. Each verification plan was generated using the PDIP algorithm in the Eclipse TPS and the 2D dose map was calculated for the planned positions. The measurement was performed in the integration mode with the same geometry and the measured dose distribution was obtained. The comparison between the calculated and measured dose distributions was performed using portal dose analysis software in the Eclipse TPS and was evaluated using the gamma index criteria [22].

5.2.4 Evaluation criteria for VMAT QA

We have used the globally normalized gamma pass rates in IM ($IM_{\gamma\%}$) and EP ($EP_{\gamma\%}$) in our study. The gamma pass rates were assessed using the 3%/3mm (Δd_M =3% and Δd_M=3 mm), 2%/2mm (Δd_M =2% and Δd_M =2 mm) and 1%/1mm (Δd_M =1% and Δd_M =1 mm) criteria. The effect of different TH values on the gamma pass rates was also assessed. Three TH values were set for each IM and EP measurement. When the TH was set to zero ($TH_{0\%}$), all the points in the measured and calculated dose distributions were included in the gamma calculation. However, when the TH was 10% ($TH_{10\%}$) and 20%

($TH_{20\%}$), the points receiving a dose smaller than 10% and 20% of the maximum dose respectively were excluded. The same evaluation methods were adopted for both the patient and hypothetical PTV plans. The difference in gamma pass rates between the $TH_{10\%}$ and $TH_{0\%}$ ($TH_{10-0\%}$) and $TH_{10\%}$ and $TH_{20\%}$ ($TH_{10-20\%}$) were evaluated for the three clinical situations when the 3%/3mm, 2%/2mm and 1%/1mm gamma criteria were used.

5.3 Results

5.3.1 Gamma index analysis of VMAT plans in hypothetical PTVs

Table 5.1 shows the mean and standard deviation (SD) in $IM_{\gamma\%}$ and $EP_{\gamma\%}$ for the VMAT plans of the four hypothetical PTVs (X-PTV, U-PTV, Z-PTV, and O-PTV). The results for $IM_{\gamma\%}$ and $EP_{\gamma\%}$ are comparable in all cases. When the commonly used 3%/3mm criterion was considered, the pass rates were above 95%; when $TH_{20\%}$ was applied, the Z-PTV exhibited the minimum value, which was $95.9\% \pm 0.80\%$ and $96.8\% \pm 0.86\%$ for IM and EP respectively. The pass rates were observed to decrease as the criteria became more stringent. Similarly, the pass rates increased for both methods when no threshold ($TH_{0\%}$) was applied and they tended to decrease for $TH_{10\%}$ and $TH_{20\%}$. In all cases, the lowest pass rates values were observed for the1%/1mm criteria when a 20% TH was applied.

Table 5.2 summarizes the mean and SD values in $IM_{\gamma\%}$ and $EP_{\gamma\%}$ for the Δ-PTV and for varying sizes of O-PTVs. Among the differently sized O-PTVs, the lowest mean and SD values for the 3%/3mm criterion and when $TH_{20\%}$ was applied were observed for the $O - PTV_{0.5cm}$; these were $81.0\% \pm 1.70\%$ and $84.3\% \pm 1.15\%$ for IM and EP respectively, and they were higher in the VMAT plans using $O - PTV_{2cm}$ and $O - PTV_{4cm}$. The Δ-PTV-based VMAT plans also exhibited a reduction in pass rates when changing form $TH_{0\%}$ ($97.2\% \pm 0.95\%$ and $97.3\% \pm 1.03\%$) to TH20% ($92.7\% \pm 2.36\%$ and $92.0\% \pm 1.25\%$). In all cases,

it can be observed that the variation in the pass rates when changing from $TH_{0\%}$ to $TH_{20\%}$ is more evident when the criteria become stringent.

5.3.2 Gamma index analysis of VMAT plans in patients

The $IM_{\gamma\%}$ and $EP_{\gamma\%}$ results were above 95% in the patient-based VMAT plans when the 3%/3mm criterion and a threshold of $TH_{10\%}$ were applied (Table 5.3). However, it must be noted that the gamma pass rates were higher in the brain cancer cases compared to the other two patient categories for all the three evaluation criteria, the maximum values for the 3%/3mm criterion were $98.3\% \pm 0.8\%$ and $98.5\% \pm 0.6\%$ for IM and EP respectively. The lowest pass rates were exhibited by the HN cases, which were $97.2\% \pm 0.7\%$ and $97.5\% \pm 2.1\%$ respectively for IM and EP and for the 3%/3mm criterion. These pass rates tended to decline as the criteria became stricter.

Figure 5.3 depicts the mean and SD for difference in gamma pass rates, calculated using the 3%/3mm, 2%/2mm and 1%/1mm evaluation criteria in the brain, prostrate and HN cancer VMAT plans. The gamma pass rates were observed to be higher when analyzed with $TH_{0\%}$ and they decreased when the threshold was increased, in both IM- and EP- based QA systems. The maximum difference in gamma pass rates was observed in the EP-based system for the HN cases and $TH_{10-0\%}$ which were $-1.8\% \pm 1.6\%$, $-9.2\% \pm 6.3\%$ and $-12.3\% \pm 5.3\%$, respectively for the 3%/3mm, 2%/2mm and 1%/1mm gamma criteria. When $TH_{10-20\%}$ was calculated for the HN cases, the maximum difference were $1.3\% \pm 1.1\%$ in IM and $7.9\% \pm 6.1\%$ and $17\% \pm 4.7\%$ in EP for the 3%/3mm, 2%/2mm and 1%/1mm gamma criteria. Similarly, in the brain and prostate cancer cases, difference in gamma pass rates were also observed to increase as the gamma criteria become more stringent.

Table 5.1: The mean and standard deviation of the gamma pass rates for hypothetical PTV-based (X-PTV, U-PTV, Z-PTV and O-PTV) VMAT plans, as evaluated using IM and EP at different threshold values ($TH_{0\%}$, $TH_{10\%}$ and $TH_{20\%}$)

VMAT plan	Gamma Criteria	$IM_{TH0\%}$	$EP_{TH0\%}$	$IM_{TH10\%}$	$EP_{TH10\%}$	$IM_{TH20\%}$	$EP_{TH20\%}$
X-PTV	3%/3mm	99.3 ± 0.24	99.5 ± 0.06	97.6 ± 0.30	98.3 ± 0.15	96.4 ± 0.40	97.2 ± 0.15
	2%/2mm	93.1 ± 0.99	92.7 ± 1.53	88.1 ± 1.20	87.2 ± 1.05	85.4 ± 1.40	84.0 ± 1.05
	1%/1mm	72.5 ± 2.68	74.0 ± 2.00	53.5 ± 2.30	55.3 ± 3.60	49.0 ± 1.28	52.3 ± 3.70
U-PTV	3%/3mm	99.2 ± 0.28	99.5 ± 0.61	98.4 ± 0.47	98.1 ± 0.29	97.1 ± 0.50	96.9 ± 0.73
	2%/2mm	94.7 ± 0.51	95.8 ± 0.72	87.1 ± 1.20	89.6 ± 0.55	86.4 ± 1.31	85.1 ± 1.20
	1%/1mm	476.3 ± 1.53	77.0 ± 1.00	56.3 ± 2.89	58.0 ± 3.00	54.1 ± 1.90	53.1 ± 3.51
Z-PTV	3%/3mm	98.7 ± 0.21	99.5 ± 0.40	97.2 ± 0.23	98.1 ± 0.12	95.9 ± 0.80	96.8 ± 0.86
	2%/2mm	93.9 ± 0.53	95.2 ± 0.59	91.2 ± 0.88	89.7 ± 2.08	85.3 ± 1.07	86.0 ± 1.00
	1%/1mm	71.3 ± 1.29	73.7 ± 1.15	59.2 ± 3.34	58.0 ± 1.00	54.8 ± 2.73	52.7 ± 2.53
O-PTV	3%/3mm	98.6 ± 0.88	98.7 ± 1.53	98.0 ± 1.28	98.6 ± 1.46	97.9 ± 1.29	97.7 ± 0.58
	2%/2mm	92.7 ± 0.58	92.8 ± 0.72	90.6 ± 2.03	89.4 ± 1.00	88.3 ± 2.31	87.7 ± 2.08
	1%/1mm	69.0 ± 1.00	73.0 ± 1.00	58.3 ± 1.15	59.7 ± 1.15	57.0 ± 2.00	56.6 ± 1.53

Table 5.2: Mean and standard deviation of the gamma pass rates for hypothetical PTV-based ($O - PTV_{0.5cm}$, $O - PTV_{2cm}$, $O - PTV_{4cm}$, and Δ-PTV) VMAT plans, as evaluated using IM and EP at different threshold values ($TH_{0\%}$,$TH_{10\%}$ and $TH_{20\%}$)

VMAT plan	Gamma Criteria	$IM_{TH0\%}$	$EP_{TH0\%}$	$IM_{TH10\%}$	$EP_{TH10\%}$	$IM_{TH20\%}$	$EP_{TH20\%}$
O-PTV0.5cm	3%/3mm	98.8 ± 0.68	98.3 ± 1.42	90.1 ± 1.01	92.3 ± 1.53	81.0 ± 1.70	84.3 ± 1.15
	2%/2mm	93.1 ± 0.64	92.1 ± 0.95	75.1 ± 1.01	78.0 ± 1.00	59.4 ± 0.65	60.3 ± 1.53
	1%/1mm	54.5 ± 1.11	58.4 ± 1.53	34.6 ± 2.17	38.3 ± 1.10	21.3 ± 1.60	21.3 ± 2.08
O-PTV2cm	3%/3mm	98.3 ± 1.16	98.8 ± 0.98	95.0 ± 0.42	97.7 ± 0.58	94.6 ± 0.85	95.3 ± 1.13
	2%/2mm	95.0 ± 1.48	96.7 ± 0.58	87.1 ± 0.54	88.0 ± 1.00	76.2 ± 1.01	78.0 ± 1.00
	1%/1mm	87.2 ± 1.08	85.8 ± 2.25	52.3 ± 1.12	58.0 ± 1.00	33.7 ± 0.23	37.7 ± 0.58
O-PTV4cm	3%/3mm	99.5 ± 0.5	99.0 ± 1.00	99.3 ± 0.61	98.3 ± 1.13	98.5 ± 1.29	97.7 ± 2.08
	2%/2mm	96.6 ± 1.00	95.1 ± 1.80	93.3 ± 0.60	92.4 ± 0.58	89.3 ± 1.20	90.3 ± 0.58
	1%/1mm	91.7 ± 1.24	92.8 ± 1.06	66.6 ± 1.20	68.9 ± 1.10	66.1 ± 1.66	65.5 ± 1.86
Δ-PTV	3%/3mm	97.2 ± 0.95	97.3 ± 1.03	94.2 ± 1.70	94.6 ± 1.40	92.7 ± 2.36	92.0 ± 1.25
	2%/2mm	90.7 ± 1.46	91.7 ± 1.53	80.9 ± 2.12	79.2 ± 0.71	76.1 ± 3.73	76.7 ± 1.15
	1%/1mm	73.1 ± 3.03	74.8 ± 0.57	46.6 ± 2.92	46.8 ± 1.11	41.8 ± 3.29	43.6 ± 0.36

Table 5.3: Mean and standard deviation of gamma pass rates for VMAT plans for brain (BR), prostate (PR) and head and neck (HN) cancer patients, obtained using a threshold of 10% ($TH_{10\%}$).

	BR		PR		HN	
Gamma Criteria	$IM_{\gamma\%}$	$EP_{\gamma\%}$	$IM_{\gamma\%}$	$EP_{\gamma\%}$	$IM_{\gamma\%}$	$EP_{\gamma\%}$
3%/3mm	98.3 ± 0.8	98.5 ± 0.6	97.7 ± 1.0	98.0 ± 0.2	97.2 ± 0.7	97.5 ± 2.1
2%/2mm	90.8 ± 2.8	92.4 ± 1.7	88.1 ± 2.0	88.5 ± 3.0	78.9 ± 4.8	80.6 ± 8.6
1%/1mm	59.0 ± 4.9	60.6 ± 3.9	54.6 ± 4.8	57.5 ± 4.94	47.7 ± 8.4	50.7 ± 7.5

5.4 Discussion

An efficient and consistent testing device has become an essential part of pre treatment verification of highly complicated delivery techniques like VMAT. In our study, we have evaluated the effect on gamma pass rates when different gamma evaluation criteria and threshold settings were used, in different hypothetical and clinical situations using the IM and EP verification systems. Different levels of complexity were attained using hypothetical PTVs of different shapes and sizes and by using three different anatomical sites (prostate, brain, and HN). Both IM and EP achieved comparable results for the various VMAT plans. The measured and calculated dose distributions showed a good correlation in both systems. Threshold settings were used to define the region of interest of the evaluation field. When no threshold was applied, the gamma calculation considered all the points in the dose plane and obtained a higher pass rate; this effect can mask the fail points inside the field where the PTVs and OARs are present. Therefore, we also have investigated the effect of gamma pass rates with 10% and 20% thresholds using the 3%/3mm, 2%/2mm, and 1%/1mm gamma criteria.

We have observed that as the threshold increased, the pass rates deceased. This reduction was significant when the stringent evaluation criteria 2%/2mm

and 1%/1mm were applied in both the hypothetical and patient-based VMAT plans. Several groups have investigated the applicability of pre treatment verification of the IMRT and VMAT techniques with MatriXX and EPID. Zhu et al.[10] compared the gamma pass rates of the VMAT QA using EPID and MatriXX and reported that the gamma pass rates were greater than 98% when the 3%/3mm gamma criterion and a threshold of 10% were applied. They have also noted a reduction in gamma pass rates when the 2%/2mm criterion was employed for variable gantry positions. Additionally, their results showed higher pass rates in the brain and prostate cancer cases than HN ones. Bailey et al. [26] analyzed the applicability of pre-treatment VMAT QA of prostate and HN cancer plans using the Varian EPID and MapCHECK systems and observed gamma pass rates of $98.2\% \pm 1.65\%$ and $95.3\% \pm 5.9\%$ in the prostate 14-arc and the HN 12-arc VMAT plans. The outcomes of all these studies are comparable with our results. The lower pass rate exhibited by the HN cases compared to the other two groups is due to the increased level of complexity in the corresponding VMAT plan. This increase in complexity can be attributed to the large dose gradient and the complex dose distribution in the HN cases.

When the measured and calculated dose distributions are evaluated, there are several sources of uncertainties that must be considered. Positional inaccuracies if any, the detector response, the daily dose variation and mechanical instabilities of the gantry and collimator of the treatment machine are errors that may modify the gamma pass rates, especially in complex techniques like VMAT [27]. Wagner and Vorwerk observed larger deviations in the gamma pass rates in VMAT plans when the field sizes were very small or very large [27]. This effect was confirmed by our studies of O-PTVs, as significant reductions of the pass points were observed when the size of the PTV was too small owing to resolution of the detector. When the fluence between the two detectors is greatly modulated, the recorded dose is lower than the calculated dose, which also contributes to the dose deviation [18]. We have also determined that most of these fail points were near the field boundaries both in the IM and EP QA

systems. This is because even small errors in the position of the collimator can result in large dose variations near the edge [18]. During rotation treatment, the angular dependence of MatriXX plays a major role in the gamma pass rates. This dependence was especially increased when the incident beam approached to 90 in MatriXX. This can be avoided by using gantry angle sensors to determine each gantry position and the corresponding corrections can be applied using the correction factors provided by the OmniPro-I'mRT software. In addition to all these errors, MatriXX overestimates the peripheral dose by 2% [14].

EPID is a good choice for the verification of plans as it easily achieves accurate positioning and can measure both high- and low-dose gradient regions. Additionally, it exhibits no angular dependence. However, the system has some issues that must be addressed, like electronic disequilibrium produced by insufficient build up material in EPID, inaccuracies in dose measurements created by scattered photons from the phosphor screen and back scattered radiation from the support arms. As the position of EPID is fixed with respect to the gantry, it is impossible to asses any errors in the gantry rotation [8]. Furthermore, EPID exhibits a small sag in its position due to gravity; this displacement also contributes to the reduction of pass rates, especially in VMAT plans in which gantry continuously rotates.

The main limitation of 2D dose verification is that, it cannot formulate a correlation between the errors detected during measurement and the dose with the OARs and PTVs. This can be addressed by introducing 3D dose verification methods in clinics. Such methods involve the implementation of an EPID system and a 3D dose reconstruction method by using either a back-projection method [28] or Monte Carlo dose simulations [29]. Furthermore, a technique using the COMPASS system (IBA Dosimetry, Germany) can determine the 3D dose distribution in the patient's anatomy [30]. However, these methods require further clinical investigations and independent commissioning before implementation in clinics. Therefore, the 2D dose verification is still a gold standard for pre-treatment plan verification. An action level must be set for the pre-treatment

QA based on the institution's protocol, the experience of the physicist and on the recommendation of the AAPM TG -119. The latter propose using 90% and 88%-90% gamma pass rate for per field and composite 2D dose verification, respectively with the 3%/3mm gamma criterion and a 10% threshold in IMRT. This recommendation is also valid for VMAT plans. The scope of the 3D analysis in the VMAT plan verification must be investigated in the future and its clinical relevance must be studied in detail.

5.5 Conclusions

We have examined the performance of the MatriXX and EPID systems for QA and verified the validity of VMAT plans. The results obtained for the two systems are comparable in terms of the measured and calculated doses, which confirmed the suitability of the equipments used and the validity of the plans. Our investigation of differently shaped hypothetical PTVs and different clinical situations has provided us with an improved perspective of the plan verification process in different complex situations. Additionally, the study results emphasize that the threshold settings significantly affect the gamma pass rates, especially in the lower gamma criteria; however this effect is reduced in the 3%/3mm criterion. Therefore, the threshold value must be selected carefully.

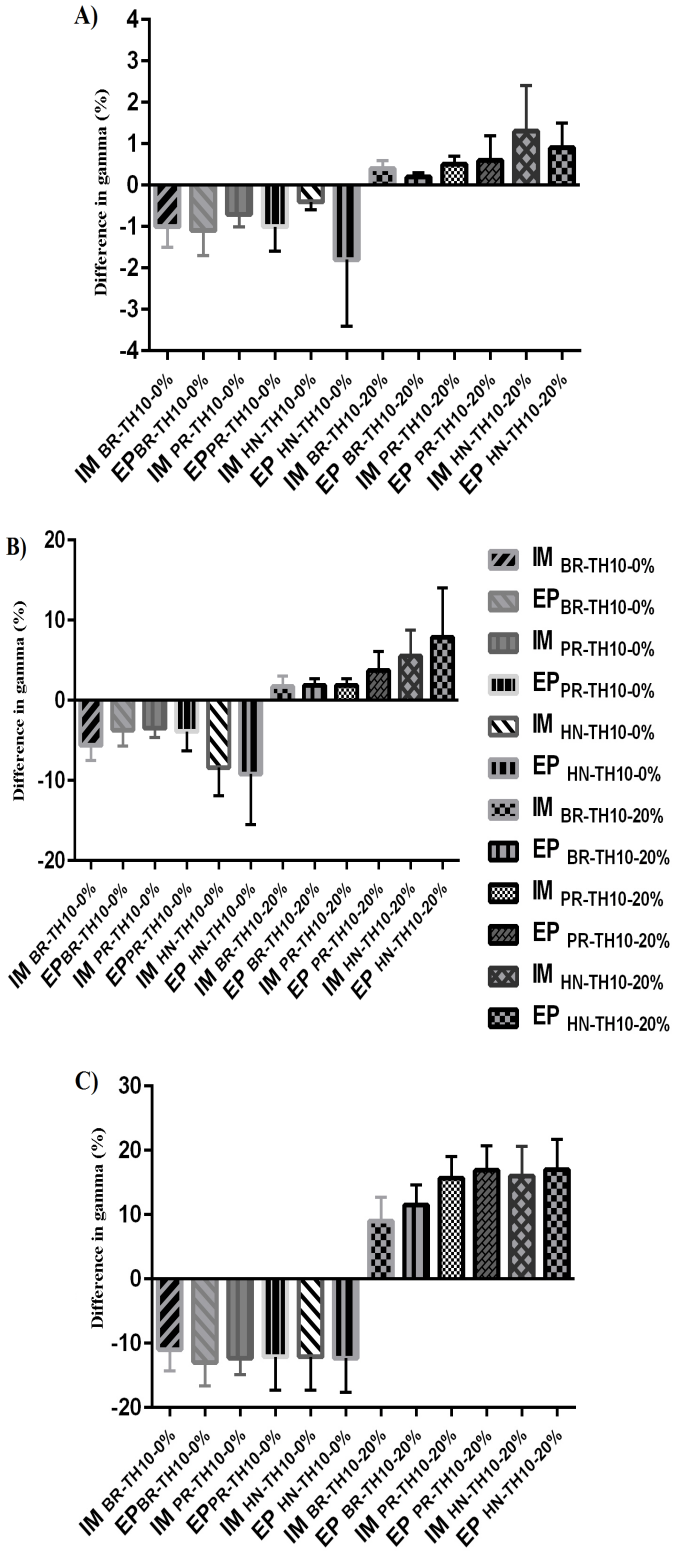

Figure 5.3: Mean and standard deviation of the percentage differences in gamma pass rates for $TH_{10-0\%}$ ($TH_{10\%}$ - $TH_{0\%}$) and $TH_{10-20\%}$ ($TH_{10\%}$ - $TH_{20\%}$) for brain (BR), prostate (PR) and Head and Neck (HN) clinical plans evaluated using MatriXX (IM) and EPID (EP) at a) 3%/3mm b) 2%/2mm c) 1%/1mm.

References

[1] VerbakelWF, Cuijpers J P, Hoffmans D, Bieker M, Slotman B J Senan S. (2009) Volumetric intensity-modulated arc therapy versus conventional IMRT in head-and-neck cancer: a comparative planning and dosimetric study Int. J. Radiat. Oncol. Biol. Phys;74: 252-9.

[2] Wolff D, Stieler F, Welzel G, Lorenz F, Abo-Madyan Y, Mai S, Herskind C, PolednikM, Steil V,Wenz F Lohr F. (2009). Volumetric modulated arc therapy (VMAT) versus serial tomotherapy, step-and-shoot IMRT and 3D-conformal RT for treatment of prostate cancer Radiother. Oncol; 93:226-33.

[3] Otto K. (2008). Volumetric modulated arc therapy: IMRT in a single gantry arc. Med Phys.;35(1):310-17.

[4] Bedford J L Warrington A P. (2009). Commissioning of volumetric modulated arc therapy (VMAT) Int. J. Radiat. Oncol. Biol. Phys; 73:537-45.

[5] Tatsumi D, Hosono M N, Nakada R, Ishii K, Tsutsumi S, Inoue M, Ichida T, Miki Y. (2011). Direct impact analysis of multi-leaf collimator leaf position errors on dose distributions in volumetric modulated arc therapy: a pass rate calculation between measured planar doses with and without the position errors. Phys Med Biol.;56 (20):237-46.

[6] Pardo Montero J and Fenwick J D. (2011). The effect of different control point sampling sequences on convergence of VMAT inverse planning Phys. Med. Biol ; 56: 2569-83.

[7] Iftimia I, Cirino ET, Xiong L, Mower HW. (2010). Quality assurance methodology for Varian RapidArc treatment plans. J Appl Clin Med Phys; 11(4):3164.

[8] Chandraraj V, Stathakis S, Manickam R, Esquivel C, Supe SS, Papanikolaou N. (2010). Consistency and reproducibility of the VMAT plan delivery using three independent validation methods. J Appl Clin Med Phys.; 12(1):3373.

[9] Hussein M, Adams EJ, Jordan TJ, Clark CH, Nisbet A. (2013). A critical evaluation of the PTW 2D-ARRAY seven29 and OCTAVIUS II phantom for IMRT and VMAT verification. J Appl Clin Med Phys.;14(6):4460.

[10] ZhuJ, Chen L, Jin G. (2013). A comparison of VMAT dosimetric verifications between fixed and rotating gantry positions. Phys.Med. Biol ; 58:1315-1322.

[11] Wolfsberger L D, Wagar M, Nitsch P, Bhagwat M S, Zygmanski P. (2010). Angular dose dependence of Matrixx TM and its calibration J. Appl. Clin. Med. Phys.;11: 241-51.

[12] Herzen J, Todorovic M, Cremers F, Platz V, Albers D, Bartels A, Schmidt R. (2007). Dosimetric evaluation of a 2D pixel ionization chamber for implementation in clinical routine Phys. Med. Biol; 52:1197-208.

[13] Li J G, Yan G Liu C. (2009). Comparison of two commercial detector arrays for IMRT quality assurance J. Appl. Clin. Med. Phys.;10: 62-74.

[14] Han Z, Ng S K, Bhagwat M S, Lyatskaya Y Zygmanski P. (2010). Evaluation of MatriXX for IMRT and VMAT dose verifications in peripheral dose regions Med. Phys.; 37:3704-14.

[15] Wiezorek T, Banz N, Schwedas M, Scheithauer M, Salz H, Georg D, Wendt TG. (2005). Dosimetric quality assurance for intensity-modulated radiother-

apy feasibility study for a filmless approach. Strahlenther Onkol; 181:468-474.

[16] Chandraraj V, Stathakis S, Manickam R, Esquivel C, Supe SS, Papanikolaou N. (2011).Comparison of four commercial devices for RapidArc and sliding window IMRT QA. J Appl Clin Med Phys.;12(2):338-349.

[17] Shimohigashi Y, Araki F, Tominaga H, et al. (2012). Angular dependence correction of MatriXX and its application to composite dose verification. J Appl Clin Med Phys. ;13(5):81-96.

[18] Boggula R, Birkner M, Lohr F, Steil V, Wenz F, Wertz H. Evaluation of a 2D detector array for patient-specific VMAT QA with different setups. (2011). Phys Med Biol. ; 56(22):7163-77.

[19] Bakhtiari M, Kumaraswamy L, Bailey DW, Boer S De, Malhotra HK, Podgorsak MB. (2011). Using an EPID for patient-specific VMAT quality assurance Using an EPID for patient-specific VMAT quality assurance. Med Phys.;38(3):1366-73.

[20] ori M, Cagni E, Paiusco M, Munro P, Nahum AE. (2010). Dosimetric verification of IMAT delivery with a conventional EPID system and a commercial portal dose image prediction tool Dosimetric verification of IMAT delivery with a conventional EPID system. Med Phys.; 37(1):377-90.

[21] Sharma DS, Mhatre V, Heigrujam M, Talapatra K, Mallik S. (2010). Portal dosimetry for pretreatment verification of IMRT plan?: a comparison with 2D ion chamber array. J Appl Clin Med Phys. ;11(4):3268.

[22] Low DA, Harms WB, Mutic S, Purdy JA. (1998). A technique for the quantitative evaluation of dose distributions. Med Phys.; 25(5):656-61.

[23] Bailey DW, Nelms BE, Attwood K, Kumaraswamy L, Podgorsak MB. (2011) Statistical variability and confidence intervals for planar dose QA pass rates. Med Phys.;38(11):6053-64.

[24] Low DA, Dempsey JF. (2003). Evaluation of the gamma dose distribution comparison method. Med Phys.;30 (9):2455-64.

[25] Das IJ, Ding GX, Ahnesj A. (2008). Small fields: nonequilibrium radiation dosimetry. Med Phys. ;35(1):206-15.

[26] Bailey DW, Kumaraswamy L, Bakhtiari M, Malhotra HK, Podgorsak MB. (2012) EPID dosimetry for pretreatment quality assurance with two commercial systems. J Appl Clin Med Phys.; 13(4):3736.

[27] Wagner D, Vorwerk H. (2011). Two years experience with quality assurance protocol for patient related Rapid Arc treatment plan verification using a two dimensional ionization chamber array. Radiat. Oncol.;6(1):21.

[28] A. Mans, P. Remeijer, I. Olaciregui-Ruiz, M. Wendling, J. J. Sonke, B. Mijnheer, M. van Herk, and J. C. Stroom. (2010). 3D dosimetric verification of volumetric-modulated arc therapy by portal dosimetry. Radiother. Oncol.;94:181-187.

[29] W. van Elmpt, S. Nijsten, A. Dekker, B. Mijnheer, P. Lambin. (2007). Treatment verification in the presence of inhomogeneities using EPID-based three dimensional dose reconstruction Med. Phys.;34:2816-2826.

[30] Boggula R, Lorenz F, Mueller L, Birkner M, Wertz H, Stieler F, Steil V, Lohr F Wenz F. (2010). Experimental validation of a commercial 3D dose verification system for intensity-modulated arc therapies Phys. Med. Biol.;55:5619-33.

[31] Mancuso GM, Fontenot JD, Gibbons JP, Parker BC, Mancuso GM, Parker BC. (2012). Comparison of action levels for patient-specific quality assurance of intensity modulated radiation therapy and volumetric modulated arc therapy treatments Comparison of action levels for patient-specific quality assurance of intensity modulated radiation therapy and volumetric modulated arc therapy treatments. Med Phys. ;39(7):4378-85.